

Gauge Higgs Unification in Extra Dimensions and Spin-3/2 Dark Matter

Mohammed Omer Ahmednoor Khojali

Supervised by: Prof. Alan S. Cornell

24th April 2018 in Johannesburg

*A Thesis submitted to the Faculty of Science, University of the Witwatersrand, Johannesburg, in
fulfillment of the requirements for the degree of Doctor of Philosophy.*



Abstract

In this thesis we discuss various gauge group structures in the gauge-Higgs unification models. The first group we considered was a toy $SU(3)$ model, where it is possible to have the unification of gauge and top Yukawa couplings, which is an attractive feature of gauge-Higgs unification models in extra-dimensions. This feature is usually considered difficult to obtain based on simple group theory analyses. We reconsider several minimal toy models calculating the renormalisation group running at one loop. Our results show that the gauge couplings unify asymptotically at high energies, and that this may result from the presence of an UV fixed point. The Yukawa coupling in our toy models is enhanced at low energies, showing that a genuine unification of gauge and Yukawa couplings may be achieved.

Furthermore, the evolution of the Cabibbo-Kobayashi-Maskawa matrix elements, the Jarlskog invariant and the quark mixings are derived for the one-loop renormalisation group equations in a five-dimensional models for an $SU(3)$ gauge group compactified on an S^1/\mathbb{Z}_2 orbifold. We have assumed that there is a fermion doublet and two singlets located at the fixed points of the extra dimension, which pointed to some interesting phenomenology in this toy model. We then explicitly test in a simplified 5-dimensional model with $SU(5)$, $SU(5) \times U(1)'$ and G_2 gauge symmetries, the evolution of the gauge couplings, by assuming that all the matter fields are propagating in the bulk, and consider orbifolds based on Abelian discrete groups which lead to 5-dimensional gauge theories compactified on an S^1/\mathbb{Z}_2 . The gauge couplings evolution is derived at one-loop level and used to test the impact on lower energy observables, in particular the Weinberg angle. For our numerical calculations we have assumed that the fundamental scale is not far from the scope of the Large Hadron Collider, where we choose the compactification radii to be the following benchmark values: 1 TeV, 4 TeV, 5 TeV, 8 TeV, 10 TeV, 15 TeV and 20 TeV.

As these gauge-Higgs unification models can also contain many additional particles,

we sought to use these particles as dark matter (DM) candidates. As many studies have already been done on various spin DM particles, we chose to focus on the more exotic spin-3/2 fermionic DM. We have allowed interactions with standard model fermions through a vector mediator in the s -channel in our first considerations. An interesting feature of the spin-3/2 nature of the standard model particles is that there exists a minimum value of the DM mass for a given coupling and mediator mass, below which the decay width of the mediator exceeds the mediator mass. We find that for pure vector couplings almost the entire parameter space in DM and mediator mass is consistent with the observed relic density, and is ruled out by the direct detection observations through DM-nucleon elastic scattering cross-section. In contrast, for pure axial-vector coupling, the most stringent constraints are obtained from mono-jet searches at the Large Hadron Collider.

We have also considered a spin-3/2 fermionic DM particle interacting with the standard model quarks through the exchange of a charged and coloured scalar or vector mediator in a simple t -channel model. It is found that for the vector mediator case almost the entire parameter space allowed by the observed relic density is already ruled out by the direct detection LUX data. There are no such bounds which exist on the interaction mediated by scalar particles. Monojet + missing energy searches at the Large Hadron Collider provide the most stringent bounds on the parameters of the model for this case. The collider bounds put a lower limit on the allowed DM masses.

These studies have shown a variety of particle phenomenology beyond the standard model, where such models can be constrained from both collider and astrophysical data.

DECLARATION

I declare that all results presented in this thesis are original except where reference is made to the work of others. The following are the list of my original works discussed in this thesis.

- **Journal papers:**

- A. Abdalgabar, **Mohammed Omer Khojali**, Alan S. Cornell, G. Cacciapaglia and A. Deandrea. Published in **Physics Letters B** **776** (2018), arXiv:1706.02313 [hep-ph].
- **Mohammed Omer Khojali**, A. Goyal, M. Kumar and Alan S. Cornell. Published in **Eur.Phys.J. C77** (2017) no.1, 25, arXiv:1608.08958 [hep-ph].

- **Conference proceedings:**

- **Mohammed Omer Khojali**, Alan S. Cornell and A. Deandrea. Published in **J. Phys. Conf. Ser.** **802** (2017) no.1, 012005, arXiv:1602.07441 [hep-th].
- **Mohammed Omer Khojali**, Alan S. Cornell, A. Deandrea and G. Cacciapaglia. Published in **J. Phys. Conf. Ser.** **878** (2017) no.1, 012024.
- **Mohammed Omer Khojali**, Alan S. Cornell, A. Deandrea and G. Cacciapaglia. Published in **J. Phys. Conf. Ser.** **889** (2017) no.1, 012012.
- **Mohammed Omer Khojali** and Alan S. Cornell. Published in **SAIP Proceeding** (2016), to be appear in **J. Phys. Conference Series**.

- **Awaiting publication:**

- **Mohammed Omer Khojali**, A. Goyal, M. Kumar and Alan S. Cornell. Submitted to **EPJC**, arXiv:1705.05149 [hep-ph].



Mohammed Omer Ahmednoor Khojali
24th April 2018 in Johannesburg

ACKNOWLEDGEMENTS

I would like to express my gratitude to my PhD advisor, Alan S. Cornell. He has helped me a lot during my PhD period, where no words can express my gratitude. I am greatly indebted to him for his unlimited support, which came without any hesitation during this work. I am very proud to be one of his students.

Special thanks to my collaborators, from University Lyon, Aldo Deandrea and Giacomo Cacciapaglia, thanks to them for giving me this chance to work with them.

I would like to express my warm gratitude to my collaborators, Ashok Goyal and Mukesh Kumar, I was very glad while I was working with them.

Many thanks also to Ammar Abdalgabar, as he is the one who introduced me to Alan, and also for his valuable discussion during my PhD time.

I would like to thank the National Research Foundation of South Africa, for the financial support given to me for three years, and SA-CERN for funds to visit CERN.

Many many thanks, to my family for their help and supporting me throughout my whole life. I would especially like to express my sincere thanks and indebtedness to my Dad, my Mom, my brothers, my sisters, and to all of my family for their encouragement and sacrifices, without them I could not be in this position.

I would like to thank all the people who support me, especially my teachers throughout my learning and educational life, thanks to all of my colleagues.

Thanks to Allah who made all of these works possible, without help of Allah, I would not have been able to finish this work.

Contents

Abstract	i
Declaration	iii
Acknowledgement	iv
List of Figures	xi
List of Tables	xiii
1 General context and overview	1
1.1 Introduction	1
1.2 The Standard Model of Particles physics	3
1.3 Some Reasons to go Beyond the SM	12
1.4 Some Ideas about Physics Beyond the SM	15
1.5 Structure of this thesis	19
2 Mathematical Background	20
2.1 Renormalisation Group Equations	20
2.2 Dimensional Regularisation Scheme	21
2.3 The RGEs for the Yukawa couplings in the SM	25
2.4 The cross-section for scattering of 2-particles into 2-particles	27
2.5 The Boltzmann equation	29
3 Unification of gauge and Yukawa couplings	33
3.1 Minimal SU(3) model with a bulk triplet	34
3.2 The RGEs for an SU(3) toy model	38
3.3 The naive dimensional analysis and asymptotic behaviour	40
3.4 Results and Discussions	40

4 Evolution of quark masses and flavour mixings in 5D for an SU(3) gauge group	42
4.1 Model construction	42
4.2 The evolution of CKM matrix in 5 dimension for an SU(3)	44
4.3 Numerical Results	46
5 Evolution of the gauge couplings and Weinberg angle in 5D for an SU(5) and flipped SU(5) gauge group	49
5.1 The gauge coupling evolution equations for an SU(5)	50
5.2 The gauge coupling evolution equations for an $SU(5) \times U(1)'$	53
6 Evolution of the gauge couplings and Weinberg angle in 5D for a G_2 gauge group	56
6.1 The G_2 Model Construction	57
6.2 The evolution of the gauge couplings and Weinberg angle	58
6.3 Results and discussions	60
7 Minimal Spin-3/2 Dark Matter in a simple s-channel model	62
7.1 Spin-3/2 Singlet DM Model	63
7.2 Constraints for the spin-3/2 singlet DM model	66
7.3 Summary and discussion	73
8 Spin-3/2 Dark Matter in a simple t-channel model	75
8.1 The simple t -channel model	76
8.2 The constraints for the simple t -channel model	79
8.3 Collider bounds	84
8.4 Summary and discussion	86
9 Conclusion	87
9.1 Summary of key results	87
9.2 Aspects for future work	88
Appendix A One-loop correction for gauge coupling coefficients in the SM	90
A.1 The strong interactions: $SU(3)_C$	90
A.2 The weak interactions: $SU(2)_L$	91
A.3 Electromagnetic interactions: $U(1)_{em}$	91
Appendix B Running of gauge and gauge-scalar couplings in 5D	92
B.1 Running of the gauge-scalar couplings	92
B.2 $SU(3)_W$ GHU model with bulk triplet	94

B.3	SU(3) _W GHU model with bulk sextet	96
Appendix C	Some calculations for one-loop β -functions	100
Appendix D	Full expression for the decay widths and cross-section	104
D.1	Decay widths	104
D.2	Cross-section	105
Appendix E	The thermal cross-section for $\chi S \rightarrow ug$	108
References		124

List of Figures

1.1	<i>The Higgs potential $V(\Phi)$ where: in the left panel, the case where $\mu^2 > 0$, and the right panel is the case where $\mu^2 < 0$, as a function of $\Phi ^2 = \Phi^\dagger \Phi$.</i>	7
1.2	<i>The one-loop Higgs correction with fermions inside the loop.</i>	13
1.3	<i>The running of the gauge couplings g_3 (green), g_2 (blue), and g_1 (red) in the SM as a function of a scale parameter t.</i>	15
2.1	<i>The contour we use to handle the integration.</i>	23
3.1	<i>Running of the normalised gauge and Yukawa couplings for the $SU(3)$ GHU model, for $1/R = 5$ TeV. The first KK mode enters at $t_{\text{KK}} \sim 4.0$.</i>	36
3.2	<i>5D NDA loop factor as a function of the energy, for $1/R = 5$ TeV.</i>	37
4.1	<i>Evolution of the mass ratio for three different values of the compactification radius we have used: 4 TeV (red line), 8 TeV (blue line), 20 TeV (green line); as a function of the scale parameter t. In the left panel is the evolution of the mass ratio m_u/m_t, and the right panel is the evolution of the mass ratio m_c/m_t.</i>	46
4.2	<i>The evolution of the CKM elements for three different values of the compactification radius we have used: 4 TeV (red line), 8 TeV (blue line), 20 TeV (green line); as a function of the scale parameter t. In the left panel is the evolution of the CKM element V_{cb}, and the right panel is the evolution of CKM element V_{ts}.</i>	47
4.3	<i>In the left panel is the evolution of the Jarlskog re-phasing-invariant parameter; the right panel is the evolution of R_{23}, for three different values of the compactification radius: 4 TeV (red line), 8 TeV (blue line) and 20 TeV (green line); as a function of the scale parameter t.</i>	47

4.4	<i>Left panel is the evolution of $\sin \theta_{23}$; the right panel is the evolution of $\sin \theta_{12}$, for three different values of the compactification radius: 4 TeV (red line), 8 TeV (blue line), 20 TeV (green line), as a function of the scale parameter t.</i>	47
5.1	<i>Left panel: The evolution of the inverse fine structure constants $\alpha_i^{-1}(\mu)$ in five dimensions as a function of t, for compactification scale $R^{-1} = 5$ TeV, where α_1^{-1} is the (red line), α_2^{-1} is the (blue line) and α_3^{-1} is the (green line). Right panel: Evolution of the Weinberg angle $\sin^2 \theta_W$ for all matter fields in the bulk, for three different compactification scales; 5 TeV (red line), 10 TeV (blue line), 20 TeV (green line) as a function of t.</i>	52
5.2	<i>Left panel: The evolution of the inverse fine structure constants $\alpha_i^{-1}(\mu)$ in five dimension as a function of $\log(E/\text{GeV})$ for compactification scale $R^{-1} = 5$ TeV, where α_1^{-1} is the (red line), α_2^{-1} is the (blue line) and α_3^{-1} is the (green line). Right panel: Evolution of the Weinberg angle $\sin \theta_W$ for all matter fields in the bulk, for two different compactification scales 1 TeV (red line), 5 TeV (blue line) and 10 TeV (green line) as a function of t.</i>	54
6.1	<i>The evolution of the inverse fine structure constants $\alpha_i^{-1}(\mu)$ in 5-dimensions for one-loop beta-functions as a function of $t = \ln(\mu/M_Z)$, for compactification scale $R^{-1} = 5$ TeV, where α_1^{-1} is the (red line), α_2^{-1} is the (blue line) α_3^{-1} is the (green line).</i>	59
6.2	<i>The evolution of the Weinberg angle $\sin^2 \theta_W$ for the one-loop beta-function, for different values of compactification scales, $R^{-1} = 1$ TeV (red), $R^{-1} = 5$ TeV (blue) and $R^{-1} = 10$ TeV (green) as a function of t.</i>	60
7.1	<i>Ratio of the mediator decay width to its mass $\Gamma/m_{Z'}$ as a functions of $m_\chi/m_{Z'}$ for a few benchmark values of the couplings: 0.1, 0.5 and 1.0. The (a) panel is for the vector couplings $g_{\chi,f}^V$, and the (b) panel is for the chiral couplings ($g_{\chi,f}^V = \pm g_{\chi,f}^A$). The (c) panel is for the axial-vector couplings $g_{\chi,f}^A$.</i>	66
7.2	<i>The contour plots between the $m_{Z'}$ and m_χ, where we have assumed that the DM χ saturates the observed DM density. The (a) and the (c) panels are for benchmark values of vector and axial-vector couplings respectively. The (b) panel is for the chiral coupling.</i>	68

7.3	<i>The spin-independent nucleon-DM cross-section σ^{SI} (left panel) and spin-dependent nucleon-DM cross-section σ^{SD} (right panel). The predicted cross-section is shown here for different values of the coupling, and are in agreement with the relic density constraints. In the plots we show the recent XENON1T data for σ^{SI}, and the XENON 100 neutron bounds for σ^{SD}.</i>	70
7.4	<i>The prediction for the DM χ annihilation rate into $b\bar{b}$ and $\tau^+\tau^-$ for benchmark values of couplings. The top, middle and bottom panels are for pure vector, chiral and axial couplings respectively. The cross-sections are obtained for $(m_\chi, m_{Z'})$ values consistent with the observed relic density. Bounds from the Fermi-LAT experiments are also shown.</i>	71
7.5	<i>The monojet cross-section in [pb] at the LHC with missing transverse energy $\cancel{E}_T + 1$ jet signal, through $pp \rightarrow Z' \rightarrow \chi\bar{\chi} + 1j$. The cross-sections are obtained by considering values of $(m_{Z'}, m_\chi)$ consistent with the observed relic density for the benchmark couplings. The allowed parameter space for spin-3/2 DM candidates lies below the CMS bound of $\sigma_{\text{monojet}} = 7.8$ fb. The (a), (b) and (c) panels are for pure vector, chiral and axial-vector couplings respectively.</i>	73
8.1	<i>Contour plots in the allowed DM mass m_χ and the mass splitting ratio $r - 1$ (with $r = m_S(m_V)/m_\chi$) in the left panels, and in the DM mass m_χ and the couplings in the right panels. We have assumed that the DM χ saturates the observed relic density. The top panels are for the dimension-4 interaction term for the vector mediator case. The middle and the bottom panels are for dimension-5 vector and scalar mediator cases respectively. In the left panels the colour gradient corresponds to the Yukawa couplings required to give the observed relic density, which in the right panels, the colour gradient corresponds to the mass splitting consistent with the observed relic density.</i>	78

8.2	<i>The spin-independent proton-DM cross-section σ^{SI}. The top and the bottom panels correspond to dimension-4 and dimension-5 vector interactions. In the left and right panel the colour gradients correspond to the Yukawa couplings and mass splittings respectively. All parameters are consistent with the observed relic density. We have also shown the graphs from the observed current upper limits from LUX [25] and PANDAX-II [24] experiments. The projected upper limit for XENON1T [23] has also been shown. Almost the entire parameter space (m_χ, m_V) for the vector mediator case considered here is already ruled out from the LUX data.</i>	82
8.3	<i>The prediction for the DM $\chi \bar{\chi}$ annihilation rate into $u \bar{u}$, as a function of the DM mass m_χ. All the parameters are chosen to be consistent with the observed relic density. The top and the middle panels are for dimension-4 and dimension-5 vector interactions respectively. The bottom panels are for the scalar interaction. The colour gradient in the left and right panels correspond to the coupling and mass splitting respectively. Bounds from the Fermi-LAT experiments are also shown [164].</i>	83
8.4	<i>The monojet cross-section in [pb] at the LHC with missing energy for two cases (i) $E_T^{\text{miss}} > 250 \text{ GeV}$ and (ii) $E_T^{\text{miss}} > 450 \text{ GeV}$. The cross-sections are obtained for all masses and couplings consistent with the observed relic density. (a) and (b) correspond to the dimension-4 and dimension-5 vector interactions terms respectively and (c) for the dimension-5 interaction term for the scalar mediator. The monojet cross-section from 8 TeV CMS collaboration data [166] based on an integrated luminosity 19.7 fb^{-1} is shown.</i>	85
B.1	<i>The diagrams contributing to the running of the gauge-scalar couplings.</i>	93
C.1	<i>Contributions to the top Yukawa coupling's RGEs in GHU models in the Landau gauge. The solid lines correspond to the top quarks, the broken lines correspond to A_5, the wavy lines correspond to the ordinary gauge bosons, while the wavy lines with a line through them correspond to the higher mode components of gauge bosons.</i>	101
D.1	<i>The Feynman diagram for the spin-3/2 DM annihilation into SM fermions $\chi \bar{\chi} \rightarrow Z' \rightarrow f \bar{f}$.</i>	105

List of Tables

1.1	<i>Summary of the SM field content and their quantum numbers.</i>	5
1.2	<i>The quantum number of the Higgs doublet.</i>	6
1.3	<i>Summary of the SM particles and their quantum numbers.</i>	12
3.1	<i>Gauge and Yukawa couplings in the $SU(3)$ GHU model compared to the SM values at the M_Z scale (for the Yukawa we use the top as a reference even though in this toy model the Yukawa corresponds to a down-type quark). We also include for completeness the QCD coupling.</i>	35
5.1	<i>Summary the cut-offs in 5 dimensions for an $SU(5)$ gauge group for three different compactification radii $R^{-1} = 5, 10$ and 20 TeV, where $t = \ln(\mu/M_Z)$.</i>	52
5.2	<i>Summary of the quarks, leptons and Higgs field content in the flipped $SU(5)$ model and their quantum numbers.</i>	54
5.3	<i>The cut-offs in 5 dimensions for the flipped $SU(5)$ gauge group for two different compactification radii $R^{-1} = 1, 5$ and 10 TeV, where $t = \ln(\mu/M_Z)$.</i>	55
6.1	<i>The cut-offs in 5 dimensions for the G_2 gauge group for three different compactification radii $R^{-1} = 1, 5$ and 10 TeV, where $t = \ln(\mu/M_Z)$.</i>	59
B.1	<i>The contribution of each diagram to the beta-function.</i>	94
B.2	<i>Coefficients of the beta-function in case A. In bold are the values corresponding to SM values (for diagram j an extra factor of $1/2$ should be taken as the SM is chiral).</i>	95
B.3	<i>Coefficients of the beta-function in case B.</i>	96
B.4	<i>Coefficients of the beta-function in case A, keeping only the values corresponding to SM running below m_{KK} (for diagram j, an extra factor of $1/2$ should be taken as the SM is chiral).</i>	98

Chapter 1

General context and overview

1.1 Introduction

The coming years could represent a new era of unexpected and exciting discoveries in high energy physics. For one thing, the CERN Large Hadron Collider (LHC) has been operating for some time and much experimental data has already been collected [1, 2]. So far, the greatest achievement of the LHC has been the discovery of the missing building block of the Standard Model (SM), the Higgs particle (or, at least, a particle which most likely is the SM Higgs particle) [3, 4]. On the other hand, no direct evidence of new physics beyond the SM has been found, yet. However, there are many reasons to believe that new physics should in fact show-up at, or about, the TeV scale [5, 6, 7].

The ways in which new physics may manifest, could be in the more poorly understood regions of the SM. For example, in the Higgs sector, and may lead to a way of resolving issues of the Higgs vacuum stability. One model to resolve this instability is with models like Gauge-Higgs Unification (GHU) in extra dimensions. This offers a very promising solution to the problem of the radiative stability of the electroweak scale (Higgs mass), by promoting the Higgs boson to a gauge field component, and then gauge invariance itself can protect the mass term from divergent radiative corrections [8]. Even though the model is an effective theory with a rather low cut-off, the finiteness of the Higgs potential allows calculability. Furthermore, we know the Universe to have dark matter (DM), where this is unexplained by the SM [9].

In order to build a successful GHU model, the first requirement is to find a gauge group that contains $SU(2)_L \times U(1)_Y$ (and optionally the strong $SU(3)_c$) and whose adjoint representation contains a doublet of $SU(2)$ to be identified with the Higgs

doublet. The group must have rank at least equal to the SM subgroup, which is 2, because the rank cannot be generally reduced by an orbifold breaking. As such, we shall consider groups of rank 2 or 4. The second step is to normalise the $U(1)$ gauge coupling so that the candidate Higgs has the correct hypercharge: this fixes the value of $\tan \theta_W$ at the cut-off scale and allows us to predict the Z mass at low energies. Finally, we need to make sure that the proper breaking of the unified group to the SM with a scalar zero mode for the Higgs doublet can be correctly done: this last step depends crucially on the symmetries of the orbifold compactification. In Ref. [10] a survey of the rank 2 groups has been done already, showing that in many cases the value of $\tan \theta_W$ at the cut-off is too far from the low energy value. However, even though the cut-off of the theory is small, the presence of many Kaluza-Klein (KK) levels below the cut-off means that the running is not logarithmic as in 4-dimensions, but starts showing a power law behaviour. Therefore, very large corrections are expected and one cannot disregard any possibility without studying the running. In this thesis we debate the minimal $SU(3)$ model with a bulk triplet, the evolution of quark masses and flavour mixings in 5-dimensions for an $SU(3)$ gauge group, as well as the evolution of the gauge couplings and Weinberg angle in 5-dimension for an $SU(5)$, flipped $SU(5)$ and G_2 gauge group.

Another great problem in the SM is that there are no strong clues to explain DM. Any new physics beyond the SM which anticipates the existence of new particles, for instance the superpartner particles (in supersymmetry) [11], KK particles (in extra dimensional models) [12, 13], also the techni-particles (such as in compositeness of the Higgs models), can seek to explain these as DM candidates [14, 15]. In the case of extra dimensions, we have the lightest KK particles, and if these particles are stable, these can become candidates for DM [16]. For instance, the spin-3/2 fermions exist in the KK model [17]. One of the additional fermions in the GHU model can be identified as a dark fermion, and thus, this dark fermion becomes the DM candidate, and it has to be the lightest of the dark particles.

Many astrophysical and cosmological observations during the last several decades provide strong evidence for the existence of DM in the Universe. The amount of DM has been precisely measured by the Planck satellite mission to be $\Omega_{DM}h^2 = 0.1188 \pm 0.0010$ [18], where the cold dark matter (CDM) content is estimated to comprise roughly 26% of the total energy in the Universe. Investigations into the nature of DM particles and their interactions has emerged as an important field of research. Weakly interacting massive particle (WIMP) DM searches constitute an important programme at the LHC, where the ATLAS and CMS collaborations [19, 20, 21] are looking for DM signatures involving missing energy accompanied by a single or two

jet events. It is expected, and there is indeed a real possibility, that the production of DM particles of any spin at 13 TeV centre-of-mass energy would be detected.

Null results from the direct detection experiments [22, 23, 24, 25], which measure nuclear-recoil in DM-nucleon elastic scattering, have provided the most stringent upper bounds on the spin-independent DM-nucleon elastic scattering cross-section over a wide range of DM masses. This has provided important constraints on the DM models considered in the literature. In addition there are indirect detection experiments whose aim is to detect the signature of annihilating or decaying DM particles into the SM particles.

As such, in this thesis we will also consider a spin-3/2 DM particle as an alternative to the conventional scalar, vector or spin-1/2 CDM particles. Where this spin-3/2 CDM has been studied in effective field theories (EFT) models and constraints from the relic density, direct and indirect observations obtained [26, 27, 28, 29]. Spin-3/2, 7.1 KeV warm dark matter (WDM) has been considered as a means to provide a viable explanation from the anomalous 3.1 KeV X-ray line observed by the XMM Newton [30]. Furthermore, the spin-3/2 DM with a Higgs portal has recently been investigated [31].

1.2 The Standard Model of Particles physics

The SM of particle physics has been a very successful model in describing most of the particle phenomenology known so far [32], even though it possesses some problems whose solution implies physics beyond the SM. The SM is a quantum field theory model based on two main principles:

- (1) The gauge principle.
- (2) The spontaneous symmetry breaking mechanism.

In order to obtain a renormalisable theory, we need to construct a Lagrangian in terms of operators of dimensionality such that the Lagrangian has dimensionality 4. Once we impose the local gauge invariance this will require the existence of the gauge bosons, which determines the interactions of these gauge bosons with fermions and also the interactions between the gauge bosons themselves. The combination of local gauge invariance with the spontaneous symmetry breaking mechanism leads to the Higgs mechanism, which generates the masses of weak vector bosons and fermions [33]. In order to determine the gauge theory we need to specify:

- (1) The gauge group.

(2) The field content in terms of its spin and its representations under the SM gauge groups.

The SM is a non-Abelian gauge theory with gauge group $SU(3)_C \times SU(2)_L \times U(1)_Y$, where the group corresponding to strong interactions is the $SU(3)_C$ colour group of quantum chromodynamics (QCD) [32, 34]. QCD describes the strong interaction between quarks, that arises from the exchange of the eight massless gluons that couple to the colour charge of the fermions, G_μ^a ($a=1,2,\dots,8$) [35]. The electroweak theory, which describes the electromagnetic and weak interactions between quarks and leptons, is basically based on the electroweak gauge group $SU(2)_L \times U(1)_Y$ [36, 37].

For the sake of completeness, let us now define the SM field content and their transformations under the SM gauge group, which are illustrated in Table 1.1.

The SM contains fermions also, where we can always write the Dirac spinor corresponding to each SM fermion as a sum of two spinors, one with left chirality P_L and the other with right chirality P_R :

$$\Psi = P_R \Psi + P_L \Psi = \Psi_R + \Psi_L = \frac{1}{2}(1 - \gamma_5)\Psi + \frac{1}{2}(1 + \gamma_5)\Psi. \quad (1.2.1)$$

The left and right-handed components of any fermion are assigned to different representations of the $SU(2)_L \times U(1)_Y$ gauge groups [38]. In order to specify the transformation properties under $SU(2)_L$ it is useful to define a new quantum number, the weak isospin T . Therefore, any particles having a weak isospin different from zero have an $SU(2)_L$ interaction, while those particles with weak isospin which is null are not sensitive to the $SU(2)_L$ interaction. For instance, the weak isospin of the fermions of left chirality is $T = 1/2$, thus the third component of the weak isospin T_3 can take values of $\pm 1/2$. Correspondingly, the quarks of left chirality are grouped into quark doublets,

$$Q_i = \begin{pmatrix} u_{iL} \\ d_{iL} \end{pmatrix}, \quad (1.2.2)$$

where i is the family index ($i = 1, 2, 3$). The left-handed leptons are grouped into the lepton doublets also,

$$L_i = \begin{pmatrix} \nu_{iL} \\ e_{iL} \end{pmatrix}. \quad (1.2.3)$$

The weak isospin is null for the fermions of right chirality, i.e. the quarks u_{iR} , d_{iR} and lepton e_{iR} . The weak hypercharge, Y , is the quantum number associated with the group $U(1)_Y$. Thus, the electric charge Q and the third component of the weak isospin T_3 are related by the Gell-Mann-Nishijima formula

$$Q = T_3 + Y. \quad (1.2.4)$$

Fields	Lorentz	$SU(3)_C$	$SU(2)_L$	$U(1)_Y$
Q_i	L	3	2	$\frac{1}{6}$
u_{iR}	R	3	1	$\frac{2}{3}$
d_{iR}	R	3	1	$-\frac{1}{3}$
L_i	L	1	2	$-\frac{1}{2}$
e_{iR}	R	1	1	-1

Table 1.1: *Summary of the SM field content and their quantum numbers.*

Therefore, the quark doublets have hypercharge 1/6, the lepton doublets have hypercharge -1/2 and the right-handed fermions u_{iR} , d_{iR} and e_{iR} have hypercharge 2/3, -1/3, and -1 respectively. The quarks are triplets under the $SU(3)_C$ group, and can interact via strong interactions, while leptons are colour singlets.

For each gauge group there is a gauge coupling associated to that gauge group, where in the case of the electroweak gauge symmetry group $SU(2)_L \times U(1)_Y$; there are two different couplings constant, $U(1)_Y$ has a gauge coupling g' , and $SU(2)_L$ has a gauge coupling g . The part of the SM Lagrangian that describes the $SU(2)_L \times U(1)_Y$ gauge interactions is given by

$$\mathcal{L}_{SM}^{Gauge} = i\bar{Q}_i D_\mu \gamma^\mu Q_i + i\bar{u}_{iR} D_\mu \gamma^\mu u_{iR} + i\bar{d}_{iR} D_\mu \gamma^\mu d_{iR} + i\bar{L}_i D_\mu \gamma^\mu L_i + i\bar{e}_{iR} D_\mu \gamma^\mu e_{iR} - \frac{1}{4} W_\mu^a W_a^{\mu\nu} - \frac{1}{4} B_{\mu\nu} B^{\mu\nu}, \quad (1.2.5)$$

where W_μ^a has a self-interacting term because of the non-Abelian nature of the $SU(2)_L$ group;

$$W_{\mu\nu}^a = \partial_\mu W_\nu^a - \partial_\nu W_\mu^a - g\epsilon_{abc} W_\mu^b W_\nu^c, \quad (1.2.6)$$

and

$$B_{\mu\nu} = \partial_\mu B_\nu - \partial_\nu B_\mu. \quad (1.2.7)$$

The covariant derivative in this case is given as

$$D_\mu = \partial_\mu + igW_\mu^a T_a + ig'B_\mu Y, \quad (1.2.8)$$

where the T_a are identified as the representations of the $SU(2)_L$ generators and are different for left handed and right handed fields. As we will see later, after spontaneous symmetric breaking, we can write the covariant derivative in terms of the gauge boson mass eigenstates

$$W_\mu^1 = \frac{W_\mu^+ + W_\mu^-}{\sqrt{2}}, \quad W_\mu^2 = \frac{i(W_\mu^+ - W_\mu^-)}{\sqrt{2}}, \quad (1.2.9)$$

and

$$W_\mu^3 = \frac{gZ_\mu + g'A_\mu}{\sqrt{g^2 + g'^2}}, \quad B_\mu = \frac{gA_\mu - g'Z_\mu}{\sqrt{g^2 + g'^2}}. \quad (1.2.10)$$

Fields	T	T_3	Y	Q
Φ^+	$\frac{1}{2}$	$\frac{1}{2}$	$\frac{1}{2}$	1
Φ^0	$\frac{1}{2}$	$-\frac{1}{2}$	$\frac{1}{2}$	0

Table 1.2: *The quantum number of the Higgs doublet.*

1.2.1 The SM Higgs and flavour.

Note that the discussion in this section based on Ref. [32]. A mass term for the gauge vectors is prevented by the gauge symmetry, therefore, in order for these gauge vectors to acquire masses, it is implied that somehow the gauge symmetry must be broken. This can be done through spontaneous symmetry breaking [39], which is a way for the gauge bosons to acquire masses, as well as the fermions, whose mass terms are also otherwise forbidden by the gauge symmetry. Note that the SM fermions in Table 1.1 are in chiral representations, and gauge symmetry in conjugation with chiral representations forbid fermion mass terms (vector-like fermions can have mass terms allowed by gauge symmetry).

The SM gauge group contains $SU(3)_C$ interactions which seem to be conserved, as long as the gluons are massless, therefore this symmetry should not be broken [40]. We therefore only need to break the other part, $SU(2)_L \times U(1)_Y$. In order to spontaneously break the gauge symmetry we need to introduce a scalar field in the theory, which is called the Higgs field, and we need this field to give mass not only to the gauge bosons but also to the SM fermions. Therefore we can introduce a complex scalar doublet as

$$\Phi = \begin{pmatrix} \Phi^+ \\ \Phi^0 \end{pmatrix}, \quad (1.2.11)$$

where the transformation of this doublet under the SM gauge group is given as:

(i) Under $SU(3)_C$ it is a singlet

$$\Phi \rightarrow \Phi. \quad (1.2.12)$$

(ii) Under $SU(2)_L$ it is a doublet

$$\Phi_r \rightarrow U_{rs} \Phi_s, \quad (1.2.13)$$

Φ_r and Φ_s are complex scalar doublet and $r, s = 1, 2$. The transformation matrix $U_{rs} \in SU(2)$.

(iii) Under $U(1)_Y$ the value of hypercharge is $Y = 1/2$.

Accordingly, the quantum number of these fields are given in the Table 1.2.

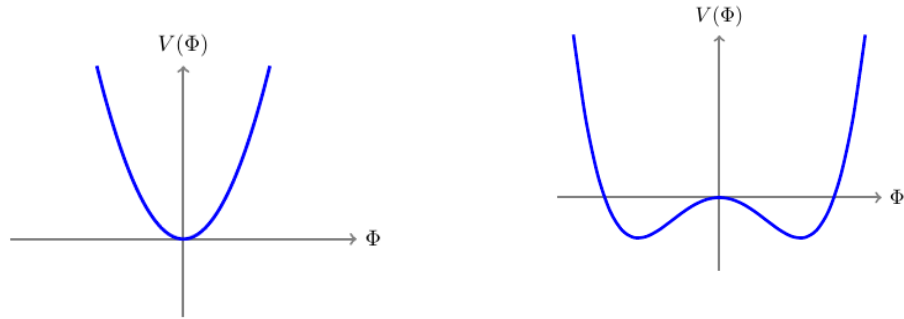


Figure 1.1: The Higgs potential $V(\Phi)$ where: in the left panel, the case where $\mu^2 > 0$, and the right panel is the case where $\mu^2 < 0$, as a function of $|\Phi|^2 = \Phi^\dagger \Phi$.

Therefore, we can write the Lagrangian for the Higgs field as

$$\mathcal{L}_\Phi = (D_\mu \Phi)^\dagger (D^\mu \Phi) - V(\Phi^\dagger \Phi), \quad (1.2.14)$$

where the Higgs potential is given by

$$V(\Phi^\dagger \Phi) = \mu^2 \Phi^\dagger \Phi + \frac{\lambda}{2} (\Phi^\dagger \Phi)^2. \quad (1.2.15)$$

The parameter λ should be non negative, otherwise the potential will not be bounded from below, and μ^2 should be real, because the Lagrangian is hermitian. μ^2 can be positive or negative, where in this case the action of the covariant derivative on the Higgs doublet is given by the following equation

$$D_\mu \Phi = \partial_\mu \Phi + ig W_\mu^a \frac{\sigma_a}{2} \Phi + ig' B_\mu \frac{1}{2} \Phi. \quad (1.2.16)$$

By minimising the Higgs potential there are two possibilities for the vacuum expectation value (VEV), see Figure 1.1:

- (i) $\mu^2 > 0$ in this case there is no $SU(2)_L \times U(1)_Y$ symmetry breaking.
- (ii) $\mu^2 < 0$ in this case there is $SU(2)_L \times U(1)_Y$ symmetry breaking.

The Higgs potential only depends on the gauge invariant combination $r^2 = \Phi^\dagger \Phi$, therefore we can rewrite the Higgs potential in terms of r^2 as

$$V(r) = \mu^2 r^2 + \frac{\lambda}{2} r^4. \quad (1.2.17)$$

When we minimise the potential in Equation (1.2.17) one can find

$$\frac{\partial V}{\partial r} = 2\mu^2 r + 2\lambda r^3 = 2r(\mu^2 + \lambda r^2) = 0. \quad (1.2.18)$$

Thus, in the case when $\mu^2 < 0$, the local and absolute minimum is given by

$$\mu^2 + \lambda r_0^2 = 0 \implies r_0^2 = -\frac{\mu^2}{\lambda}, \quad (1.2.19)$$

which is a positive quantity because $\mu^2 < 0$. This quantity is called the electroweak symmetry breaking scale squared, and we denote it by v^2 :

$$\frac{v^2}{2} = -\frac{\mu^2}{\lambda}. \quad (1.2.20)$$

The ground state is degenerate, as there are many possible values of the Higgs VEV that correspond to the same value

$$|\langle \Phi \rangle|^2 = \frac{v^2}{2}. \quad (1.2.21)$$

Accordingly, any such value of the VEV is possible as a ground state. Moreover the ground state is not invariant under the SM gauge group, which means that the SM gauge group is spontaneously broken. As an example, given any $\langle \Phi \rangle$ such that $|\langle \Phi \rangle| = v/\sqrt{2}$, there exists an $SU(2)_L$ transformation U such that

$$\langle \Phi \rangle = U \begin{pmatrix} 0 \\ \frac{v}{\sqrt{2}} \end{pmatrix}, \quad (1.2.22)$$

where without loss of the generality, we can then assume that the ground state is of the form

$$\langle \Phi \rangle = \begin{pmatrix} 0 \\ \frac{v}{\sqrt{2}} \end{pmatrix}. \quad (1.2.23)$$

In order to show how the gauge group is broken, let us remember that a generator is unbroken if the VEV is invariant under the associated (or generated) transformation

$$\mathcal{U} |\Phi\rangle = |\Phi\rangle, \quad (1.2.24)$$

with

$$\mathcal{U} = e^{i\theta U} \Rightarrow U|\Phi\rangle = 0. \quad (1.2.25)$$

The SM gauge group is spontaneously broken, except for the generators corresponding to $U(1)_{\text{em}} \times SU(3)_C$. Let us call $T_A^{(3)}$ the $SU(3)_C$ generators, $T_a^{(2)}$ the $SU(2)_L$ generators and Y the hypercharge generator. Then the most general generator is the superposition of all of these,

$$T = \sum_{A=1}^8 \alpha_A T_A^{(3)} + \sum_{a=1}^3 \beta_a T_a^{(2)} + \gamma Y, \quad (1.2.26)$$

where α_A , β_a and γ are real, and the generator T is unbroken only if

$$T \langle \Phi \rangle = 0. \quad (1.2.27)$$

As we know the Higgs doublet does not feel strong interactions, therefore

$$T_A^{(3)}\langle\Phi\rangle = 0. \quad (1.2.28)$$

Thus, this will lead to the following

$$0 = T\langle\Phi\rangle = (\beta_a T_a^{(2)} + \gamma Y)\langle\Phi\rangle = \frac{v}{2} \begin{pmatrix} \beta_1 - i\beta_2 \\ \gamma - \beta_3 \end{pmatrix}. \quad (1.2.29)$$

Accordingly, from the previous equation, we will get

$$\beta_1 - i\beta_2 = 0 \implies \beta_1 = \beta_2 = 0,$$

and

$$\gamma - \beta_3 = 0 \implies \gamma = \beta_3.$$

Hence, we can rewrite the most general generator as

$$\begin{aligned} T &= \alpha_A T_A^{(3)} + \gamma(T_3 + Y) \\ &= \alpha_A T_A^{(3)} + \gamma Q. \end{aligned} \quad (1.2.30)$$

Thus, Equation (1.2.30) shows that the unbroken generators are $T_A^{(3)}$ and Q , which are the generators of $U(1)_{\text{em}} \times SU(3)_C$. Therefore, in the SM the electroweak symmetry, if broken, is always correctly broken to $U(1)_{\text{em}}$, and always $v \geq 0$, with VEV Equation (1.2.23) which do not have any complex relative phase, thus CP is not spontaneously broken.

1.2.2 The gauge boson masses.

The SM gauge group contains twelve generators, where the number of the unbroken generators is nine, accordingly, this means that the remaining three generators are the broken generators. If the symmetry was a global symmetry the spectrum should contain three massless physical degrees of freedom, the Nambu-Goldstone bosons [41, 42, 43]. Out of the four generators of the electroweak group only one is unbroken, which means that three are broken. We then expect three vector bosons to acquire a mass (W_μ^+ , W_μ^- and Z_μ bosons) and three Higgs real degree of freedom (the Goldstones) to be eaten up by them. Out of the four real (two complex) Higgs degrees of freedom, only one then correspond to physical scalar, the Higgs boson [44, 45].

In order to write the spectrum following from spontaneous symmetry breaking, we should rewrite the Higgs doublet Φ in terms of the displacement from the ground state as follows:

$$\Phi = \langle\Phi\rangle + \Phi', \quad (1.2.31)$$

and by applying Equation (1.2.16) to the VEV, one can get the following

$$\begin{aligned} D_\mu \langle \Phi \rangle &= \partial_\mu \langle \Phi \rangle + ig W_\mu^a \frac{\sigma^a}{2} \langle \Phi \rangle + ig' B_\mu \frac{1}{2} \langle \Phi \rangle \\ &= \frac{iv}{2\sqrt{2}} \begin{pmatrix} g(W_\mu^1 - iW_\mu^2) \\ g' B_\mu - g W_\mu^3 \end{pmatrix}. \end{aligned} \quad (1.2.32)$$

Therefore, by substituting $D_\mu \Phi = D_\mu \langle \Phi \rangle + D_\mu \Phi'$ into Equation (1.2.14), we realise that these gauge bosons acquire a mass, given as:

$$\begin{aligned} (D_\mu \langle \Phi \rangle)^\dagger (D^\mu \langle \Phi \rangle) &= \frac{v^2}{8} [2g^2 W_\mu^- W^{+\mu} + (g^2 + g'^2) Z_\mu Z^\mu] \\ &= M_W^2 W_\mu^- W^{+\mu} + \frac{1}{2} M_Z^2 Z_\mu Z^\mu. \end{aligned} \quad (1.2.33)$$

The masses of the W_μ^\pm and Z_μ gauge bosons are given by

$$M_W^2 = \frac{g^2 v^2}{4}, \quad M_Z^2 = (g^2 + g'^2) \frac{v^2}{4}, \quad (1.2.34)$$

where all the other gauge fields associated to the unbroken generators remain massless. We can define an angle $\theta_W \in [0, \pi/2]$, called the Weinberg angle, via

$$\tan \theta_W \equiv \frac{g'}{g}, \quad (1.2.35)$$

such that

$$\cos \theta_W = \frac{g}{\sqrt{g^2 + g'^2}}, \quad \sin \theta_W = \frac{g'}{\sqrt{g^2 + g'^2}}. \quad (1.2.36)$$

The physical bosons observed in interactions are the photon A_μ , W_μ^\pm and Z_μ bosons. Thus the W_μ^\pm bosons are mass eigenstates,

$$W_\mu^\pm = \frac{1}{\sqrt{2}} (W_{1\mu} \mp i W_{2\mu}), \quad (1.2.37)$$

while the W_μ^3 and B_μ mix to give us two physical bosons A_μ and Z_μ ,

$$Z_\mu = \cos \theta_W W_\mu^3 - \sin \theta_W B_\mu \quad \text{and} \quad A_\mu = \sin \theta_W W_\mu^3 + \cos \theta_W B_\mu. \quad (1.2.38)$$

The value of v can be fixed from the measurement of the W mass as follows

$$v = \frac{2M_W}{g} \simeq 246 \text{GeV}. \quad (1.2.39)$$

1.2.3 The fermion masses.

In order to obtain the fermion masses we need to introduce the Yukawa Lagrangian, which is given by

$$\mathcal{L}_{Yukawa} = \lambda_{ij}^U \bar{Q}_{Li} \tilde{\Phi} u_{Rj} + \lambda_{ij}^D \bar{Q}_{Li} \Phi d_{Rj} + \lambda_{ij}^E \bar{L}_{Li} \Phi e_{Rj} + \text{h.c.}, \quad (1.2.40)$$

where $\tilde{\Phi} = i\sigma_2\Phi^\dagger$, here we have included all three SM families through the family indices $i, j = 1, 2, 3$. Accordingly, each of the three Yukawa couplings in Equation (1.2.40) is a 3×3 complex matrix. Therefore, once the Higgs acquires a VEV, all the SM fermions acquire a mass also, and these masses are proportional to their Yukawa couplings. We can rewrite the Higgs field in terms of the unitary gauge, where in this case the Goldstone bosons are removed from the Higgs fields. Therefore

$$\Phi = \begin{pmatrix} 0 \\ \frac{v + \varphi}{\sqrt{2}} \end{pmatrix}, \quad (1.2.41)$$

and hence, the Lagrangian becomes

$$\mathcal{L}_{Yukawa} = \mathcal{L}_{Yukawa}^{Mass} + \mathcal{L}'_\phi, \quad (1.2.42)$$

where the first part in Equation (1.2.42) is given by

$$\mathcal{L}_{Yukawa}^{Mass} = \frac{v}{\sqrt{2}} \lambda_{ij}^U \bar{u}_{iR}^\alpha u_{jL}^\alpha + \frac{v}{\sqrt{2}} \lambda_{ij}^D \bar{d}_{iR}^\alpha d_{jL}^\alpha + \frac{v}{\sqrt{2}} \lambda_{ij}^E \bar{e}_{iR}^\alpha e_{jL}^\alpha + \text{h.c.}, \quad (1.2.43)$$

which gives the fermions masses

$$m_{ij}^U = v\lambda_{ij}^U, \quad m_{ij}^D = v\lambda_{ij}^D, \quad m_{ij}^E = v\lambda_{ij}^E. \quad (1.2.44)$$

While the second term in Equation (1.2.42) shows the Yukawa interaction of the Higgs, φ , with the fermions,

$$\mathcal{L}'_\phi = \frac{\lambda_{ij}^U}{\sqrt{2}} \bar{u}_{iR}^\alpha u_{jL}^\alpha \varphi + \frac{\lambda_{ij}^D}{\sqrt{2}} \bar{d}_{iR}^\alpha d_{jL}^\alpha \varphi + \frac{\lambda_{ij}^E}{\sqrt{2}} \bar{e}_{iR}^\alpha e_{jL}^\alpha \varphi + \text{h.c.} \quad (1.2.45)$$

Thus, these interactions are diagonal in the mass eigenstate basis, which diagonalises λ_{ij}^U , λ_{ij}^D and λ_{ij}^E . Therefore, there are no flavour changing Higgs interactions at the tree level in the SM. Flavour changing interactions are generated at the loop level in the quark sector, due to quark mixing, but not in the lepton sector. The individual lepton matrices are in fact conserved in the SM (in the limit in which neutrinos are massless). Finally, the Higgs squared mass is given by $m_H^2 = \lambda_H v^2$, and is proportional to the electroweak symmetry breaking scale squared, and to the Higgs self-coupling λ_H . While the electroweak scale has long been known from the measurement of the Fermi constant G_F , the Higgs boson has been discovered only relatively recently, and its mass has been measured to be $m_H \simeq (125.5 \pm 0.5)$ GeV [2, 3]. The mass matrices in Equation (1.2.44) are in flavour basis, and not in the mass basis. In order to diagonalise them and define the real mass eigenstates, we introduce unitary matrices which affect, in the quark sector, the interactions containing both quark types with W^\pm . This will lead to a non diagonal term in the Yukawa Lagrangian which ensures couplings between different type of quark generations through the CKM matrix (for more details see section 4.2).

Particles	colour	spin	Q	mass [v]
e, μ , τ	(1)	1/2	-1	$\lambda_{e,\mu,\nu}/\sqrt{2}$
ν_e , ν_μ , ν_τ	(1)	1/2	0	0
u , c , t	(3)	1/2	+2/3	$\lambda_{u,c,t}/\sqrt{2}$
d , s , b	(3)	1/2	-1/3	$\lambda_{d,s,b}/\sqrt{2}$
h	(1)	0	0	$\sqrt{2\lambda}$
W^\pm	(1)	1	± 1	$g/2$
Z	(1)	1	0	$\sqrt{g^2 + g'^2}/2$
A	(1)	1	0	0
G	(8)	1	0	0

Table 1.3: *Summary of the SM particles and their quantum numbers.*

The neutrinos remain massless in the SM [46, 47, 48]:

$$m_{\nu_e} = m_{\nu_\mu} = m_{\nu_\tau} = 0. \quad (1.2.46)$$

The neutrino oscillations suggest that the neutrinos mass difference are measured to be non-zero [49, 50], and the SM thus needs to be extended.

Finally, as a summary, one can write the full renormalisable part of the SM Lagrangian as follows:

$$\begin{aligned} \mathcal{L}_{SM} = & -i\bar{Q}_i D_\mu \gamma^\mu Q_i - i\bar{u}_{iR} D_\mu \gamma^\mu u_{iR} - i\bar{d}_{iR} D_\mu \gamma^\mu d_{iR} - i\bar{L}_i D_\mu \gamma^\mu L_i \\ & - i\bar{e}_{iR} D_\mu \gamma^\mu e_{iR} - \frac{1}{4} W_{\mu\nu}^a W_a^{\mu\nu} - \frac{1}{4} B_{\mu\nu} B^{\mu\nu} - \frac{1}{4} G_a^{\mu\nu} G_{a\mu\nu} \\ & + (\lambda_{ij}^U \bar{Q}_{Li} \tilde{\Phi} u_{Rj} + \lambda_{ij}^D \bar{Q}_{Li} \Phi d_{Rj} + \lambda_{ij}^E \bar{L}_{Li} \Phi e_{Rj} + \text{h.c.}) \\ & - (D_\mu \Phi)^\dagger (D^\mu \Phi) - \lambda (\Phi^\dagger \Phi - v^2/2)^2, \end{aligned} \quad (1.2.47)$$

where $i, j = 1, 2, 3$. We summarise in Table 1.3 the mass eigenstates of the SM, their masses in terms of the VEV, as well as their $SU(3)_C \times U(1)_{\text{em}}$ quantum numbers.

1.3 Some Reasons to go Beyond the SM

The SM has been accepted as the current best description we have, and all the parameters has been measured experimentally, where these tests have been done with extremely high accuracy. Despite all of its successes, the SM is believed to be only an effective low energy theory for numerous reasons, such as:

- (1) **Quantum Gravity and the Dark Matter Puzzle:** The SM describes three out of four fundamental interactions at the quantum level. While gravity is

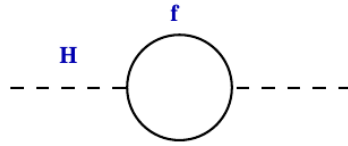


Figure 1.2: *The one-loop Higgs correction with fermions inside the loop.*

only treated classically and therefore, any quantum discussion for gravity has to be contemplated as an effective field theory, which will only be valid up to certain scales, smaller than the Planck scale ($M_{pl} = \sqrt{G\hbar/c^3} \simeq 10^{19} \text{ GeV}$) [51]. At this scale the quantum effects of gravity have to be included, where at this scale the Einstein theory has the problem of being a non-renormalisable theory, and accordingly unable to give us reliable observables beyond this scale. On the other hand, DM, which makes up one quarter of our universe, also has no explanation in the SM, and there are no candidates for DM in the SM [52, 53].

(2) **The Hierarchy Problem (The Naturalness Problem):** Mainly, the hierarchy problem is the question of why there are totally different energy scales; $(M_{ew}/M_{pl}) \simeq 10^{-15} \text{ GeV}$. This problem is also called the naturalness problem, where in this case the radiative corrections to the Higgs mass are quadratically divergent, which calls for “magical” cancellations to stabilise the Higgs mass at its tree level value [53]. In order to understand this problem correctly let us look for an example in the Higgs potential,

$$V(H) = \mu^2 |H|^2 + \lambda |H|^4, \quad \text{where } \mu^2 < 0. \quad (1.3.1)$$

As we know from the experimental point of view, the minimisation of such a potential leads to $\langle H \rangle = \sqrt{-\mu^2/2\lambda}$, and it is around 246 GeV. This means that the bare mass of Higgs is approximately 100 GeV, which implies that $m_H^2 \simeq (100 \text{ GeV})^2$. So we need to look to the radiative corrections, by considering the SM fermions couplings to the Higgs [54]

$$-\mathcal{L}_Y = \lambda_f H \bar{f}_L f_R + \text{h.c..} \quad (1.3.2)$$

By computing the 2-point function, with fermions running inside the loop, and two external lines identified as zero momentum for the Higgs, it can be shown (diagrammatically in Figure 1.2) that

$$\begin{aligned} i\Pi_{HH}^f &= - \int \frac{d^4 p}{(2\pi)^4} \text{Tr} \left[\left(-\frac{i\lambda_f}{\sqrt{2}} \right) \frac{i}{p' - m_f} \left(-\frac{i\lambda_f}{\sqrt{2}} \right) \frac{i}{p' - m_f} \right] \\ &= -2\lambda_f^2 \int \frac{d^4 p}{(2\pi)^4} \left[\frac{1}{p^2 - m_f^2} + \frac{2m_f^2}{(p^2 - m_f^2)^2} \right]. \end{aligned} \quad (1.3.3)$$

Therefore, the one-loop correction to the Higgs mass is given as:

$$\Delta m_H^2 \simeq \frac{\Lambda^2}{16\pi^2} (-2\lambda_f^2), \quad (1.3.4)$$

where in this case Λ is the UV cut-off, and naturally it should be around the TeV scale, because the idea is to protect the Higgs mass. Therefore, the SM should appear as an effective theory valid up to the $E < M_{\text{eff}} \sim \text{TeV}$ scale.

- (3) **The cosmological constant problem:** The cosmological constant problem is the question of why $(\tilde{\Lambda}/M_{pl})^4 \sim 10^{-120} \ll 1$, where $\tilde{\Lambda}$ is called the energy density of free space time, thus, this puzzle is probably the biggest problem in theoretical physics, and it is similar to the hierarchy problem, which is an issue of naturalness [53, 55].
- (4) **Flavour problem:** The flavour problem is the questions of why there are large mass hierarchy of fermion and are not in the same order, note that the electron mass is about 0.511 MeV and the top mass is around 173 GeV [56]. Also the question of why in the SM we have exactly three copies of the fermions [57]. The SM is unable to generate a baryon asymmetry of the Universe of sufficient size, the Universe is baryon-antibaryon asymmetric [58, 59].
- (5) **Gauge coupling unification:** In the SM, aside from the electroweak (EW) scale, there is a new scale of order 10^{15} GeV, called the Grand Unified scale. It arises from the fact that in the SM we have three gauge couplings which run according to the following Renormalisation Group Equations (RGEs) [60]:

$$\frac{1}{\alpha_i(\mu)} \equiv \frac{4\pi}{g_i^2(\mu)} = \frac{b_i}{2\pi} \ln \left(\frac{\mu}{\Lambda_i} \right) \quad i = 1, 2, 3. \quad (1.3.5)$$

Therefore, at the EW scale when $\mu = M_Z$, there is a hierarchy between the couplings

$$\alpha_1(M_Z) < \alpha_2(M_Z) < \alpha_3(M_Z). \quad (1.3.6)$$

The RGEs will make this hierarchy between the gauge couplings, Equation (1.3.6), change with the energy scale. In principle, let us assume there are no particles other than the SM particles, thus at a much higher scale, such as the Grand Unified scale ($M_{\text{GUT}} \sim 10^{15}$ GeV), all the three couplings tend to unify [61]. We have in the SM the numerical coefficients appearing in Equation (1.3.5), and are given by ¹ [62, 63]:

$$b_i = \left(\frac{41}{10}, -\frac{19}{6}, -7 \right), \quad (1.3.7)$$

¹These coefficients are derived in Appendix A.

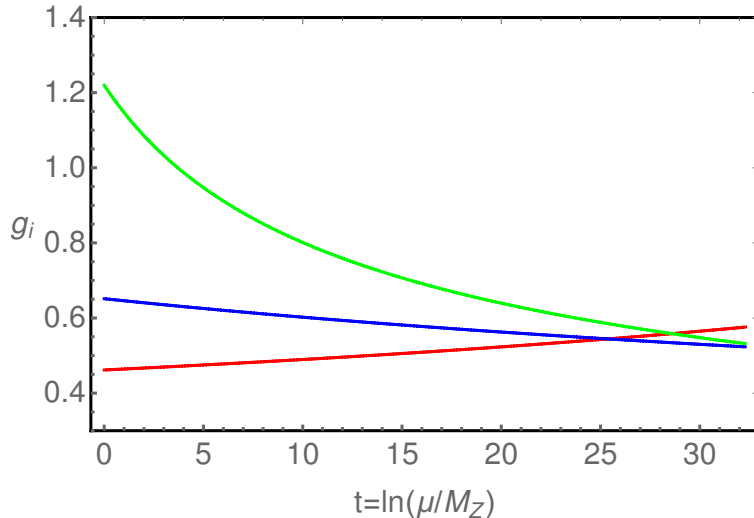


Figure 1.3: *The running of the gauge couplings g_3 (green), g_2 (blue), and g_1 (red) in the SM as a function of a scale parameter t .*

and accordingly, the running of the SM gauge couplings are shown in Figure 1.3, where the couplings g_1 , g_2 and g_3 are corresponding to $U(1)_Y$, $SU(2)_L$ and $SU(3)_C$ gauge groups respectively.

1.4 Some Ideas about Physics Beyond the SM

The SM is not the fundamental theory of the Universe, but is only an effective theory describing the interactions of the strong, weak and electromagnetic interactions at low energies. We need to find an extension that may solve some (or all) of the problems mentioned above in order to generalise the SM. Accordingly, the idea now is to go beyond the SM, and in order to do that there are several approaches we can take. For example [51], one way is by adding new particles, or adding interactions (as we shall do in chapter 7 and chapter 8, where we consider a spin-3/2 fermionic DM interacting with SM fermions through a vector mediator in the s -channel [64], as well as the t -channel [65]).

Another way is motivated from our previous discussion of the SM, in that it is mainly based on two kinds of symmetries. The first one is the internal symmetry, which is the gauge group of the SM, while the other is the space-time symmetry, or the Poincare symmetry in 4 dimensions. The Poincare group is the group which contains rotations and boosts. There are extensions of the 4 dimensional Poincare group, as well as more general internal symmetries [51], such as supersymmetry (SUSY), the most attractive aspect of SUSY is that it provides a solution to the hierarchy

problem due to cancellations between the contributions of bosons and fermions to electroweak scale, defined by the Higgs mass. As an example, for more general internal symmetries, we consider the Grand Unification Theories (GUT), where in this case the SM gauge group is the result of the breaking of a larger symmetry group as follows [53]

$$G_{GUT} \xrightarrow{M \approx 10^{15} \text{ GeV}} G_{SM} \xrightarrow{M \approx 10^2 \text{ GeV}} \text{SU}(3) \times \text{U}(1)_{\text{em}}, \quad (1.4.1)$$

where G_{GUT} is a larger symmetry group and G_{SM} is the SM gauge group.

1.4.1 Extra spacetime dimensions.

The idea here is to add more dimensions to space-time, in which case the Poincare symmetries of the SM, and the general coordinate transformations of general relativity, are significantly enhanced. This leads to the well known KK theories [51, 53].

In order to understand the idea of extra dimensions we shall consider as an example the scalar field scenario in extra dimensions. For a massless 5-dimensional scalar field $\phi(x^\mu, y)$, the action is given as:

$$S_{5D} = \int d^5x \left(\partial^M \phi \partial_M \phi - M^2 \phi^\dagger \phi \right), \quad (1.4.2)$$

where one can presume that the scalar field is a periodic function on this new coordinate (this new coordinate is compactified as a circle of radius R). Therefore, we can expand the field $\phi(x^\mu, y)$ in a Fourier expansion along the new coordinate as

$$\phi(x^\mu, y) = \sum_{n=-\infty}^{\infty} \phi_n(x^\mu) \exp\left(\frac{iny}{R}\right), \quad (1.4.3)$$

where the Fourier coefficients are functions of the standard 4-dimensional coordinates. Therefore, they are a set of 4-dimensional scalar fields. The infinite number of Klein Gordon equations for the massive 4-dimensional fields are then given by

$$\partial^\mu \partial_\mu \phi_n(x^\mu) - \left(M^2 + \frac{n^2}{R^2} \phi_n(x^\mu) \right) = 0, \quad (1.4.4)$$

which means that each Fourier mode ϕ_n is a 4-dimensional particle with mass

$$m_n^2 = M^2 + \frac{n^2}{R^2}, \quad (1.4.5)$$

where R is the compactification radius, the mass eigenstates can be labeled by their parity assignment with respect to the generators of the symmetry group of the orbifold and by the KK numbers (n) [66].

As another example, let us presume the Higgs sector, which is comprised of the following kinetic term, as well as the potential term [66]:

$$\mathcal{L}_H = \int_0^{2\pi R} dy \left[(D_M H(x, y))^\dagger (D^M H(x, y)) - \mathcal{V}(H^\dagger(x, y), H(x, y)) \right]. \quad (1.4.6)$$

Here an even parity, $y \rightarrow -y$, is presumed for the five dimensional Higgs doublet, the one extra spatial dimension coordinate y is compactified on the orbifold S^1/\mathbb{Z}_2 with radius R . Thus the corresponding KK expansion is given as:

$$H(x, y) = \frac{1}{\sqrt{2\pi R}} H^{(0)}(x) + \sum_{n=1}^{\infty} \frac{1}{\sqrt{\pi R}} H^{(n)}(x) \cos\left(\frac{ny}{R}\right). \quad (1.4.7)$$

Therefore, one can expand the covariant derivative as $(D_\mu H)$ and $(D_5 H)$, in terms of the KK modes, and then by integrating out the y coordinate, we can rewrite the kinetic term as:

$$\begin{aligned} \mathcal{L}_{4HK} &= \int_0^{2\pi R} dy \left[(D_M H)^\dagger(x, y) (D^M H)(x, y) \right] \\ &= (D_\mu H)^{(0)\dagger}(x) (D^\mu H)^{(0)}(x) + (D_\mu H)^{(n)\dagger}(x) (D^\mu H)^{(n)}(x) \\ &\quad + (D_5 H)^{(n)\dagger}(x) (D^5 H)^{(n)}(x). \end{aligned} \quad (1.4.8)$$

The repetition of the indices signify a summation. Thus the four dimensional covariant derivative objects $(D_\mu H)^{(0)}$, $(D_\mu H)^{(n)}$ and $(D_5 H)^{(n)}$ are written as follows:

$$\begin{aligned} (D_\mu H)^{(0)} &= D_\mu^{(0)} H^{(0)} - \left(i g \frac{\sigma^a}{2} W_\mu^{(n)a} + i g' \frac{Y}{2} B_\mu^{(n)} \right) H^{(n)}, \\ (D_\mu H)^{(n)} &= D_\mu^{(nm)} H^{(m)} - \left(i g \frac{\sigma^a}{2} W_\mu^{(n)a} + i g' \frac{Y}{2} B_\mu^{(n)} \right) H^{(0)}, \\ (D_5 H)^{(n)} &= D_5^{(nm)} H^{(m)} - \left(i g \frac{\sigma^a}{2} W_5^{(n)a} + i g' \frac{Y}{2} B_5^{(n)} \right) H^{(0)}, \end{aligned} \quad (1.4.9)$$

where $D_\mu^{(0)}$, $D_\mu^{(nm)}$ and $D_5^{(nm)}$ appearing in the above equation are given by:

$$\begin{aligned} D_\mu^{(0)} &= \partial_\mu - i g \frac{\sigma^a}{2} W_\mu^{(0)a} - i g' \frac{Y}{2} B_\mu^{(0)}, \\ D_\mu^{(nm)} &= \delta^{nm} D_\mu^{(0)} - \Delta^{nrm} \left(i g \frac{\sigma^a}{2} W_\mu^{(r)a} + i g' \frac{Y}{2} B_\mu^{(r)} \right), \\ D_5^{(nm)} &= -\delta^{nm} \frac{n}{R} - \Delta'^{nrm} \left(i g \frac{\sigma^a}{2} W_5^{(r)a} + i g' \frac{Y}{2} B_5^{(r)} \right), \end{aligned} \quad (1.4.10)$$

where Δ^{nrm} and Δ'^{nrm} are:

$$\begin{aligned} \Delta^{nrm} &= \frac{1}{\sqrt{2}} (\delta^{r,n+m} + \delta^{n,r+m} + \delta^{m,n+r}), \\ \Delta'^{nrm} &= \frac{1}{\sqrt{2}} (\delta^{r,n+m} + \delta^{n,r+m} - \delta^{m,n+r}). \end{aligned} \quad (1.4.11)$$

The Higgs potential appearing in Equation (1.4.6) is given by:

$$\mathcal{V} = \int_0^{2\pi R} dy \left[\mu^2 H^\dagger(x, y) H(x, y) + \lambda_5 \left(H^\dagger(x, y) H(x, y) \right)^2 \right], \quad (1.4.12)$$

hence, by integrating out the fifth coordinate, we obtain the following:

$$\begin{aligned} \mathcal{V}_{4D} = & \mu^2 \left(H^{(0)\dagger} H^{(0)} \right) + \lambda \left(H^{(0)\dagger} H^{(0)} \right)^2 + \left[\mu^2 + 2\lambda \left(H^{(0)\dagger} H^{(0)} \right) \right] \left(H^{(n)\dagger} H^{(n)} \right) \\ & + \lambda \left(H^{(0)\dagger} H^{(n)} + H^{(n)\dagger} H^{(0)} \right) \left(H^{(0)\dagger} H^{(n)} + H^{(n)\dagger} H^{(0)} \right) \\ & + 2\lambda \Delta^{npq} \left(H^{(0)\dagger} H^{(n)} + H^{(n)\dagger} H^{(0)} \right) \left(H^{(p)\dagger} H^{(q)} \right) \\ & + \lambda \Delta^{npqr} \left(H^{(n)\dagger} H^{(p)} \right) \left(H^{(q)\dagger} H^{(r)} \right), \end{aligned} \quad (1.4.13)$$

where $\lambda = \lambda_5/2\pi R$ and

$$\begin{aligned} \Delta^{npqr} = & \frac{1}{2} \left[\delta^{r,n+p+q} + \delta^{n+p,q+r} + \delta^{n+q,p+r} + \delta^{n+r,p+q} \right. \\ & \left. + \delta^{n,p+q+r} + \delta^{p,n+q+r} + \delta^{q,n+p+r} \right]. \end{aligned} \quad (1.4.14)$$

Finally, let us have a look to the Abelian gauge field Lagrangian, which is given as follows

$$\begin{aligned} \mathcal{L}_{\text{gauge}} = & \int_0^{2\pi R} dy \left[-\frac{1}{4} B_{MN}(x, y) B^{MN}(x, y) - \frac{1}{4} W_{MN}^a(x, y) W_a^{MN}(x, y) \right. \\ & \left. - \frac{1}{4} G_{MN}^A(x, y) G_A^{MN}(x, y) \right], \end{aligned} \quad (1.4.15)$$

where $B_{MN}(x, y)$, $W_{MN}^a(x, y)$ and $G_{MN}^A(x, y)$ are the field strength tensors related to the five dimensional gauge groups $U(1)_Y$, $SU(2)_L$ and $SU(3)_C$ respectively. We presume that the $A_\mu^a(x, y)$, where $(A \equiv G, W, B)$, are the components of the five dimensional gauge fields of even parity $y \rightarrow -y$. Thus the KK decomposition are given by

$$A_\mu^a(x, y) = \frac{1}{\sqrt{2\pi R}} A_\mu^{(0)a}(x) + \sum_{n=1}^{\infty} \frac{1}{\sqrt{\pi R}} A_\mu^{(n)a}(x) \cos \left(\frac{n y}{R} \right), \quad (1.4.16)$$

and therefore, an odd parity is allocated to the A_5^a . A_5^a 's Fourier expansion is

$$A_5^a(x, y) = \sum_{n=1}^{\infty} \frac{1}{\sqrt{\pi R}} A_5^{(n)a}(x) \sin \left(\frac{n y}{R} \right), \quad (1.4.17)$$

and by integrating out the y coordinate, the effective 4 dimensional Lagrangian is

$$\begin{aligned} \mathcal{L}_{\text{gauge}}^{\text{4D}} = & -\frac{1}{4} \left(B_{\mu\nu}^{(0)} B^{(0)\mu\nu} + B_{\mu\nu}^{(n)} B^{(n)\mu\nu} + 2 B_{\mu 5}^{(n)} B^{(n)\mu 5} \right) \\ & -\frac{1}{4} \left(W_{\mu\nu}^{(0)a} W^{(0)a\mu\nu} + W_{\mu\nu}^{(n)a} W^{(n)a\mu\nu} + 2 W_{\mu 5}^{(n)a} W^{(n)a\mu 5} \right) \\ & -\frac{1}{4} \left(G_{\mu\nu}^{(0)A} G^{(0)A\mu\nu} + G_{\mu\nu}^{(n)A} G^{(n)A\mu\nu} + 2 G_{\mu 5}^{(n)A} G^{(n)A\mu 5} \right). \end{aligned} \quad (1.4.18)$$

1.5 Structure of this thesis

The structure of this thesis is as follows: In chapter 2 we shall give a brief summary for the RGEs, the dimensional regularisation scheme, the cross section for the scattering of two particles into a two particle final states, as well as some basic ideas about the Boltzmann equation.

In chapter 3 we introduce the model in five-dimensions, compactified on an interval S^1/\mathbb{Z}_2 , with bulk gauge groups $SU(3)_c \times SU(3)_W$ and a bulk fermion transforming as a bi-fundamental. In chapter 4 we derive the evolution of the Cabibbo-Kobayashi-Maskawa matrix elements, the Jarlskog invariant and the quark mixings in a five-dimensional model for an $SU(3)$ gauge group. In chapter 5 we explore the evolution of the gauge couplings in five dimensions for $SU(5)$ and flipped $SU(5)$, and will extend the discussion in chapter 6 for the G_2 gauge group.

In chapter 7 we consider a spin-3/2 fermionic DM interacting with SM fermions through a vector mediator in the s-channel, and will extend our discussion for the *t*-channel in chapter 8. In chapter 9, we will give our overall conclusions.

Chapter 2

Mathematical Background

In this chapter we shall discuss the mathematical tools, which we will use during this thesis, such as RGEs, dimensional regularisation, the averaged cross-section for scattering, and the Boltzmann equation.

2.1 Renormalisation Group Equations

In this section we are going to introduce the most important object that we need during this thesis: the β -functions. The crucial role of this object is that we need it in order to determine the evolution of the coupling constants. Generally, by considering a theory with n -couplings, g_i , we need to solve a coupled set of differential equations of the following form [67],

$$\beta_i = \mu \frac{dg_i}{d\mu} = \frac{dg_i}{dt}, \quad (2.1.1)$$

where $t = \ln[\mu/M_Z]$. The behaviour of the gauge coupling g_i as a function of μ , as shown in Equation (2.1.1), is called the renormalisation group flow of g_i . In general the β -functions depend on all the couplings and all the masses in the theory. However, we can remove all the masses by focusing only on the universal ultra-violet (UV) relevant coefficients. As an example, one can focus on the Yukawa coupling evolution equations, where in this case we can write the general term for the Yukawa interaction of the fermion and the boson as $\lambda \bar{\psi}_L \psi_R \phi$. Therefore, let us write the terms in this coupling as renormalisable quantities, or by rescaling [68]

$$\psi_R = Z_{\psi_R}^{1/2} \psi_R^R, \quad (2.1.2)$$

$$\psi_L = Z_{\psi_L}^{1/2} \psi_L^R, \quad (2.1.3)$$

$$\phi = Z_\phi^{1/2} \phi^R. \quad (2.1.4)$$

By using Equations (2.1.2), (2.1.3) and (2.1.4) one can rewrite the Yukawa interaction of the fermion and the boson in terms of the renormalisable quantities as follows:

$$\lambda \bar{\psi}_L \psi_R \phi = \lambda^R Z_{\text{coupling}} \bar{\psi}_L^R \psi_R^R \phi^R. \quad (2.1.5)$$

Accordingly, from Equation (2.1.5), we can write this as

$$\lambda = Z_{\text{coupling}} Z_{\psi_L}^{-1/2} Z_{\psi_R}^{-1/2} Z_\phi^{-1/2} \lambda^R. \quad (2.1.6)$$

While the bare parameters are independent of the renormalisation scale μ , we thus have:

$$\mu \frac{\partial \ln \lambda^R}{\partial \mu} = \frac{1}{2} \mu \frac{\partial \ln Z_{\psi_R}}{\partial \mu} + \frac{1}{2} \mu \frac{\partial \ln Z_{\psi_L}}{\partial \mu} + \frac{1}{2} \mu \frac{\partial \ln Z_\phi}{\partial \mu} - \mu \frac{\partial \ln Z_{\text{coupling}}}{\partial \mu}, \quad (2.1.7)$$

where λ^R is the renormalised Yukawa coupling constant. Z_ϕ , Z_{ψ_L} and Z_{ψ_R} are called the wave function renormalisation constants, corresponding to the Higgs boson, left-handed and right-handed fermions respectively. Generally, the wave function renormalisation constants have the following form:

$$Z_{\text{coupling}} = 1 - \frac{\gamma_{\text{wave}}}{2\pi} \ln \left(\frac{\mu}{\mu_0} \right), \quad (2.1.8)$$

where γ_{wave} is the anomalous dimension, and is given as

$$\gamma_{\text{wave}} = \frac{1}{2} \mu \frac{\partial \ln Z_{\text{wave}}}{\partial \mu}. \quad (2.1.9)$$

When we calculate these wave function renormalisation constants, we ignore the mass term in the propagators, since they have nothing to do with the divergent part of the one loop diagrams [69].

2.2 Dimensional Regularisation Scheme

In this section we will mainly discuss the method of dimensional regularisation, where this scheme will be a very important tool in our calculations during this thesis. In QFT there at least three types of divergences: infra-red (IR), UV and collinear; where here we are going to deal only with the UV divergences. The Feynman diagrams involving loops lead to divergent integrals, and in order to handle this type of divergent integral we need to cut them off at some high scale to avoid these UV divergences. This can be done by giving them a finite upper limit. This way of regularising infinite integrals is not very convenient in dealing with theories which have a local symmetry, however, in this thesis we shall use dimensional regularisation, which preserves the local symmetries.

In order to understand the dimensional regularisation scheme let us use an example of the 1-loop 4-point functions. In this scenario the Feynman diagram would have two propagators and one integral, thus the integral is given as [70]

$$J_\Lambda(p^2, m^2) = \int \frac{d^4 k}{(2\pi)^4} \frac{1}{(k^2 - m^2 + i\epsilon)((p - k)^2 - m^2 + i\epsilon)}. \quad (2.2.1)$$

This integral is logarithmically divergent in 4-space-time dimensions, however, it is convergent if the space-time dimension is less than four. Accordingly, we will perform this integration in an arbitrary dimension D , and after obtaining an answer which is dependent on D , we can continue the result analytically to $D = 4$. Therefore, the D -dimensional integral can be written as [71]

$$J_\Lambda(p^2, m^2) = \int \frac{d^D k}{(2\pi)^D} \frac{1}{(k^2 - m^2 + i\epsilon)((p - k)^2 - m^2 + i\epsilon)}. \quad (2.2.2)$$

In order to tackle the above integral, one useful technique developed by Feynman (called Feynman parametrisation), deals with the product of two propagators, A and B , in the denominator, by writing them in one term as follows:

$$\frac{1}{AB} = \int_0^1 dx \frac{1}{[Ax + B(1-x)]^2}. \quad (2.2.3)$$

Therefore, we can rewrite J_Λ in Equation (2.2.1) by using the Feynman parametrisation from Equation (2.2.3), namely,

$$J_\Lambda(p^2, m^2) = \int \frac{d^D k}{(2\pi)^D} \int_0^1 dx \frac{1}{[k^2 + p^2 x(1-x) - m^2 + i\epsilon]^2}. \quad (2.2.4)$$

We can now do the k integral in Minkowski space,

$$k^2 = k_0^2 - \vec{k}^2, \quad (2.2.5)$$

where in this scenario the dimension of \vec{k} is $(D - 1)$, and the dimension of k_0 is one. We can handle the k_0 integration by using Cauchy's residue theorem. However, in this case the poles in the complex plane are located at [71]

$$k_0^2 - \vec{k}^2 + p^2 x(1-x) - m^2 + i\epsilon = 0, \quad (2.2.6)$$

or

$$k_0 = \pm \sqrt{\vec{k}^2 - p^2 x(1-x) + m^2 + i\epsilon}. \quad (2.2.7)$$

If we take the external momentum to be $p^2 > 0$ (time-like), the square root is real, because the $+i\epsilon$ shifts the poles. Hence, by considering the contour in Figure 2.1, and if we used Cauchy's residue theorem, the integral around this closed contour gives us zero, because in this case there is no pole inside this closed contour. If we

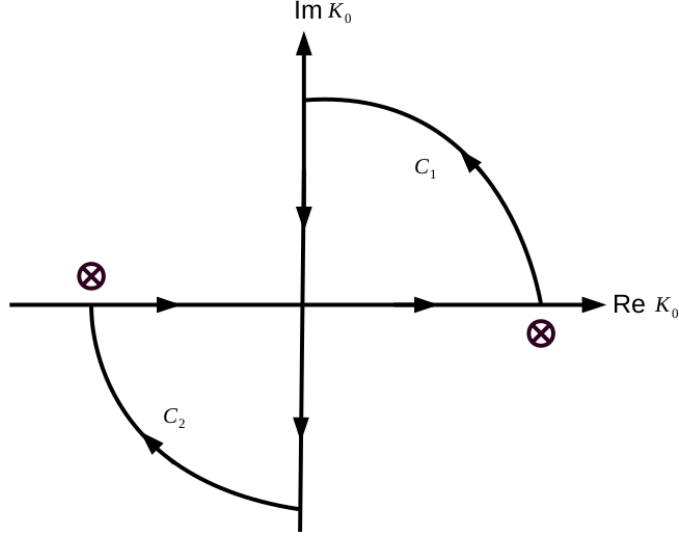


Figure 2.1: The contour we use to handle the integration.

look at the C_1 and C_2 parts, this goes to zero in the limit $R \rightarrow \infty$. From the fact that the total contour integral is zero, this tell us that the integral around the real axis is the same as the one around the imaginary axis. So by using Cauchy's residue theorem one can see [71]

$$\begin{aligned} \int_0^1 dx \int_{-\infty}^{\infty} dk_0 \int \frac{d^{D-1} \vec{k}}{(2\pi)^D} \frac{1}{[k^2 + p^2 x(1-x) - m^2 + i\epsilon]^2} = \\ \int_0^1 dx \int_{-i\infty}^{i\infty} dk_0 \int \frac{d^{D-1} \vec{k}}{(2\pi)^D} \frac{1}{[k^2 + p^2 x(1-x) - m^2 + i\epsilon]^2}. \end{aligned} \quad (2.2.8)$$

We can then change the variable k_0 , by using a Wick rotation $k_0 \rightarrow ik_D$. J_Λ can be written in terms of the Euclidean integral

$$J_\Lambda(p^2, m^2) = \int_0^1 dx \int_{-\infty}^{\infty} dk_D \int \frac{d^{D-1} \vec{k}}{(2\pi)^D} \frac{1}{[k_E^2 + p^2 x(1-x) - m^2]^2}, \quad (2.2.9)$$

where we can now drop the $i\epsilon$. Note that the integration above has rotational symmetry, which can be used to separate the integral into a radial part, as the angular part can be done as follows:

$$J_\Lambda(p^2, m^2) = \int_0^1 dx \int \frac{k^{D-1} dk}{(2\pi)^D} \frac{V_{S^{D-1}}}{[k^2 + p^2 x(1-x) - m^2]^2}, \quad (2.2.10)$$

where $V_{S^{D-1}}$ is the volume of a unit sphere in D-dimensional Euclidean space, and

is given by

$$V_{S^{D-1}} = \frac{2\pi^{D/2}}{\Gamma(D/2)}. \quad (2.2.11)$$

The $\Gamma(D/2)$ is the Gamma function, and is given by:

$$\Gamma(z) = \int_0^\infty dt e^{-t} t^{z-1} \quad \text{Re}(z) > 0, \quad (2.2.12)$$

and has the important property that it can be analytically continued to the complex z -plane. It also has poles at $z = 0$. In the limit when $z \rightarrow 0$, the Gamma-function behaves like:

$$\Gamma(z) = \frac{1}{z} + \text{finite term}. \quad (2.2.13)$$

We can calculate the radial integral in Equation (2.2.10) with the help of the following general formula:

$$\int_0^\infty \frac{u^\delta}{(u+A)^\sigma} du = A^{\delta+1-\sigma} \frac{\Gamma(\delta+1) \Gamma(\sigma-\delta-1)}{\Gamma(\sigma)}. \quad (2.2.14)$$

By using Equation (2.2.14), we can write Equation (2.2.10) as:

$$J_\Lambda(p^2, m^2) = \frac{V_{S^{D-1}}}{2(2\pi)^D} \Gamma\left(\frac{D}{2}\right) \Gamma\left(\frac{4-D}{2}\right) \int_0^1 dx [-x(1-x)p^2 + m^2]^{(D-4)/2}. \quad (2.2.15)$$

We now want to continue the result to $D = 4$. To do this let us take $D - 4 = z$. The Gamma function appearing in $V_{S^{D-1}}$ is finite, even though the $\Gamma(z/2)$ diverges, this divergence from Equation (2.2.13) behaves like

$$\Gamma\left(\frac{z}{2}\right) \xrightarrow{z \rightarrow 0} \frac{2}{z} - \gamma + \mathcal{O}(z), \quad (2.2.16)$$

where the finite term $\gamma = 0.5772\dots$ is called the Euler-Macheroni number. It is now easy to see that as $D \rightarrow 4$ ($z \rightarrow 0$) Equation (2.2.15) reduces to [71]

$$\begin{aligned} J_\Lambda(p^2, m^2) &= \frac{1}{8\pi^2} \frac{1}{z} - \frac{1}{16\pi^2} \int_0^1 dx \ln[-x(1-x)p^2 + m^2] \\ &= \frac{1}{8\pi^2} \frac{1}{z} - \frac{1}{16\pi^2} \int_0^1 dx \left[\ln m^2 + \ln \left(1 - x(1-x) \frac{p^2}{m^2} \right) \right], \end{aligned} \quad (2.2.17)$$

where the term $(1/16\pi^2) \int_0^1 dx \ln m^2$ does not depend on p . This means that:

$$J_\Lambda(p^2, m^2) = \frac{1}{8\pi^2} \frac{1}{z} \frac{1}{16\pi^2} \int_0^1 dx \ln \left[1 - x(1-x) \frac{p^2}{m^2} \right] + \text{constant} + \mathcal{O}(z), \quad (2.2.18)$$

where to evaluate $J_\Lambda(p^2, m^2)$ when $p^2 = 0$ we get

$$J_\Lambda(0, m^2) = \frac{1}{8\pi^2} \frac{1}{z} + \text{constant}. \quad (2.2.19)$$

Equation (2.2.17) can then be written as follows:

$$J_\Lambda(p^2, m^2) - J_\Lambda(0, m^2) = -\frac{1}{16\pi^2} \int_0^1 dx \ln \left[1 - x(1-x) \frac{p^2}{m^2} \right]. \quad (2.2.20)$$

The idea is to determine the finite expression in Equation (2.2.20). Thus we have to subtract a divergent quantity from J_Λ , which is not an unique procedure. For example, we could subtract just the $(1/8\pi^2 z)$ from J_Λ , thus we see that we still obtain a finite result, however this result should be independent of p . The quantity which was subtracted is defined by the scheme we employ, and when we subtract the pole parts only, this renormalisation scheme is called the Minimal Subtraction scheme (MS) [71].

2.3 The RGEs for the Yukawa couplings in the SM

In this section we will discuss the RGEs for the Yukawa couplings in the SM, where the tools introduced here will be used extensively in chapter 3. We will write the most generic formula for the Yukawa evolution equations in the SM, and define the Yukawa coupling matrices to be y_u , y_d and y_e . In the SM they run with momentum according to the following formula [72, 73]:

$$\begin{aligned} 16\pi^2 \frac{dy_u}{dt} &= y_u \left[T - G_u + \frac{3}{2} (y_u^\dagger y_u - y_d^\dagger y_d) \right], \\ 16\pi^2 \frac{dy_d}{dt} &= y_d \left[T - G_d + \frac{3}{2} (y_d^\dagger y_d - y_u^\dagger y_u) \right], \\ 16\pi^2 \frac{dy_e}{dt} &= y_e \left[T - G_e + \frac{3}{2} y_e^\dagger y_e \right]. \end{aligned} \quad (2.3.1)$$

The quantities T , G_u , G_d , and G_e are given as follows:

$$\begin{aligned} T &= \text{Tr} \left[3y_u^\dagger y_u + 3y_d^\dagger y_d + y_e^\dagger y_e \right], \\ G_u &= \frac{17}{12} g_1^2 + \frac{9}{4} g_2^2 + 8 g_3^2, \\ G_d &= \frac{5}{12} g_1^2 + \frac{9}{4} g_2^2 + 8 g_3^2, \\ G_e &= \frac{15}{4} g_1^2 + \frac{9}{4} g_2^2. \end{aligned} \quad (2.3.2)$$

The relation between the y 's couplings appearing in Equations (2.3.1) and (2.3.2) and the couplings in Equation (1.2.40) are give by

$$\begin{aligned} \lambda_{ij}^U &= \text{diag} (y_u, y_c, y_t), \\ \lambda_{ij}^D &= \text{diag} (y_d, y_s, y_b), \\ \lambda_{ij}^E &= \text{diag} (y_e, y_\mu, y_\tau). \end{aligned} \quad (2.3.3)$$

The g_1 , g_2 and g_3 correspond to the $U(1)_Y$, $SU(2)_L$, and $SU(3)_C$ gauge couplings respectively, where the $U(1)_Y$ should be normalised correctly in the $SU(5)$ normalisation. Note that an $SU(5)$ normalisation is required in order to have the couplings, as in the SM, almost tend to unify [74]. This can be done by multiplying the coefficients in front of g_1^2 by factors of $3/5$ [75].

By defining the following variables $M_u = y_u^\dagger y_u$, $M_d = y_d^\dagger y_d$ and $M_e = y_e^\dagger y_e$, and then by multiplying both sides of Equation (2.3.1) by y_u^\dagger , y_d^\dagger and y_e^\dagger respectively, the left hand side becomes

$$\begin{aligned} 16\pi^2 y_u^\dagger \frac{dy_u}{dt} &= y_u^\dagger y_u \left[T - G_u + \frac{3}{2} (y_u^\dagger y_u - y_d^\dagger y_d) \right], \\ 16\pi^2 y_d^\dagger \frac{dy_d}{dt} &= y_d^\dagger y_d \left[T - G_d + \frac{3}{2} (y_d^\dagger y_d - y_u^\dagger y_u) \right], \\ 16\pi^2 y_e^\dagger \frac{dy_e}{dt} &= y_e^\dagger y_e \left[T - G_e + \frac{3}{2} y_e^\dagger y_e \right]. \end{aligned} \quad (2.3.4)$$

By taking the Hermitian conjugate of Equation (2.3.1) and then by multiplying both sides by y_u , y_d and y_e respectively, we get

$$\begin{aligned} 16\pi^2 \frac{dy_u^\dagger}{dt} y_u &= \left[T - G_u + \frac{3}{2} (y_u^\dagger y_u - y_d^\dagger y_d) \right] y_u^\dagger y_u, \\ 16\pi^2 \frac{dy_d^\dagger}{dt} y_d &= \left[T - G_d + \frac{3}{2} (y_d^\dagger y_d - y_u^\dagger y_u) \right] y_d^\dagger y_d, \\ 16\pi^2 \frac{dy_e^\dagger}{dt} y_e &= \left[T - G_e + \frac{3}{2} y_e^\dagger y_e \right] y_e^\dagger y_e. \end{aligned} \quad (2.3.5)$$

Therefore, by adding Equation (2.3.4) to Equation (2.3.5), we get the following formula

$$\begin{aligned} 16\pi^2 \frac{dy_u^\dagger y_u}{dt} &= 2 y_u^\dagger y_u \left[T - G_u + 3 y_u^\dagger y_u \right] - \frac{3}{2} \{y_u^\dagger y_u, y_d^\dagger y_d\}, \\ 16\pi^2 \frac{dy_d^\dagger y_d}{dt} &= 2 y_d^\dagger y_d \left[T - G_d + 3 y_d^\dagger y_d \right] - \frac{3}{2} \{y_d^\dagger y_d, y_u^\dagger y_u\}, \\ 16\pi^2 \frac{dy_e^\dagger y_e}{dt} &= 2 y_e^\dagger y_e \left[T - G_e \right] + 3 (y_e^\dagger y_e)^2. \end{aligned} \quad (2.3.6)$$

And by defining $M_i = y_i^\dagger y_i$,

$$\begin{aligned} 16\pi^2 \frac{dM_u}{dt} &= 2 (T - G_u) M_u + 3 M_u^2 - \frac{3}{2} \{M_u, M_d\} \\ 16\pi^2 \frac{dM_d}{dt} &= 2 (T - G_d) M_d + 3 M_d^2 - \frac{3}{2} \{M_d, M_u\} \\ 16\pi^2 \frac{dM_e}{dt} &= 2 (T - G_e) M_e + 3 M_e^2. \end{aligned} \quad (2.3.7)$$

At some momentum scale, μ , the matrices M_u and M_d can be diagonalised by using

two different unitary matrices U_u and U_d :

$$U_u M_u U_u^\dagger = \text{diag}(\lambda_u^2, \lambda_c^2, \lambda_t^2), \quad (2.3.8)$$

$$U_d M_d U_d^\dagger = \text{diag}(\lambda_d^2, \lambda_s^2, \lambda_b^2). \quad (2.3.9)$$

Accordingly, the CKM matrix at that scale μ will be given as

$$V_{\text{CKM}} = U_u U_d^\dagger. \quad (2.3.10)$$

2.4 The cross-section for scattering of 2-particles into 2-particles

To continue our introduction of tools to be used in coming chapters, we now show how to calculate the averaged cross-section for the scattering of two particles into two particle final states, which is important for our studies in chapters 7 and 8. In what follows we will give the formula for the n -particle Lorentz invariant phase space, and it is defined as follows [76]

$$d\text{Lips}(p_1, p_2, \dots, p_n) \equiv \prod_{i=1}^n \frac{d^3 p_i}{(2\pi)^3 2 E_i}. \quad (2.4.1)$$

Here we have $p_i = (E_i; \vec{p})$ and $E_i = (|\vec{p}|^2 + m_i^2)^{1/2}$, where in this case the corresponding n -particle phase space integral is given as [76]:

$$R_n(s) \equiv \int d\text{Lips}(p_1, p_2, \dots, p_n) (2\pi)^4 \delta \left(p - \sum_i p_i \right). \quad (2.4.2)$$

s is a Lorentz invariant quantity given by $s \equiv p^2$ here, where we now presume the case of two particles scattering to two particles, $A + B \rightarrow a + b$, with four momentum vectors, p_A , p_B , p_a , and p_b respectively. The s above is the well known Mandelstam variable, where we define the following Lorentz invariant variables [77]:

$$\begin{aligned} s &= (p_A + p_B)^2 = (p_a + p_b)^2 \\ t &= (p_A - p_a)^2 = (p_b - p_B)^2 \\ u &= (p_A - p_b)^2 = (p_a - p_B)^2, \end{aligned} \quad (2.4.3)$$

having used the conservation of four-momentum, $p_A + p_B = p_a + p_b$, to define the full-set. These Mandelstam variables can be evaluated in any reference frame, therefore, it will be suitable to work in the centre of mass frame, as in this case we have $\vec{p}_B = -\vec{p}_A$ and $\vec{p}_b = -\vec{p}_a$. Thus, the four momentum of the scattering process are given by the following formulas:

$$p_A = (E_A; \vec{p}_A), \quad p_B = (E_B; -\vec{p}_A), \quad p_a = (E_a; \vec{p}_a), \quad p_b = (E_b; -\vec{p}_a). \quad (2.4.4)$$

It is appropriate to define the magnitudes of the final and initial centre of mass momenta, and they are defined as follows:

$$p_i \equiv |\vec{\mathbf{p}}_A| = |\vec{\mathbf{p}}_B|, \quad p_f \equiv |\vec{\mathbf{p}}_a| = |\vec{\mathbf{p}}_b|. \quad (2.4.5)$$

Therefore the mass shell conditions are given as:

$$E_A = (p_i^2 + m_A^2)^{1/2}, \quad E_B = (p_i^2 + m_B^2)^{1/2}, \quad (2.4.6)$$

and

$$E_a = (p_f^2 + m_a^2)^{1/2}, \quad E_b = (p_f^2 + m_b^2)^{1/2}. \quad (2.4.7)$$

From Equation (2.4.4) we have the following,

$$s = (E_A + E_B)^2, \quad \text{and} \quad t = m_A^2 + m_a^2 - 2 E_A E_a + 2 p_i p_f \cos \theta. \quad (2.4.8)$$

Using momentum and energy conservation, along with the mass shell condition, in order to get the expression for the centre of mass frame energies as well as the three momentum, we arrive at the following formulae [76]:

$$\begin{aligned} E_A &= \frac{s + m_A^2 - m_B^2}{2\sqrt{s}}, & E_B &= \frac{s + m_B^2 - m_A^2}{2\sqrt{s}}, \\ E_a &= \frac{s + m_a^2 - m_b^2}{2\sqrt{s}}, & E_b &= \frac{s + m_b^2 - m_a^2}{2\sqrt{s}}, \end{aligned} \quad (2.4.9)$$

and

$$p_i = \frac{1}{2\sqrt{s}} \lambda^{1/2}(s, m_A^2, m_B^2), \quad p_f = \frac{1}{2\sqrt{s}} \lambda^{1/2}(s, m_a^2, m_b^2). \quad (2.4.10)$$

In the above expressions we have used $\lambda^{1/2}(s, m_A^2, m_B^2)$ and $\lambda^{1/2}(s, m_a^2, m_b^2)$, these are the square root of the triangle function, which is defined as [77]

$$\lambda^{1/2}(x, y, z) = \sqrt{x^2 + y^2 + z^2 - 2xy - 2xz - 2yz}. \quad (2.4.11)$$

We now introduce the total cross section for the scattering of two particles into two particles in the final states:

$$\sigma = \frac{1}{4\sqrt{(p_A \cdot p_B)^2 - m_A^2 m_B^2}} \int d\text{Lips} (2\pi)^4 \delta^4 \left(p_A + p_B - \sum_f p_f \right) \sum_f |\mathcal{M}_{fi}|^2, \quad (2.4.12)$$

where \mathcal{M}_{fi} is the invariant scattering amplitude, and it is summed over all the internal spin degrees of freedom. We shall estimate the spin averaged cross section, via the summing of the squared matrix element over the initial spin states, then dividing by $(2J_A + 1)(2J_B + 1)$. Accordingly

$$\frac{d\sigma}{d\Omega} = \frac{1}{2\lambda^{1/2}(s, m_A^2, m_B^2)} \frac{dR_2(s)}{d\Omega} \frac{1}{(2J_A + 1)(2J_B + 1)} \sum_{i,f} |\mathcal{M}_{fi}|^2, \quad (2.4.13)$$

where $(2 J_A + 1)(2 J_B + 1)$ is the total number of the initial spin states, $\Omega \equiv (\phi, \theta)$ refers to the centre of mass frame. The ϕ and θ refer to the azimuthal and polar angles respectively, where ϕ of particle a in the centre of mass frame corresponds to the rotation around the z -axis. As such the integral over Ω is given as:

$$d\Omega = 2\pi d\cos\theta = \frac{4\pi s}{\lambda^{1/2}(s, m_A^2, m_B^2) \lambda^{1/2}(s, m_a^2, m_b^2)} dt. \quad (2.4.14)$$

Therefore, the formula for the cross-section for the scattering of two particles A and B into a two particles a and b is:

$$\frac{d\sigma}{d\cos\theta} = \frac{1}{2s} \frac{\lambda^{1/2}(s, m_A^2, m_B^2) \lambda^{1/2}(s, m_a^2, m_b^2)}{16\pi\lambda(s, m_A^2, m_B^2)} \frac{1}{(2J_A + 1)(2J_B + 1)} \sum_{i,f} |\mathcal{M}_{fi}|^2. \quad (2.4.15)$$

And,

$$\sigma = \int_{-1}^1 \left(\frac{1}{32\pi s} \frac{\lambda^{1/2}(s, m_a^2, m_b^2)}{\lambda^{1/2}(s, m_A^2, m_B^2)} \frac{1}{(2J_A + 1)(2J_B + 1)} \sum_{i,f} |\mathcal{M}_{fi}|^2 \right) d\cos\theta. \quad (2.4.16)$$

2.5 The Boltzmann equation

The following section based on Ref. [78]. To get the relic density contributions of the DM particles, as in chapters 7 and 8, we will need to solve the Boltzmann equation numerically. Recall that in the early hot Universe the densities of all the particles were produced from a thermal bath, and consequently the densities swiftly drop when the temperature of the expanding Universe decreases. This type of behaviour is described by the Boltzmann equation.

The Boltzmann equation describes the evolution of the phase space distribution of the particles, for instance, let us say we have a particle $\mathcal{A}(\mathbf{p}, \mathbf{x}, t)$, hence the Boltzmann equation is given as:

$$\mathbf{L} [\mathcal{A}] = \mathbf{C} [\mathcal{A}], \quad (2.5.1)$$

where we have the Liouville operator \mathbf{L} as given by:

$$\mathbf{L} = p^\alpha \frac{\partial}{\partial x^\alpha} - \Gamma_{\beta\gamma}^\alpha p^\beta p^\gamma \frac{\partial}{\partial p^\alpha}. \quad (2.5.2)$$

\mathbf{C} is the collision operator, which is described by the interactions which occur between the particles. For simplicity we will assume that the phase space distribution is isotropic and homogeneous, this means that $\mathcal{A}(\mathbf{p}, \mathbf{x}, t) = \mathcal{A}(E, t)$. We can then

consider the metric which describes an isotropic and homogeneous expanding space time called the Roberston-Walker metric,

$$ds^2 = -dt^2 + a(t)^2 g_{\alpha\beta} dx^\alpha dx^\beta \quad \text{for } \alpha, \beta = 0, 1, 2, 3. \quad (2.5.3)$$

In this space we have $a(t)$, which is the scale factor of the Universe, thus, the affine connections (Christoffel symbols) are given by:

$$\Gamma_{\alpha\beta}^\mu = \frac{g^{\mu\nu}}{2} \left[\frac{\partial g_{\alpha\nu}}{\partial x^\beta} + \frac{\partial g_{\beta\nu}}{\partial x^\alpha} - \frac{\partial g_{\alpha\beta}}{\partial x^\nu} \right]. \quad (2.5.4)$$

Accordingly, the Liouville operator acting on \mathcal{A} takes the following simple formula:

$$\mathbf{L}[\mathcal{A}] = E \frac{\partial \mathcal{A}}{\partial t} - H p^2 \frac{\partial \mathcal{A}}{\partial E}. \quad (2.5.5)$$

The Hubble expansion rate in Equation (2.5.5) is given by:

$$H = \frac{\dot{a}(t)}{a(t)}. \quad (2.5.6)$$

By substituting Equation (2.5.5) into (2.5.1), and then multiplying the left-hand side and the right-hand side by $d^3 p / ((2\pi)^3 E)$, followed by integrating with respect to the full phase space, we get

$$\int \frac{d^3 p}{(2\pi)^3} \frac{\partial \mathcal{A}}{\partial t} - H \int \frac{p^2}{E} \frac{\partial \mathcal{A}}{\partial E} \frac{d^3 p}{(2\pi)^3} = \int \frac{\mathbf{C}[\mathcal{A}]}{E} \frac{d^3 p}{(2\pi)^3}. \quad (2.5.7)$$

Here we have the following relation:

$$\frac{\partial E}{\partial p} = \frac{1}{2} \frac{1}{\sqrt{p^2 + m^2}} 2p = \frac{p}{E}, \quad (2.5.8)$$

which we can use to rewrite the second term in Equation (2.5.7) as

$$H \int \frac{p^2}{E} \frac{\partial \mathcal{A}}{\partial E} \frac{d^3 p}{(2\pi)^3} = \frac{H}{(2\pi)^3} \int p \frac{\partial \mathcal{A}}{\partial p} d^3 p. \quad (2.5.9)$$

We can now integrate out the angular parts of the previous integral, by invoking the isotropic and homogeneous properties of the space. This will introduce factors of 4π and p^2 in the integrand. Using integration by parts on Equation (2.5.9), we get:

$$\frac{4\pi H}{(2\pi)^3} \int_0^\infty p^3 \frac{\partial \mathcal{A}}{\partial p} dp = \frac{4\pi H}{(2\pi)^3} \left([p^3 \mathcal{A}]_0^\infty - 3 \int_0^\infty p^2 \mathcal{A} dp \right). \quad (2.5.10)$$

Thus, Equation (2.5.7) can be written as:

$$\frac{dn}{dt} + 3Hn = \int \frac{\mathbf{C}[\mathcal{A}]}{E} \frac{d^3 p}{(2\pi)^3}. \quad (2.5.11)$$

The number density of particles, n is given by

$$n = \frac{g}{(2\pi)^3} \int \mathcal{A}(p) d^3p. \quad (2.5.12)$$

For simplicities sake let us take the following $2 \rightarrow 2$ interaction $A + B \leftrightarrow a + b$, therefore, the collision term for the particle A is given by [79]

$$\begin{aligned} \int \frac{\mathbf{C}[\mathcal{A}]}{E} \frac{d^3p}{(2\pi)^3} = & - \sum_{\text{spin}} \int \left[\mathcal{A}_A \mathcal{A}_B (1 \pm \mathcal{A}_a) (1 \pm \mathcal{A}_b) |\mathcal{M}_{AB \rightarrow ab}|^2 \right. \\ & \left. - \mathcal{A}_a \mathcal{A}_b (1 \pm \mathcal{A}_A) (1 \pm \mathcal{A}_B) |\mathcal{M}_{ab \rightarrow AB}|^2 \right] \\ & \times (2\pi)^4 \delta^4(p_A + p_B - p_a - p_b) d\tau_A d\tau_B d\tau_a d\tau_b, \end{aligned} \quad (2.5.13)$$

where \mathcal{A}_i is the phase-space densities for the particles i , and the phase-space integration factors $d\tau_i \equiv d^3p_i / ((2\pi)^3 2E_i)$.

As we shall apply the Boltzmann equation to studies of DM candidate particles, we can avoid calculating the full Boltzmann equation for the number density as a function of time. As such we shall suppose that some type of interactions keep the DM candidate generally to be in thermal equilibrium with the SM particles, and also the DM will be able to annihilate.

In the early Universe the chemical potentials for the all particles are very small, so they can be neglected, thus the number density in the absence of Bose-Einstein condensation is given by [80]:

$$n_\chi = \frac{g_\chi}{2\pi^2} \int_0^\infty dp \frac{p^2}{\exp\left(\left[\sqrt{p^2 + m_\chi^2}\right]/T\right) \pm 1}. \quad (2.5.14)$$

g_χ is called the number of internal degrees of freedom, T is the temperature, and m_χ the mass of the relic particle. By defining $x \equiv m_\chi/T$ and $\kappa \equiv p/T$, we can write n_χ as:

$$n_\chi = \frac{g_\chi}{2\pi^2} T^3 I_\pm(x), \quad (2.5.15)$$

with

$$I_\pm(x) = \int_0^\infty d\kappa \frac{\kappa^2}{e^{\sqrt{\kappa^2 + x^2}} \pm 1}. \quad (2.5.16)$$

We can use in the following standard integration

$$\int_0^\infty d\xi \frac{\xi^n}{e^\xi - 1} = \zeta(n+1) \Gamma(n+1), \quad (2.5.17)$$

where $\zeta(n)$ is the Riemann Zeta-function. In the relativistic limit we have $m_\chi \ll T$, and in this limit the integration of Equation (2.5.16) is reduced to

$$I_\pm(0) \simeq \int_0^\infty d\kappa \frac{\kappa^2}{e^\kappa \pm 1}. \quad (2.5.18)$$

Accordingly, for the bosons we have $I_{\pm}(0) = 2\zeta(3)$, and for the fermions we have $I_{\pm}(0) = 3\zeta(3)/4$. Thus, we get

$$n_{\chi} = \frac{\zeta(3)}{\pi^2} g_{\chi} T^2 \begin{cases} 3/4 & \text{fermions} \\ 1 & \text{bosons} \end{cases} \quad (2.5.19)$$

On the other hand, in the limit $m_{\chi} \gg T$, we have a similar integration formula for both the fermions as well as the bosons, and in this limit the integration in Equation (2.5.16) reduces to

$$I_{\pm}(x) \simeq \int_0^{\infty} d\kappa \frac{\kappa^2}{e^{\sqrt{\kappa^2 + x^2}}}. \quad (2.5.20)$$

We can then perform a Taylor expansion for the square root in the denominator $(\sqrt{\kappa^2 + x^2})$, to lowest order in κ . We can use the Taylor expansion to write Equation (2.5.20) as:

$$\begin{aligned} I_{\pm}(x) &\simeq \int_0^{\infty} d\kappa \frac{\kappa^2}{e^{x + \kappa^2/(2x)}} = e^{-x} \int_0^{\infty} d\kappa \kappa^2 e^{-\kappa^2/2x} \\ &= (2x)^{3/2} e^{-x} \int_0^{\infty} d\kappa \kappa^2 e^{-\kappa^2}. \end{aligned} \quad (2.5.21)$$

From Equation (2.5.21) we get:

$$I_{\pm} = \sqrt{\frac{\pi}{2}} (x)^{3/2} e^{-x}, \quad (2.5.22)$$

which implies the following formula for the number density:

$$n_{\chi} = g_{\chi} \left(\frac{m_{\chi} T}{2\pi} \right)^{3/2} e^{-m_{\chi}/T}. \quad (2.5.23)$$

The effective number of the relativistic degrees of freedom in the thermal equilibrium case is given by the following expression:

$$g_{*}(T) = \sum_{j=\text{bosons}} g_j + \frac{7}{8} \sum_{k=\text{fermions}} g_k, \quad (2.5.24)$$

$g_{\text{bosons}} = 28$ and $g_{\text{fermions}} = 90$ and hence $g_{*} = 106.75$.

The relic density for the DM candidate χ is defined conventionally to be the ratio of the current DM mass density $\rho_{\chi}(x_0) \equiv m_{\chi} s_0 Y_{\chi}(x_0)$, and the critical density, which is given as $\rho_c \equiv 3H_0^2/8\pi$. s_0 refers to the current values of the entropy and is equal to $2889.2 \text{ cm}^{-3} (T_0/2.725 \text{ K})^3$ [81, 82], $Y_{\chi}(x_0)$ refers to the present relic abundance, and the critical mass density value equal to $1.0537 \times 10^{-5} h^2 \text{ GeV cm}^{-3}$ [82]. More generally the density parameter is defined to be the ratio between the density of the pertinent substance and the critical density, this relevant substance can be matter, DM and dark energy. The distribution of this density parameter is $\Omega_{\Lambda} = 68.3\%$, $\Omega_{\text{DM}} = 26.8\%$ and $\Omega_{\text{M}} = 4.9\%$ for dark energy, DM and matter respectively [83].

Chapter 3

Unification of gauge and Yukawa couplings

In this chapter we shall begin our investigation of GHU models by looking at the situation in five-dimensions, where the extra-dimension is compactified on an interval S^1/\mathbb{Z}_2 , with bulk gauge groups $SU(3)_c \times SU(3)_W$ and a bulk fermion transforming as a bi-fundamental. The content of this chapter is based on our paper Ref. [84]. Our paper [84] was motivated by the discovery of a Higgs boson at the LHC experiments, which opened up a new era in particle physics. Aside from being the last missing particle predicted by the SM, it has allowed a direct probe of the EW symmetry breaking sector of the SM. In particular, the fact that its mass is close to the EW scale itself, has materialised the issue of naturalness. Mass terms for scalar fields are not protected by any quantum symmetry, therefore any new physics sector that couples to it will feed into the value of the mass. In the SM the EW scale seems to be shielded from high energy scales, like the Planck one, however, no reason for this is present in the SM itself. Another intriguing hint for new physics is the approximate unification of gauge couplings, that occurs at high energies once one takes into account the renormalisation group evolution of the couplings. This has lead to the development of GUT. The fact that the mass of the top quark is close to the EW scale also suggests that the Yukawa coupling of the top may have a similar origin.

The proposal of low-scale extra-dimensions [85, 86, 87, 88], mainly supported by string theory constructions, opened new avenues for model building. One of the most interesting ideas is developed in GHU models [89, 90, 91]. Extra-dimensional models, in fact, contain a special class of scalar fields, that arise as an additional

polarisation of vector gauge fields aligned with the extra compact space. If the Higgs can be identified as such a scalar, its couplings with the fermions (the top quark in particular) are also related to the gauge coupling. In addition, mass terms for the Higgs would be forbidden by gauge invariance in the bulk of the extra-dimensions. If the gauge symmetry is suitably broken by boundary conditions, a massless scalar emerges in the spectrum, whose potential is then radiatively generated and finite [92, 93].

The GHU models are rather attractive as they address, at the same time, gauge-Yukawa unification and naturalness. The main challenge is to find a gauge group, \mathcal{G}_{GHU} , that successfully predicts the values of the SM couplings. The requirement that it contains the EW gauge symmetry of the SM, i.e. $SU(2)_L$ and the $U(1)_Y$ of hypercharge, and at the same time broken generators transforming as the Higgs doublet field, strongly limits the possible choices. Most of these possibilities, though, would seem to give incorrect predictions [94]. In this chapter we show that this conclusion is modified once the energy evolution of the couplings is properly taken into account. In fact, as the extra-dimensions are to be considered as an effective theory, the unified predictions are only valid at the cut-off of the theory. However, the experimental values refer to the EW scale, and the couplings may well change due to the running via renormalisation group equations. This fact is well studied and understood in extra-dimensional GUTs [60, 95]. Even though the cut-off of the effective theory may be rather low, the running in extra-dimensions is not logarithmic but follows a power law [60, 96, 97], thus it is much faster than in four dimensions. We will show that, taking into account the running, the tree-level predictions are strongly modified and the low energy values of the SM couplings can match the experimental values, even if starting from completely different tree-level values. For the top Yukawa, the running tends to ease the tension due to the largeness of the top Yukawa at low energy compared to the gauge couplings.

3.1 Minimal SU(3) model with a bulk triplet

We will focus here on the simplest GHU group that allows us to embed both the EW symmetry and the Higgs: $\mathcal{G}_{\text{GHU}} = SU(3)_W$ [98]. This group, of rank 2 like the EW symmetry, contains an $SU(2) \times U(1)$ subgroup that can be identified with the gauged EW one. Furthermore, the remaining 4 broken generators correspond to a doublet of $SU(2)$ with non-vanishing hypercharge, like the Higgs doublet in the SM. Fixing the hypercharge of the doublet fixes the relation between the $SU(2)$ and $U(1)$ couplings. Finally, a fermion field in the fundamental representation decomposes into a doublet

	$SU(2)_L$ g	$U(1)_Y$ g'	Yuk. y	$SU(3)_c$ g_s
SU(3) GHU	g_{GHU}	$\sqrt{3} g_{\text{GHU}}$	$g_{\text{GHU}}/\sqrt{2}$	-
SM	0.66	0.35	1.0	1.2

Table 3.1: *Gauge and Yukawa couplings in the $SU(3)$ GHU model compared to the SM values at the M_Z scale (for the Yukawa we use the top as a reference even though in this toy model the Yukawa corresponds to a down-type quark). We also include for completeness the QCD coupling.*

and singlet of the $SU(2)$: once the hypercharge of the Higgs candidate is fixed, the hypercharges of the doublet and singlet matches those of the left-handed quarks and the right-handed down-type ones. While we would like to describe the top quark as a bulk field, we will consider this simple model as a toy to test our idea. Note that other possible gauge groups which may satisfy these requirements will be explored in the next three chapters.

We also want to check if the running can enhance the Yukawa coupling at low energies with respect to the unified value. Note that other SM fermions can be added as localised degrees of freedom [94, 98], however, their couplings to the bulk Higgs will be suppressed, thus explaining fermion masses below the EW scale. The $SU(3)$ predictions for the gauge and Yukawa couplings, in terms of the unified coupling g_{GHU} , are shown in Table 3.1, together with the SM values of the couplings at the EW scale (i.e. M_Z). For the Yukawa we consider the top Yukawa as our benchmark value because it is the largest one. It is clear that the tree-level GHU predictions are different from the SM values, however, they only apply at the cut-off of the effective theory, which may be very far from the EW scale. We show that the running will strongly modify the predictions.

We thus study the running effects in a concrete model based on a single extra-dimension compactified on an interval S^1/\mathbb{Z}_2 . The boundary conditions at the two end points of the interval, $x_5 = 0$ and $x_5 = \pi R$ (where R is the radius of the extra-dimension), are such that the GHU group is broken to the EW one. The spectrum will thus contain massless gauge bosons plus a massless scalar associated to the broken generators. Furthermore, the bulk fermion transforming as the fundamental of $SU(3)_W$ is assigned boundary conditions such that only two massless fermions appear and we identify them with the third generation quark doublet and down-type singlet (the missing SM fermions are assumed to be localised). At low energy, therefore, the field content matches that of the SM. The running of the couplings

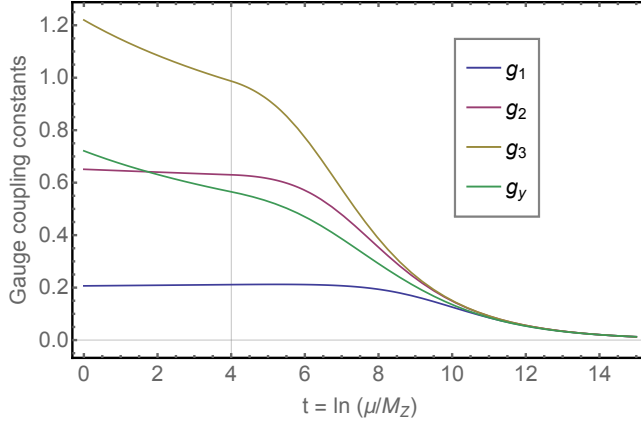


Figure 3.1: *Running of the normalised gauge and Yukawa couplings for the SU(3) GHU model, for $1/R = 5$ TeV. The first KK mode enters at $t_{\text{KK}} \sim 4.0$.*

will be affected by the presence of the KK states once the mass thresholds are met, starting at $m_{\text{KK}} = 1/R$.

In Figure 3.1 we show the running of the couplings as a function of the energy scale μ , normalised to the unified values as in Table 3.1:

$$\{g_1, g_2, g_3, g_y\} = \left\{ \frac{g'}{\sqrt{3}}, g, g_s, \sqrt{2} y \right\}. \quad (3.1.1)$$

Detailed calculations for the running of the couplings can be found in Appendix B. The normalisations simply follow from the group theory structure of the $SU(3)_W$ matrices, while the QCD coupling is, in principle, unrelated. The couplings follow SM evolutions up to the scale where the first KK resonances appear, i.e.

$$t_{\text{KK}} = \ln \frac{1}{M_Z R}. \quad (3.1.2)$$

From there on the running is modified by the extra-dimensions, and it features the expected linear behaviour. The figure clearly shows that the gauge couplings asymptotically tend to the same value.¹ This is more evident from the plot in Figure 3.2, where we show, as a function of the energy, a naive estimate of the 5-dimensional loop factor, obtained by using naive dimensional analysis (NDA) [100, 101]:

$$\alpha_i^{\text{NDA}}(\mu) \sim \frac{g_i^2(\mu)}{8\pi} \mu R. \quad (3.1.3)$$

While all the couplings run asymptotically to zero, their ratio clearly tends to 1. Thus it looks as if the unified value of the gauge couplings is an UV attractor of the one loop running. It may seem surprising that the strong coupling also falls

¹This behaviour for the gauge coupling evolution matches previous results, see for instance Ref. [99].

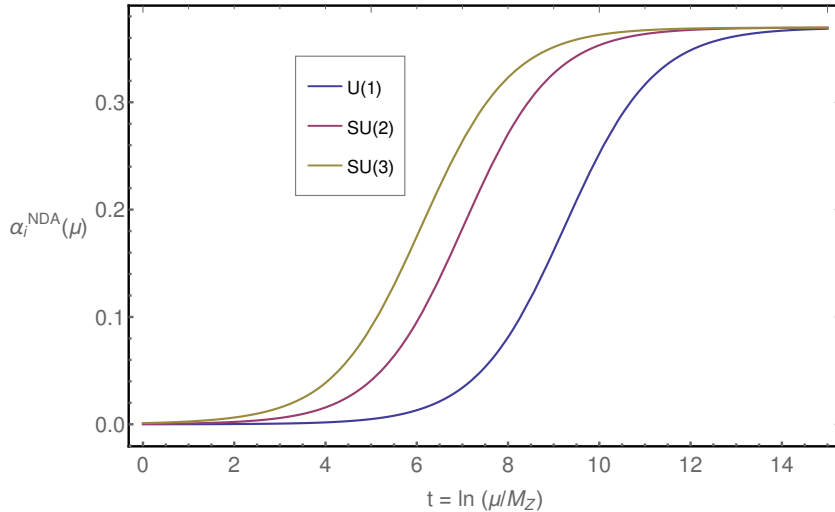


Figure 3.2: 5D NDA loop factor as a function of the energy, for $1/R = 5$ TeV.

very close. However, the GHU model contains two SU(3) gauge structures, one associated to QCD and the other to the EW gauge sector, and the bulk fermion is a bi-fundamental. This allows for the existence of a \mathbb{Z}_2 symmetry between the two sectors at high energy that implies equal couplings. Note, finally, that the NDA loop factor, which can be thought of as a 5D 't Hooft coupling (as μR counts the number of KK tiers below energy μ), can be used as a marker of the energy, where the calculability of the extra-dimensional theory is lost. The fact that the values stay small seems to suggest that the theory under study may have a more extended validity than previously thought.

The initial value of the Yukawa coupling, corresponding to $y(m_Z) = 0.51$, is tuned to achieve unification in the UV. This value depends only mildly on the scale of the extra-dimension $1/R$. It should be noted that the running of the Yukawa coupling does not follow the gauge ones at high energy, due to the fact that the compactification of the extra-dimension clearly singles out the scalar component of the bulk gauge field. However, in the UV, the running needs to be replaced by the running of the 5D gauge coupling. Our results show that the value of the Yukawa coupling at low energy is larger than the values at unification, $y = g_2/\sqrt{2}$, however the enhancement is not enough to explain the Yukawa coupling of the top, $y = 1$. It should be remarked that the value we obtain is a solid prediction of this toy model. Nevertheless two loop corrections, and the embedding of the top in a more realistic model, may further improve the agreement. One possibility is to replace the bulk fermion triplet with a larger representation that can contain a singlet with the correct hypercharge to match the right-handed top: the minimal possibility is to use a 2-index symmetric representation (sextet). The sextet would contain a doublet

and singlet matching the quantum numbers of the SM quarks, plus an SU(2) triplet. Thus, one can define two independent Yukawa couplings. Furthermore, the triplet acquires a mass by marrying to a localised chiral fermion, which is also needed to cancel residual 4-dimensional gauge anomalies. We also performed the running in this model, following the same prescriptions as before. However, we noticed that the NDA loop factor estimate for the EW gauge couplings run to non-perturbative values well before unification occurs, thus rendering the perturbative running unreliable. This result seems to indicate that only models with small representations of the bulk gauge symmetries can provide useful predictions for the low energy values of the couplings in the model.

3.2 The RGEs for an SU(3) toy model

The renormalisation group equations allow us to resum the leading energy-dependent corrections to any coupling in terms of a differential equation. The solutions are energy-dependent couplings whose values run with the scale at which the physics is probed. While in four dimensions the running is logarithmic, in five dimensional models it becomes linear in the energy. The generic structure of the running of the gauge couplings at one loop level is given by [6]:

$$16\pi^2 \frac{dg_i}{dt} = b_i^{\text{SM}} g_i^3 + (S(t) - 1) b_i^{\text{GHU}} g_i^3, \quad (3.2.1)$$

where $t = \ln(\mu/M_Z)$ and contains the energy scale parameter μ . We chose to use the Z mass as a reference scale, so that for $\mu = M_Z$ we have $t = 0$ and we can fix the initial conditions of the running. The coefficients b_i^{SM} and b_i^{GHU} can be computed once the field content of the model is specified: the former are equal to the values in the SM, while the latter include the effects of the KK modes in the bulk of the extra-dimension. This effect only starts contributing above the mass of the first mode, equal to the inverse radius $m_{\text{KK}} = 1/R$. The function $S(t)$, defined as

$$S(t) = \begin{cases} \mu R = M_Z R e^t & \text{for } \mu > 1/R, \\ 1 & \text{for } M_Z < \mu < 1/R, \end{cases} \quad (3.2.2)$$

encodes the linear running due to the extra-dimension. This continuum approximation has been tested against the discrete sum over the KK modes, and the results are in excellent agreement. For the SU(3) GHU model the b coefficients for the SM gauge couplings, $g_i = \{g', g, g_s\}$, are

$$b_i^{SM} = \left[\frac{41}{10}, -\frac{19}{6}, -7 \right], \quad b_i^{SU(3)} = \left[-\frac{17}{6}, -\frac{17}{2}, -\frac{17}{2} \right]. \quad (3.2.3)$$

This result can be easily understood: $-17/2$ is the beta function of the unified SU(3) model (recall that $b_1^{SU(3)}$ has an additional normalisation of $1/3$), and the result matches the fact that each KK tier contains a complete representation of SU(3). For the hypercharge running the normalisation factor has been taken into account.

Similarly, the general form of the running of the one loop β -function for the Yukawa coupling y can be written as [102]:

$$16\pi^2 \frac{dy}{dt} = \beta_y^{SM} + (S(t) - 1) \beta_y^{GHU}, \quad (3.2.4)$$

where

$$\beta_y = y \left[c_y y^2 + \sum_i d_i g_i^2 \right]. \quad (3.2.5)$$

Computing the coefficients for the Yukawa running is not as straightforward as for the gauge ones: already at one loop, vertices involving different KK modes contribute. Thus to simplify the calculation, we assigned the SM values to the new couplings. Note though that the choice needs to be done in a consistent way. As such, we decided on the following policy: for couplings between bosons, we always associate the coupling to a gauge one, while couplings to fermions depend on the quantum numbers of the boson (thus for doublets we associate the coupling to the Yukawa)². We also checked that the numerical results do not depend crucially on this choice³. For the model under study the coefficients assume the following values

$$c_y^{SM} = \frac{9}{2}, \quad c_y^{SU(3)} = \frac{21}{2}, \quad (3.2.6)$$

and

$$d_i^{SM} = \left[-\frac{5}{12}, -\frac{9}{4}, -8 \right], \quad d_i^{SU(3)} = \left[-\frac{35}{24}, -\frac{39}{8}, -4 \right]. \quad (3.2.7)$$

It is interesting to notice that imposing the unification relations between the EW couplings and the Yukawa, compare to Table 3.1, one would obtain a beta function of

$$\frac{1}{2}c_y^{SU(3)} + 3d_1^{SU(3)} + d_2^{SU(3)} = -4, \quad (3.2.8)$$

which is the same value of $d_3^{SU(3)}$ for the QCD contribution. Thus, the running of the scalar coupling, even in the unification regime, is different from the running of the vector couplings. This is due to the intrinsic violation of 5D gauge invariance encoded in the compactification of the extra-dimension.

²Note that for larger bulk representations this is the only physically meaningful choice. For instance, in the case of a sextet, two Yukawa couplings can be identified that run differently from each other.

³The detail of the calculation appear in Appendix B and Appendix C.

The evolution equations for the gauge couplings can be solved analytically as, at one loop level, they are not coupled. On the other hand, the Yukawa coupling is related to the gauge couplings, therefore we have performed a numerical calculation, whose results are given in Figure 3.1.

3.3 The naive dimensional analysis and asymptotic behaviour

The asymptotic behaviour of the running of the gauge couplings can be easily understood when rewriting Equation (3.2.1) in terms of α^{NDA} (as defined in Equation (3.1.3))

$$\frac{d\alpha^{\text{NDA}}}{dt} = \alpha^{\text{NDA}} + \frac{b^{\text{SU}(3)}}{\pi}(\alpha^{\text{NDA}})^2, \quad (3.3.1)$$

where we only retain the term proportional to $S(t)$ that grows with energy. As such, for negative b , the above equation allows for an UV fixed point, where the coupling stops running, that is

$$\alpha^{\text{NDA}}|_{\text{UV}} = -\frac{\pi}{b^{\text{SU}(3)}} = \frac{2\pi}{17}. \quad (3.3.2)$$

The value above matches the numerical value we found in Figure 3.2 and, as discussed earlier, it remains perturbative. We also estimated the two loop contribution which adds to Equation (3.3.1) the following term

$$+ \frac{b_{\text{2loop}}^{\text{SU}(3)}}{2\pi^2}(\alpha^{\text{NDA}})^3, \quad (3.3.3)$$

with $b_{\text{2loop}}^{\text{SU}(3)} = -44$. The zero of the beta function is marginally corrected and now appears at $\alpha^{\text{NDA}}|_{\text{UV}} \sim 0.3$. This confirms that the perturbative expansion is well behaved. The presence of an UV fixed point is less certain, as there are non-perturbative indications against its presence [103, 104].

3.4 Results and Discussions

Our results show that the running cannot be neglected and is crucial to test the feasibility of gauge-Higgs-Yukawa unification in extra-dimensions. We have performed a one loop calculation within the approximation of neglecting the finite parts of the loops. The result can be improved by including the finite contributions, that may also depend linearly on the energy [105] and thus be non-negligible. For increased accuracy the two loop running may also be computed. For the purpose of this chapter, the accuracy we achieved at one loop is sufficient to enforce our conclusions.

Note that the effect of the running on the Yukawa coupling applies to any GHU model and we expect qualitatively similar results to apply, i.e. an enhancement of the Yukawa coupling at low energy. Thus the predictions of realistic models, such as the ones in Refs. [106, 107, 108], will be affected by these running effects, in particular for the Yukawa couplings. The unification of the couplings should occur in any GHU model (as long as the running remains perturbative) as we showed that it is due to an attractor in the UV. The simplicity of this model contrasts previous attempts made in the literature to address the issue of the mismatch between tree-level predictions and the low energy SM values. The value of the gauge couplings can be easily modified by adding an extra gauged $U(1)_X$ in the extra-dimension. The hypercharge is thus identified with a combination of the $U(1)$ contained in the unified group \mathcal{G}_{GHU} and of the new $U(1)_X$, and the gauge coupling g_X can be tuned to the correct value. Additionally, localised kinetic terms [109] for the SM gauge subgroups (that are not broken on the boundaries) also modify the unified relation. The challenge presented by the top Yukawa is more critical. One possibility is to embed the top in an higher dimensional representation in order to gain a group theory factor [110] at the price of lowering the cut-off of the theory. Another possibility is to modify the geometry of the extra-dimension by including a curvature: in such a case, playing with the localisation of the zero mode wave functions, with an enhanced overlap with the Higgs being obtained. The latter mechanism has been used in warped space [111, 112], leading to a revival of composite Higgs models. Properly taking into account the running, maybe none of the above complications would be necessary. Note that obtaining the masses of light fermions is rather easy, as one can use localisation in flat space to suppress the overlap with the Higgs [113], or include light fermions as degrees of freedom localised on the boundaries [98].

To summarise, in this chapter we have introduced the simplest five-dimensional GHU scenario, where we have used the gauge symmetry to be $SU(3)_c \times SU(3)_W$, this is the smallest group that contains $SU(2) \times U(1)$ as a maximal subgroup. We have focused on the EW symmetry and the Higgs, where the gauge boson arises from the 4-dimensional components of the 5-dimensional gauge fields, whilst the Higgs field arise from the internal components of the $SU(3)$ gauge group. We will study in the next chapter the evolution of the quark masses and the flavour mixings in 5D for an $SU(3)$ gauge group which is compactified on an S^1/\mathbb{Z}_2 orbifold, where the RGEs are also derived at one-loop level.

Chapter 4

Evolution of quark masses and flavour mixings in 5D for an $SU(3)$ gauge group

4.1 Model construction

This chapter shall discuss the evolution of the Cabibbo-Kobayashi-Maskawa (CKM) matrix elements, the Jarlskog invariant as well as the quark mixings in a five-dimensional model for an $SU(3)$ gauge group compactified on an S^1/\mathbb{Z}_2 orbifold.¹ Note that this is very similar to the model investigated in chapter 3, with the exception that in this chapter we will assume that the fermion doublet and the two singlets are located at the fixed points of the extra-dimension. As such the quark masses and the flavour mixings are derived at one-loop level [115]. The SM of particle physics is believed to be an effective low energy theory for a number of reasons, where one of these reasons is to try and understand the fermion mass hierarchy and quark mixings. In the SM there is a hierarchy of the quark masses belonging to various generations of the up-type quark masses (m_t, m_c, m_u) and also the down-type quark masses (m_b, m_s, m_d) [116]:

$$m_t \gg m_c \gg m_u, \quad m_b \gg m_s \gg m_d. \quad (4.1.1)$$

In gauge theories, the renormalisable fermion masses come from mass terms such as $\bar{f}Mf$, and also arise from Yukawa terms like $\bar{f}Yf\Phi$. For these Yukawa terms, once the Higgs doublet acquires a VEV, all the SM fermions acquire a mass, where this mass is proportional to their Yukawa couplings [116]:

$$Y_{t,c,u} = \frac{m_{t,c,u}}{v} \quad Y_{b,s,d} = \frac{m_{b,s,d}}{v}. \quad (4.1.2)$$

¹The work of this chapter is based on our published conference proceeding [114].

$Y_{t,c,u}$ and $Y_{b,s,d}$ are the Yukawa coupling eigenvalues, v is the VEV of the Higgs field, where this value can be fixed from the measurement of the W boson mass:

$$v = \frac{2M_W}{g} \simeq 246 \text{GeV}. \quad (4.1.3)$$

In the standard EW model with three quark families, the quark sector contains ten free parameters, six quark masses and also four flavour mixing parameters [117]. In order to look into the dynamics of fermion mass and flavour mixing, we need to extend the SM. We expected that any new physics beyond the SM shall appear above the $M_Z \sim 91.2$ GeV scale. In order to build a mass model of quarks at the high energy scale, one can use the RGEs. We need this technique to fill in the space between the predictions of the model at $\mu \gg M_Z$ and the experimental ones at $\mu \leq M_Z$ [118]. Therefore, we are using these RGEs in order to study the asymptotic behaviour of the Lagrangian parameters, such as Yukawa couplings for both up-type quarks and down-type quarks and also the mixing angles θ_{12} , θ_{13} and θ_{23} [119]. In order to compute the running of quark masses above the M_Z scale we are going to use the quark masses and the mixing parameters, which are obtained at the M_Z scale to determine the Yukawa couplings Y_u and Y_d . After doing this, we need to solve the RGEs of the Yukawa couplings, in order to get the running of the quark masses at any energy scale [118]. In order to diagonalise the quark mass matrices, one can use an unitary matrix as follows [116, 120]:

$$u_L = (U_{u_L})u'_L, \quad u_R^c = (U_{u_R^c})^\dagger u'_R, \quad d_L = (U_{d_L})d'_L, \quad d_R^c = (U_{d_R^c})^\dagger d'_R. \quad (4.1.4)$$

However, this will lead to the following:

$$(U_{u_R^c})^\dagger Y_u (U_{u_L}) = \text{diag}(y_u, y_c, y_t), \quad (4.1.5)$$

$$(U_{d_R^c})^\dagger Y_d (U_{d_L}) = \text{diag}(y_d, y_s, y_b), \quad (4.1.6)$$

or equivalently we can diagonalise the quark mass matrices appearing in the Lagrangian of Yukawa interactions by using the bi-unitary transformation [116, 117]:

$$(U_{u_L})^\dagger M_u (U_{u_R^c}) = \text{diag}(m_u, m_c, m_t), \quad (4.1.7)$$

$$(U_{d_L})^\dagger M_d (U_{d_R^c}) = \text{diag}(m_d, m_s, m_b). \quad (4.1.8)$$

Accordingly, we use this bi-unitary transformation in order to change all our quark fields from their flavour eigenstate basis to the basis of mass eigenstates [117]. Let us assume that we are working in the basis where the Yukawa couplings for the up-type quark Y_u is diagonal, as appears in Equation (4.1.5), then the mass eigenstates of the down-type quarks are connected to their weak eigenstates by the CKM matrix V_{CKM} [118]:

$$V_{CKM}^\dagger Y_d Y_d^\dagger V_{CKM} = \text{diag}(l_d^2, l_s^2, l_b^2). \quad (4.1.9)$$

For the other way around, that is, if we are working in the basis in which the Yukawa couplings for the down-type quarks are diagonal, then the mass eigenstates of the up-type quarks are given by:

$$V_{CKM}^\dagger Y_u Y_u^\dagger V_{CKM} = \text{diag}(k_d^2, k_s^2, k_b^2). \quad (4.1.10)$$

Furthermore, we can build the Yukawa couplings for the down-type quarks from their eigenvalues and also from the CKM matrix [118].

There are many ways to look at the quark mass hierarchy and flavour mixings, we shall investigate an $SU(3)$ gauge group compactified on an S^1/\mathbb{Z}_2 orbifold which has size $R^{-1} = 4$ TeV, 8 TeV and 20 TeV.

4.2 The evolution of CKM matrix in 5 dimension for an $SU(3)$

The SM of particle physics has been very successful in describing most of the particle phenomenology known to date [32], but it possesses some problems whose solution could imply physics beyond the SM. The SM is not like QCD and QED, it is a theory which violates parity (P), time reversal (T) and charge conjugation (C). The C and P separately are not a good symmetry of the SM, but the combination CP, in the case of only one family of matter fields, or even if we have two families, is a good symmetry. Since we have three families in the SM, CP is also not a good symmetry. All of the SM Lagrangian is invariant under CP transformations, except the part where the CKM matrix appears.

In order to study the CKM matrix, let us start with a simple expression $\bar{u}_{iL} \gamma^\mu d_{iL}$ and express it in terms of mass eigenstates, this will be given as

$$\bar{u}_{iL} \gamma^\mu d_{iL} = \bar{u}'_{hL} (U^{uL})_{hi} \gamma^\mu (U^{dL})_{ij}^\dagger d'_{jL} = (U^{uL})_{hi} (U^{dL})_{ij}^\dagger \bar{u}'_{hL} \gamma^\mu d'_{jL}. \quad (4.2.1)$$

Because the above equation the two matrices are different, when we compute the product of two unitary matrices we still get a unitary matrix. This unitary matrix is called the CKM matrix

$$(U^{uL})_{hi} (U^{dL})_{ij}^\dagger \equiv V_{hj}. \quad (4.2.2)$$

In order to parameterise the quark sector's flavour mixing we need the CKM matrix [121]. The CKM matrix can be parameterised in terms of its 9 parameters [122] as:

$$V = \begin{pmatrix} e^{i\tau_1} & 0 & 0 \\ 0 & e^{i\tau_2} & 0 \\ 0 & 0 & e^{i\tau_3} \end{pmatrix} V_{st} \begin{pmatrix} e^{i\sigma_1} & 0 & 0 \\ 0 & e^{i\sigma_2} & 0 \\ 0 & 0 & e^{i\sigma_3} \end{pmatrix}, \quad (4.2.3)$$

where V_{st} is the standard parametrisation and it is given as follows

$$V_{st} = \begin{pmatrix} 1 & 0 & 0 \\ 0 & c_{23} & s_{23} \\ 0 & -s_{23} & c_{23} \end{pmatrix} \begin{pmatrix} c_{13} & 0 & s_{13}e^{i\delta} \\ 0 & 1 & 0 \\ -s_{13}e^{-i\delta} & 0 & c_{13} \end{pmatrix} \begin{pmatrix} c_{12} & s_{12} & 0 \\ -s_{12} & c_{12} & 0 \\ 0 & 0 & 1 \end{pmatrix}, \quad (4.2.4)$$

where $c_{ij} \equiv \cos \theta_{ij}$, and $s_{ij} \equiv \sin \theta_{ij}$ [123]. From the standard parameterisation, which appears in Equation (4.2.4), the CKM matrix has the following form [124]

$$V_{st} = \begin{pmatrix} c_{12}c_{13} & s_{12}c_{13} & s_{13}e^{-i\delta} \\ -s_{12}c_{23} - c_{12}s_{23}s_{13}e^{i\delta} & c_{12}c_{23} - s_{12}s_{23}s_{13}e^{i\delta} & s_{23}c_{13} \\ s_{12}s_{23} - c_{12}c_{23}s_{13}e^{i\delta} & -c_{12}s_{23} - s_{12}c_{23}s_{13}e^{i\delta} & c_{23}c_{13} \end{pmatrix}. \quad (4.2.5)$$

Thus, from the experimental point of view, we know the following relationship

$$\sin \theta_{13} \ll \sin \theta_{23} \ll \sin \theta_{12} \ll 1, \quad (4.2.6)$$

and we can express this hierarchy using the Wolfenstein parametrisation [125]:

$$\sin \theta_{23} = \frac{|V_{cb}|}{\sqrt{|V_{ud}|^2 + |V_{us}|^2}}, \quad (4.2.7)$$

and

$$\sin \theta_{12} = \frac{|V_{us}|}{\sqrt{|V_{ud}|^2 + |V_{us}|^2}}. \quad (4.2.8)$$

The RGEs for the CKM matrix beyond the R^{-1} scale is given as [126]:

$$16\pi^2 \frac{dV_{i\gamma}}{dt} = 12S(t) \left[\sum_{\sigma, j \neq i} \frac{k_i^2 + k_j^2}{k_i^2 - k_j^2} l_\sigma^2 V_{i\sigma} V_{j\sigma}^* V_{j\gamma} + \sum_{j, \sigma \neq \gamma} \frac{l_\gamma^2 + l_\sigma^2}{l_\gamma^2 - l_\sigma^2} k_j^2 V_{j\sigma}^* V_{j\gamma} V_{i\sigma} \right], \quad (4.2.9)$$

where the energy scale parameter $t = \ln(\mu/M_Z)$ and $S(t) = M_Z R e^t$, and as we mentioned earlier, our renormalisation point is the Z boson mass. Furthermore, we can introduce the Jarlskog re-phasing invariant parameter J , which is a crucial object in measuring the CP violation, and it is given through the unitarity properties of V_{CKM} , as follows [117]:

$$\text{Im}(V_{k\alpha} V_{l\beta} V_{k\beta}^* V_{l\alpha}^*) = J \sum_{m, \delta} (\varepsilon_{klm} \varepsilon_{\alpha\beta\delta}), \quad (4.2.10)$$

where the subscript (k, l or m) runs over the (u, c, t) quarks and the subscript (α, β or δ) runs over the (d, s, b) quarks. In particular, in this chapter we are using the following J to present the CP violation phenomena:

$$J = \text{Im}(V_{cs} V_{tb} V_{cb}^* V_{tb}^*). \quad (4.2.11)$$

Therefore, one can write its square as:

$$J^2 = |V_{tb}|^2 |V_{cs}|^2 |V_{ts}|^2 |V_{cb}|^2 - \frac{1}{4} \left(1 - |V_{tb}|^2 - |V_{cs}|^2 - |V_{ts}|^2 - |V_{cb}|^2 + |V_{tb}|^2 |V_{cs}|^2 + |V_{ts}|^2 |V_{cb}|^2 \right). \quad (4.2.12)$$

We can then define the RGE invariant quantity in the hierarchical limit $m_b \gg m_s$ as follows [127]:

$$R_{23} = \sin(2\theta_{23}) \sinh \left[\ln \left(\frac{m_b}{m_s} \right) \right] \Rightarrow R_{23} = \sin \theta_{23} \cos \theta_{23} \left(\frac{m_b}{m_s} \right). \quad (4.2.13)$$

4.3 Numerical Results

In Figure 4.1 we present the evolution of the mass ratio for the one-loop calculation for three different compactification scales: $R^{-1} = 4$ TeV, 8 TeV and 20 TeV. We expect new physics to come into play when we reach our cut-off, where the cut-off for our effective theory is when $t = 4.1, 4.4, 4.9$ for $R^{-1} = 4$ TeV, 8 TeV, 20 TeV respectively. In the left panel we present the evolution of m_u/m_t , in this case one can see that the SM (the black line) behaves like λ^8 , where $\lambda \sim 0.22$. Through the numerical analysis of the one-loop calculation, we observe that when the fifth dimension contributions switch on, the mass ratio m_u/m_t decreases whenever the energy increases, and this creates a significant change of order of λ^8 . In the right panel we are showing the evolution of m_c/m_t , in this case we see that the SM behaves like λ^4 , and when the fifth dimension KK-modes become kinematically accessible the mass ratio m_c/m_t decreases with increasing energy, and in this case the change is of the order of λ^4 .

In Figure 4.2 we plot the evolution of the CKM parameters, in the left panel we plot $|V_{cb}|$ and in the right panel $|V_{ts}|$. We see that once the fifth dimension contributions switch on, one can see that there are new contributions coming from the fifth dimension. Accordingly the evolution of the CKM parameters $|V_{cb}|$ and $|V_{ts}|$ are rapidly increasing, this significant increase is of order of λ^2 .

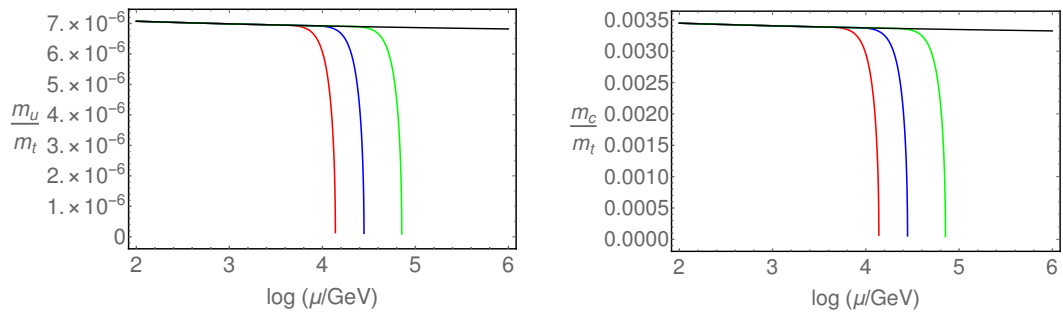


Figure 4.1: *Evolution of the mass ratio for three different values of the compactification radius we have used: 4 TeV (red line), 8 TeV (blue line), 20 TeV (green line); as a function of the scale parameter t . In the left panel is the evolution of the mass ratio m_u/m_t , and the right panel is the evolution of the mass ratio m_c/m_t .*

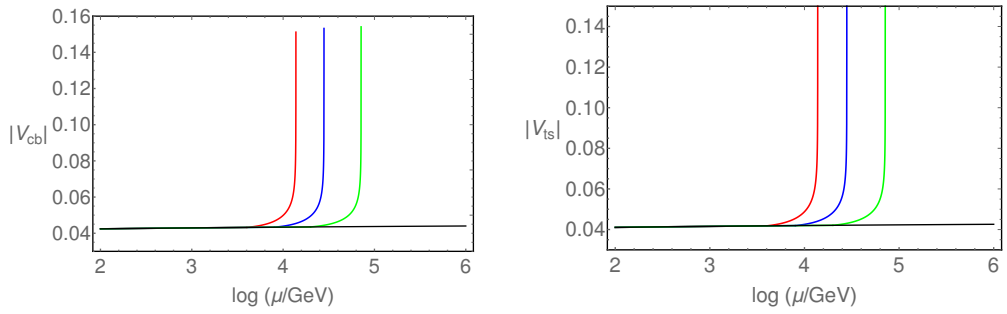


Figure 4.2: *The evolution of the CKM elements for three different values of the compactification radius we have used: 4 TeV (red line), 8 TeV (blue line), 20 TeV (green line); as a function of the scale parameter t . In the left panel is the evolution of the CKM element $|V_{cb}|$, and the right panel is the evolution of CKM element $|V_{ts}|$.*

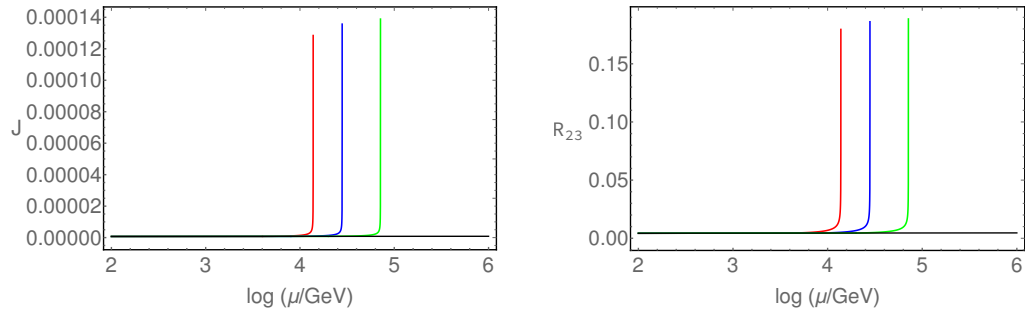


Figure 4.3: *In the left panel is the evolution of the Jarlskog re-phasing-invariant parameter; the right panel is the evolution of R_{23} , for three different values of the compactification radius: 4 TeV (red line), 8 TeV (blue line) and 20 TeV (green line); as a function of the scale parameter t .*

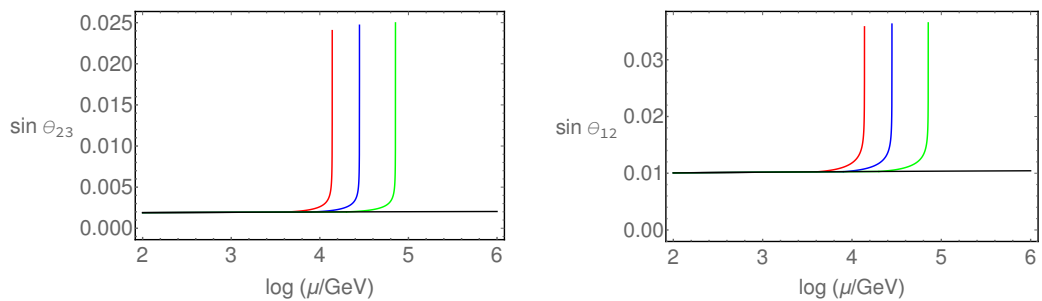


Figure 4.4: *Left panel is the evolution of $\sin \theta_{23}$; the right panel is the evolution of $\sin \theta_{12}$, for three different values of the compactification radius: 4 TeV (red line), 8 TeV (blue line), 20 TeV (green line), as a function of the scale parameter t .*

In Figure 4.3, left panel, we plot the Jarlskog invariant parameter. As we mentioned earlier, this gives us a good indication of the amount of CP violation in the quark sector. As can be seen, once the fifth dimension contributions are reached, the value of Jarlskog invariant increases sharply until we reach the cut-off. In the right panel we present the evolution of the renormalisation invariant R_{23} , where this quantity describes the relationship between the mixing angles ($\sin \theta_{23}$ and $\cos \theta_{23}$) and the mass ratio (m_b/m_s) as it appears in Equation (4.2.13). This renormalisation invariant quantity starts to increase rapidly when the fifth dimension contributions switch one, therefore, this rapid increase causes increases in the mixing angles, which is suppressed by the mass ratio m_b/m_s . Similarly, in Figure 4.4, in the left panel, we present the evolution of the mixing angle $\sin \theta_{23}$, and in the right panel we plot the evolution of the mixing angle $\sin \theta_{12}$, where in this case after, the fifth dimension is switched on, the mixing angles $\sin \theta_{23}$ and $\sin \theta_{12}$ increase rapidly. However, this increase is suppressed by $|V_{cb}|$ and $|V_{us}|$ respectively, as is shown in Equation (4.2.7) and Equation (4.2.8).

The discussion in this chapter related to the evolution of the mass ratio (only some selected mass ratio plots have been shown), the evolution of the CKM elements (such as $|V_{cb}|$ and $|V_{ts}|$), the evolution of the Jarlskog re-phasing invariant parameter, the evolution of R_{23} as well as the evolution of $\sin \theta_{23}$ and $\sin \theta_{12}$. We note that when the fifth dimension KK-modes switch on, all the above mentioned parameters increased rapidly until we reach the cut-off. Up to this point we have only consider an SU(3) GHU model (with and without additional fermions), we shall now extend this to include different bulk gauge groups. As such, in the next chapter we qualitatively discuss the evolution of the gauge couplings in 5D for an SU(5) as well as the flipped SU(5) groups.

Chapter 5

Evolution of the gauge couplings and Weinberg angle in 5D for an $SU(5)$ and flipped $SU(5)$ gauge group

In this chapter we extend upon the works of chapters 3 and 4, by now considering a simplified 5-dimensional model with a $SU(5)$ and $SU(5) \times U(1)'$ gauge symmetry. We will only look at the evolution of the gauge couplings, where in this scenario the gauge couplings evolution will be derived at one-loop level and will be used to test the impact on lower energy observables, in particular the Weinberg angle.¹ The idea of GUTs is to embed the SM gauge group ($G_{SM} \equiv SU(3)_C \times SU(2)_L \times U(1)_Y$) into a large group G , where as we know the SM group is rank 4, which means that the gauge group G must be at least rank 4. In this chapter we shall study the non-supersymmetric extensions of the SM based on the gauge group $SU(5)$ and flipped $SU(5)$. In particular, we will study higher-dimensional non-supersymmetric orbifold models [94]. By considering orbifolds based on Abelian discrete groups which lead to a 5-dimensional gauge theory compactified on an S^1/\mathbb{Z}_2 , we will assume that all matter fields are propagating in the bulk. The extra dimension is compactified on a circle of radius R with \mathbb{Z}_2 orbifold, therefore, the 5-dimensional KK modes of the weak doublet (Q) and the singlet (q), as well as the gauge fields (A), are given by [129, 130]:

$$Q(x, y) = \frac{1}{\sqrt{2\pi R}} Q_L^0(x) + \frac{1}{2\sqrt{\pi R}} \sum_{n=1}^{\infty} \left[Q_L^n(x) \cos\left(\frac{ny}{R}\right) + Q_R^n(x) \sin\left(\frac{ny}{R}\right) \right], \quad (5.0.1)$$

¹The work of this chapter is based on our published conference proceeding [128].

$$q(x, y) = \frac{1}{\sqrt{2\pi R}} q_R^0(x) + \frac{1}{2\sqrt{\pi R}} \sum_{n=1}^{\infty} \left[q_R^n(x) \cos\left(\frac{ny}{R}\right) + q_L^n(x) \sin\left(\frac{ny}{R}\right) \right], \quad (5.0.2)$$

$$A(x, y) = \frac{1}{\sqrt{2\pi R}} A_0(x) + \frac{1}{2\sqrt{\pi R}} \sum_{n=1}^{\infty} A_n(x) \cos\left(\frac{ny}{R}\right), \quad (5.0.3)$$

where the zero modes are the 4-dimensional SM fields and there is a left- and a right-handed KK mode for each SM chiral fermion, whilst the Higgs and the gauge fields are \mathbb{Z}_2 even fields [129].

The chapter is structured as follows: In section 5.1 we discuss the evolution of the gauge couplings and Weinberg angle in 5-dimensions for an SU(5) gauge group, whilst in section 5.2 we discuss the evolution of the gauge couplings and Weinberg angle in 5-dimensions for an $SU(5) \times U(1)'$ gauge group.

5.1 The gauge coupling evolution equations for an SU(5)

In this section we shall explore the evolution of the gauge couplings and Weinberg angle in five dimensions for an SU(5) gauge group, in order to have a unified theory above some energy scale M_X , with n_g generation of fermions, where we need at least 12 new gauge bosons; an $SU(2)_L$ doublet, colour triplet and their antiparticles, plus an $SU(2)_L$ singlet of the Higgs scalars h_α [131]. We put the electroweak doublet and the colour triplet in the 5-dimensional fundamental representation as follows:

$$5_H = \begin{pmatrix} h^r \\ h^g \\ h^b \\ \Phi^+ \\ \Phi^0 \end{pmatrix}. \quad (5.1.1)$$

$SU(3)_C$ acts on the first 3 components, and $SU(2)_L$ acts on the last two, where the SU(5) gauge group breaks into the SM gauge group, when a scalar field 24_H such as the Higgs field acquires a VEV, and this VEV is proportional to the hypercharge generator [131]. The Higgs sector is made up of an adjoint 24_H , which acquires a VEV from the spontaneous breaking $SU(5) \rightarrow SU(3)_C \times SU(2)_W \times U(1)_Y$:

$$\langle 24_H \rangle = \frac{v}{\sqrt{30}} \begin{pmatrix} 2 & 0 & 0 & 0 & 0 \\ 0 & 2 & 0 & 0 & 0 \\ 0 & 0 & 2 & 0 & 0 \\ 0 & 0 & 0 & -3 & 0 \\ 0 & 0 & 0 & 0 & -3 \end{pmatrix}. \quad (5.1.2)$$

Therefore, we can write the full $SU(3)_C \times SU(2)_L \times U(1)_Y$ right handed representation of the creation operators as follows [132]:

$$\begin{aligned} u^\dagger \oplus d^\dagger \oplus e^\dagger \oplus \bar{Q}^\dagger \oplus \bar{l}^\dagger &= (3, 1, 2/3) \oplus (3, 1, -1/3) \oplus (1, 1, -1) \\ &\oplus (\bar{3}, 2, -1/6) \oplus (1, 2, 1/2). \end{aligned} \quad (5.1.3)$$

The new gauge bosons are called X and Y and they violate baryon and lepton number and carry flavour and colour. The gauge bosons are given by the adjoint representation of the $SU(5)$ gauge group:

$$24 \rightarrow (8, 1, 0) \oplus (1, 3, 0) \oplus (1, 1, 0) \oplus (3, 2, -5/6) \oplus (\bar{3}, 2, 5/6), \quad (5.1.4)$$

where $(8,1,0)$ is identified as the $SU(3)_C$ gauge bosons G_β^α , $(1,3,0)$ is identified as the W^\pm and W^0 gauge bosons, $(1,1,0)$ is identified as the B gauge boson, $(3,2,-5/6)$ is identified as the $A_\alpha^\tau = (X_\alpha, Y_\alpha)$ gauge boson and $(\bar{3},2,5/6)$ is identified as the $A_\beta^\alpha = (X_\alpha, Y_\alpha)^T$ gauge boson. Therefore, the covariant derivative for a fundamental representation is given by the following formula

$$D_\mu = \partial_\mu - ig \sum_{a=1}^{24} \frac{\lambda_a}{2} A_\mu^a \equiv \partial_\mu - ig \mathcal{A}_\mu, \quad (5.1.5)$$

and the matrix of the gauge bosons becomes

$$\mathcal{A}_\mu = \frac{1}{\sqrt{2}} \begin{pmatrix} G_r^r & G_g^r & G_b^r & \bar{X}_r & \bar{Y}_r \\ G_r^g & G_g^g & G_b^g & \bar{X}_g & \bar{Y}_g \\ G_r^b & G_g^b & G_b^b & \bar{X}_g & \bar{Y}_g \\ X^r & X^g & X^b & \frac{W_3}{\sqrt{2}} & W^+ \\ Y^r & Y^g & Y^b & W^- & -\frac{W_3}{\sqrt{2}} \end{pmatrix} + \sqrt{\frac{3}{5}} \begin{pmatrix} -\frac{B_\mu}{3} & 0 & 0 & 0 & 0 \\ 0 & -\frac{B_\mu}{3} & 0 & 0 & 0 \\ 0 & 0 & \frac{B_\mu}{2} & 0 & 0 \\ 0 & 0 & 0 & \frac{B_\mu}{2} & 0 \\ 0 & 0 & 0 & 0 & \frac{B_\mu}{2} \end{pmatrix}. \quad (5.1.6)$$

The new gauge bosons X and Y are clearly carrying colour, and they have electric charge $4/3$ and $1/3$ respectively. The one-loop beta functions for the gauge couplings in 4-dimensions for $SU(5)$ are given by:

$$16\pi^2 g_1^{-3} \beta_{g_1} = \frac{81}{20}, \quad (5.1.7)$$

$$16\pi^2 g_2^{-3} \beta_{g_2} = -\frac{19}{6}, \quad (5.1.8)$$

$$16\pi^2 g_3^{-3} \beta_{g_3} = -\frac{41}{6}. \quad (5.1.9)$$

While the one-loop beta functions for the gauge couplings in 5-dimension for $SU(5)$ are given by:

$$16\pi^2 g_1^{-3} \beta_{g_1} = (S(t) - 1) \left(\frac{81}{10} \right), \quad (5.1.10)$$

Scenario	$t(R_1)$	$t(R_2)$	$t(R_3)$
5D $SU(5)$	7.51	8.19	8.86

Table 5.1: *Summary the cut-offs in 5 dimensions for an $SU(5)$ gauge group for three different compactification radii $R^{-1} = 5, 10$ and 20 TeV, where $t = \ln(\mu/M_Z)$.*

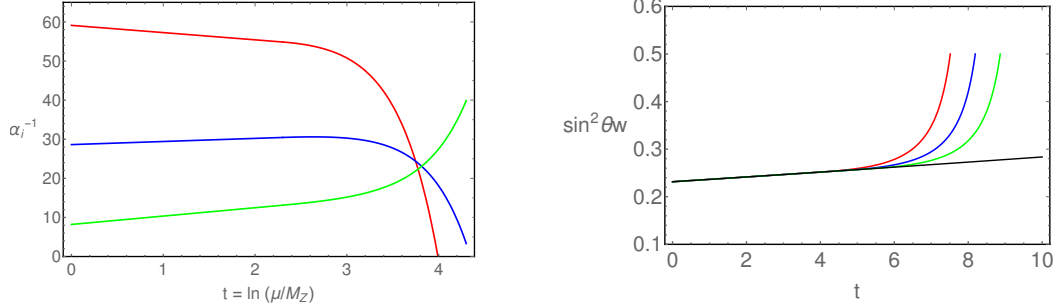


Figure 5.1: *Left panel: The evolution of the inverse fine structure constants $\alpha_i^{-1}(\mu)$ in five dimensions as a function of t , for compactification scale $R^{-1} = 5$ TeV, where α_1^{-1} is the (red line), α_2^{-1} is the (blue line) and α_3^{-1} is the (green line). Right panel: Evolution of the Weinberg angle $\sin^2 \theta_W$ for all matter fields in the bulk, for three different compactification scales; 5 TeV (red line), 10 TeV (blue line), 20 TeV (green line) as a function of t .*

$$16\pi^2 g_2^{-3} \beta_{g_2} = (S(t) - 1) \left(\frac{7}{6} \right), \quad (5.1.11)$$

$$16\pi^2 g_3^{-3} \beta_{g_3} = (S(t) - 1) \left(-\frac{5}{2} \right), \quad (5.1.12)$$

where $t = \ln(S(t)/M_Z R)$, $S(t) = \mu R$ for $M_Z < \mu < 1/R$.

In Figure 5.1, left panel, we present the evolution of the inverse fine structure constants in five dimensions for the one-loop beta-function, by assuming that all the matter fields are in the bulk. We see that α_1^{-1} and α_2^{-1} approximately meet at $\log(E/GeV) \sim 3.67$, α_1^{-1} and α_3^{-1} approximately meet at $\log(E/GeV) \sim 3.72$ and α_3^{-1} and α_2^{-1} approximately meet at $\log(E/GeV) \sim 3.78$. In Figure 5.1, right panel, we present the evolution of the Weinberg angle $\sin^2 \theta_W$ for the one-loop beta-function, for different values of compactification radius, for the model discussed above. Notice that the prediction that the Weinberg angle for an $SU(5)$ gauge group is $\sin^2 \theta_W \sim 3/8$ at M_X is over-shot by approximately 20%. We have summarised our results, in Table 5.1, of the cut-offs for the case of an $SU(5)$ gauge group in 5 dimensions, these values correspond to the point where $g_1 = \sqrt{5/3} g_2$.

5.2 The gauge coupling evolution equations for an $SU(5) \times U(1)'$

In this section we shall explore the evolution of the gauge couplings and Weinberg angle in five dimensions for an $SU(5) \times U(1)'$ gauge group, where the flipped $SU(5)$ gauge group is different from $SU(5)$ gauge group in the electric charge generators. As it does not lie completely in the $SU(5)$ gauge group, the flipped $SU(5)$ is just an embedding of $SU(5) \times U(1)$ into an $SO(10)$ gauge group. Note that the flipped $SU(5)$ model is a very special GUT [133]. The flipped $SU(5)$ gauge group contains three generations of quarks and leptons, a $(10, \bar{10})$ Higgs boson, and therefore they have the following representation [134]:

$$F_{(10)} = [Q, d^c, \nu^c]; \quad \bar{f}_{(\bar{5})} = [L, u^c]; \quad l_1 = e^c, \quad (5.2.1)$$

and

$$H_{(10)} = [Q_H, d_H^c, \Phi_H] \quad \bar{H}_{(\bar{10})} = [Q_{\bar{H}}, d_{\bar{H}}^c, \Phi_{\bar{H}}], \quad (5.2.2)$$

where the components Φ_H , $\Phi_{\bar{H}}$ break the flipped $SU(5)$ gauge group to the SM gauge group, once Φ_H , and $\Phi_{\bar{H}}$ acquires a VEV:

$$SU(5) \times U(1)' \rightarrow SU(3)_C \times SU(2)_L \times U(1)_Y \times U(1)', \quad (5.2.3)$$

and then the gauge group, $SU(3)_C \times SU(2)_L \times U(1)_Y \times U(1)'$, is spontaneously broken to $SU(3)_C \times U(1)_{em}$, once Φ_5 acquires a VEV:

$$SU(3)_C \times SU(2)_L \times U(1)_Y \times U(1)' \rightarrow SU(3)_C \times U(1)_{em}. \quad (5.2.4)$$

The flipped $SU(5)$ gauge group includes $SU(5)$ gauge bosons W^\pm , W_3 , B , X , Y and \tilde{B} , which is a $U(1)'$ gauge boson. The electric charge generator Q , in the flipped $SU(5)$ model, is given as follows:

$$Q = T_3 - \frac{1}{5}Y' + \frac{2}{5}\tilde{Y}, \quad (5.2.5)$$

where Y' is the $U(1)$ inside $SU(5)$ and \tilde{Y} is the one outside $SU(5)$. The hypercharges of the known quarks, leptons and Higgs field in the flipped $SU(5)$ gauge group are given as shown in Tabel 5.2 [133, 134]. The one-loop beta functions for the gauge couplings in 4-dimensions for $SU(5) \times U(1)'$ are given by:

$$16\pi^2 g_1^{-3} \beta_{g_1} = \frac{53}{6}, \quad (5.2.6)$$

$$16\pi^2 g_2^{-3} \beta_{g_2} = -\frac{19}{6}, \quad (5.2.7)$$

$$16\pi^2 g_3^{-3} \beta_{g_3} = -\frac{41}{6}. \quad (5.2.8)$$

Fields	$SU(3)_C$	$SU(2)_L$	$Y_5/2$
Q	3	2	$\frac{1}{6}$
L	1	2	$-\frac{1}{2}$
u^c	$\bar{3}$	1	$-\frac{2}{3}$
d^c	$\bar{3}$	1	$\frac{1}{3}$
e^c	1	1	1
Φ_5	1	2	$\frac{1}{2}$
\bar{H}_{10}	$\bar{3}$	1	$-\frac{1}{3}$

Table 5.2: *Summary of the quarks, leptons and Higgs field content in the flipped $SU(5)$ model and their quantum numbers.*

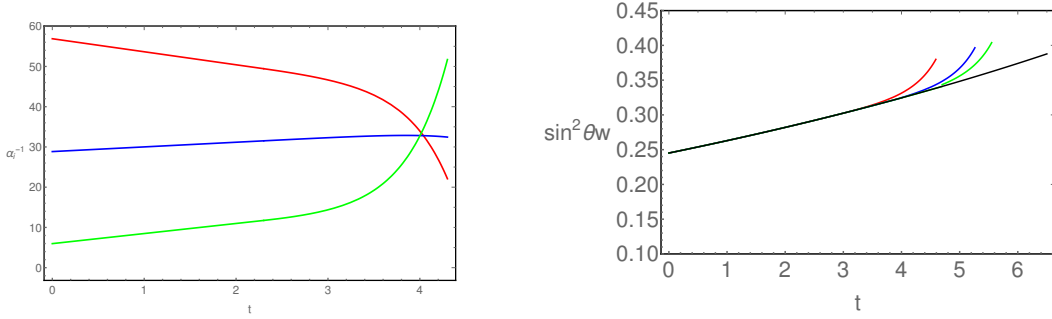


Figure 5.2: *Left panel: The evolution of the inverse fine structure constants $\alpha_i^{-1}(\mu)$ in five dimension as a function of $\log(E/\text{GeV})$ for compactification scale $R^{-1} = 5 \text{ TeV}$, where α_1^{-1} is the (red line), α_2^{-1} is the (blue line) and α_3^{-1} is the (green line). Right panel: Evolution of the Weinberg angle $\sin \theta_W$ for all matter fields in the bulk, for two different compactification scales 1 TeV (red line), 5 TeV (blue line) and 10 TeV (green line) as a function of t .*

While the one-loop beta functions for the gauge couplings in 5-dimensions for $SU(5) \times U(1)'$ are given by:

$$16\pi^2 g_1^{-3} \beta_{g_1} = (S(t) - 1) \left(\frac{105}{24} \right), \quad (5.2.9)$$

$$16\pi^2 g_2^{-3} \beta_{g_2} = (S(t) - 1) \left(-\frac{7}{24} \right), \quad (5.2.10)$$

$$16\pi^2 g_3^{-3} \beta_{g_3} = (S(t) - 1) \left(-\frac{5}{2} \right). \quad (5.2.11)$$

In Figure 5.2, left panel, we show the evolution of the α_i^{-1} in 5-dimensions for the one-loop beta-function, and in this case one can see that α_1^{-1} , α_2^{-1} and α_3^{-1} approximately unify at $\log(E/\text{GeV}) \sim 4.0$ for compactification scale $R^{-1} = 5 \text{ TeV}$. In the right panel we present the evolution of the Weinberg angle for the one-loop beta-function, for different values of compactification scales $R^{-1} = 1 \text{ TeV}$ and 5 TeV .

Scenario	$t(R_1)$	$t(R_2)$	$t(R_3)$
5D flipped $SU(5)$	4.55	5.08	5.55

Table 5.3: *The cut-offs in 5 dimensions for the flipped $SU(5)$ gauge group for two different compactification radii $R^{-1} = 1, 5$ and 10 TeV, where $t = \ln(\mu/M_Z)$.*

TeV, for the flipped $SU(5)$ model. As an example, for $R^{-1} = 5$ TeV, $\sin^2 \theta_W \sim 0.37$ at $t \sim 5.08$.

To summarise, in this chapter we have discussed the evolution of the gauge couplings in 5D for an $SU(5)$ and flipped $SU(5)$ gauge group, where we have derived these evolutions at one-loop level and used it to test the impact on lower energy observables, especially the evolution of the Weinberg angle. This chapter has shown that the evolution of the inverse fine structure constants for both $SU(5)$ and flipped $SU(5)$ gauge groups tend to almost unify. The Weinberg angle for an $SU(5)$ gauge group is over-shot by approximately 20% and for the flipped $SU(5)$ it over-shots by roughly 7%. In the next chapter we shall extend our discussion to the G_2 gauge group.

Chapter 6

Evolution of the gauge couplings and Weinberg angle in 5D for a G_2 gauge group

We will study in this chapter the evolution of the gauge couplings and Weinberg angle in 5-dimensions for a G_2 gauge group.¹ Recall that theories which contain light elementary scalars can look unnatural, because their masses receive quadratically divergent loop corrections. This problem is known as the hierarchy problem of the SM, as in this case the masses are pushed up to a cut-off scale [94]. In order to solve this problem we need to lower the cut-off scale (as was done in the case of large extra dimensional models), or to embed the Higgs field in a multiplet of a symmetry group larger than the 4-dimensional Poincare group (such as SUSY) [136]. As we know, SUSY is a space-time symmetry mapping particles and fields of integer spin (bosons) into particles and fields of half integer spin (fermions), and vice-versa. Aside from SUSY there are other extensions of the 4-dimensional Poincare group, the most natural such choice would be to use the Poincare group of a higher dimensional gauge theory [91, 137]. A gauge theory defined in more than four dimensions can have many attractive features, one of these features is that the interactions at low energies may be truly unified and some of the distinct fields in four dimensions can be integrated in a single multiplet in higher dimensions, where the Higgs fields could be a part of the gauge fields. Another feature is that the topology and structure of the extra-dimension may provide us with new ways of breaking symmetries, accounting for, at the same time, the hierarchy problem [138]. As such the SM Higgs field may originate from extra components of a higher dimensional gauge field. We therefore

¹The work of this chapter is based on our published conference proceeding [135].

plan to discuss the evolution equations of the gauge couplings and Weinberg angle for a G_2 gauge group. In this model we consider the evolution of the gauge couplings and Weinberg angle in 5D, we know that the proton decay is a well-known problem for many gauge-unification model, the model under consideration is a toy model, thus we do not addressed the proton decay.

The structure of this chapter is as follows: In section 6.1 we outline the G_2 model construction, in section 6.2 we explore the evolution of the gauge couplings and Weinberg angle for a G_2 gauge group. Our results and discussions will be given in section 6.3.

6.1 The G_2 Model Construction

In order to build a successful model we are first required to find a gauge group that contains $SU(2)_L \times U(1)_Y$ (and optionally the strong $SU(3)_c$), where the adjoint representation contains a doublet of $SU(2)$ to be identified with the Higgs doublet. The second step is to normalise the $U(1)$ gauge coupling so that the candidate Higgs has the correct hypercharge.

In this section we will explore a simple five-dimensional gauge Higgs unification scenario, where we use the gauge symmetry to be G_2 . The extra dimension is compactified on a circle of radius R with a \mathbb{Z}_2 orbifolding [139]. This orbifold is given as $\mathbb{Z}_2 : y \rightarrow -y$, so our physical space is in the interval $y \in [0, \pi R]$ and has two fixed points at $y = 0$ and $y = \pi R$ [6, 60]. We assume that all matter fields are propagating in the bulk. The gauge bosons arise from the 4-dimensional components of the 5-dimensional gauge fields, whilst the Higgs field arises from the internal components of the gauge group G_2 compactified on an S^1/\mathbb{Z}_2 orbifold [6, 139, 140].

The G_2 gauge group contains $SU(3)$ as its maximal subgroup, and the decomposition under $SU(3)$ is given by:

$$\mathbf{14} = \mathbf{8} + \mathbf{3} + \bar{\mathbf{3}}. \quad (6.1.1)$$

From this we can see that there are two possible doublets, one contained in the adjoint of $SU(3)$, and the other in the triplets, where in the first case $g_1 = \sqrt{3}g_2$ while in the other case $g_1 = g_2/\sqrt{3}$. The decomposition under $SU(2) \times U(1)$ is given by:

$$\mathbf{14} = \left(\mathbf{3}_0 + (2 + \bar{2})_{\sqrt{3}/2} + \mathbf{1}_0 \right) + (2 + \bar{2})_{1/2\sqrt{3}} + (1 + \bar{1})_{-1/\sqrt{3}}. \quad (6.1.2)$$

The other maximal subgroup is $SU(2) \times SU(2)$ under which:

$$\mathbf{14} = (\mathbf{1}, \mathbf{3}) + (\mathbf{3}, \mathbf{1}) + (\mathbf{2}, \mathbf{4}), \quad (6.1.3)$$

where in this case the first $SU(2)$ has to be identified with the one contained in the $SU(3)$ gauge group, and then in this case we can perform two possible breakings for the group. That is, either its rotation, which is now breaks $G_2 \rightarrow SU(3)$, and hence the glide to $SU(2) \times SU(2)$, or vice-versa. The fundamental representations under $SU(3)$ decompose as:

$$7 = \mathbf{3} + \bar{\mathbf{3}} + \mathbf{1}, \quad (6.1.4)$$

and the fundamental representations under $SU(2) \times U(1)$ decompose as:

$$7 = (2 + \bar{2})_{1/2\sqrt{3}} + (1 + \bar{1})_{-1/\sqrt{3}} + 1_0. \quad (6.1.5)$$

We need the RGEs to fill in the space between the predictions of the model at $\mu \gg M_Z$ and the experimental ones at $\mu \leq M_Z$. We can describe the contributions from the SM and KK modes to the beta-functions in two separate terms, which are different and independent [60, 141].

6.2 The evolution of the gauge couplings and Weinberg angle

The evolution of the gauge couplings in 4-dimensions for the G_2 gauge group at one-loop is given by:

$$16\pi^2 \frac{dg_i}{dt} = b_i^G g_i^3, \quad (6.2.1)$$

where the numerical coefficients in Equation (6.2.1) are given by:

$$b_i^G = \left[\frac{53}{6}, -\frac{21}{6}, -\frac{63}{6} \right]. \quad (6.2.2)$$

We can then rewrite Equation (6.2.1) in terms of α_i^{-1} as follows:

$$\frac{1}{\alpha_i(\mu)} \frac{d \ln \alpha_i(\mu)}{d \ln \mu} = \frac{b_i}{2\pi}. \quad (6.2.3)$$

The one-loop beta functions for the gauge couplings in 5-dimensions for the G_2 gauge group are given by:

$$16\pi^2 g_3^{-3} \frac{dg_3}{dt} = -(S(t) - 1) \left(\frac{14}{6} \right), \quad (6.2.4)$$

$$16\pi^2 g_2^{-3} \frac{dg_2}{dt} = (S(t) - 1) \left(\frac{7}{24} \right), \quad (6.2.5)$$

$$16\pi^2 g_1^{-3} \frac{dg_1}{dt} = (S(t) - 1) \left(\frac{35}{8} \right), \quad (6.2.6)$$

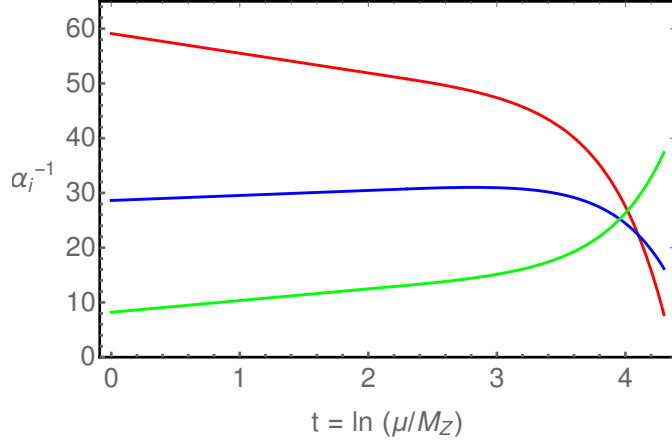


Figure 6.1: *The evolution of the inverse fine structure constants $\alpha_i^{-1}(\mu)$ in 5-dimensions for one-loop beta-functions as a function of $t = \ln(\mu/M_Z)$, for compactification scale $R^{-1} = 5 \text{ TeV}$, where α_1^{-1} is the (red line), α_2^{-1} is the (blue line) α_3^{-1} is the (green line).*

where $S(t) = M_Z R e^t$ is the number of KK states, $t = \ln(\mu/M_Z)$ is the energy scale parameter, for $M_Z < \mu < 1/R$. We have chosen the Z boson mass as the renormalization point, that is when the energy $\mu = 1/R$ or $S(t) = 1$, in this case the whole beta-function reduces to the normal beta-functions [102, 142].

Scenario	$t(R_1)$	$t(R_2)$	$t(R_3)$
5D G ₂	4.529	5.045	5.245

Table 6.1: *The cut-offs in 5 dimensions for the G₂ gauge group for three different compactification radii $R^{-1} = 1, 5$ and 10 TeV , where $t = \ln(\mu/M_Z)$.*

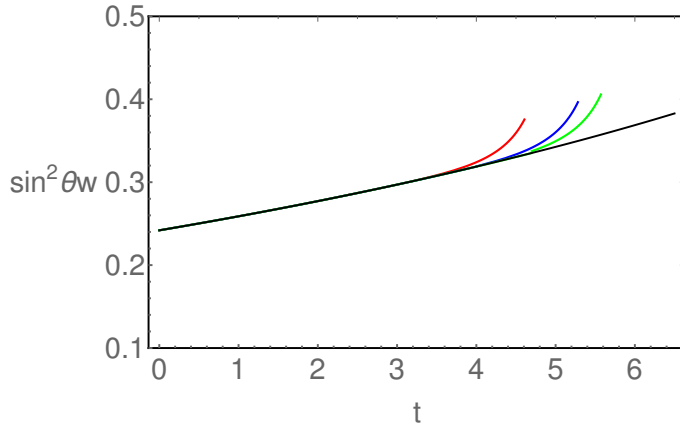


Figure 6.2: *The evolution of the Weinberg angle $\sin^2 \theta_W$ for the one-loop beta-function, for different values of compactification scales, $R^{-1} = 1$ TeV (red), $R^{-1} = 5$ TeV (blue) and $R^{-1} = 10$ TeV (green) as a function of t .*

6.3 Results and discussions

We present in Figure 6.1 the evolution of the α_i^{-1} in 5-dimensions for the one-loop beta-function for the G_2 gauge group. From this one can see that α_1^{-1} , α_2^{-1} and α_3^{-1} are approximately unified at $t \sim 4.0$.

In Figure 6.2 we present the evolution of the Weinberg angle for the one-loop beta-functions, for different values of compactification scale. As an example, for $R^{-1} = 10$ TeV, $\sin^2 \theta_W \sim 0.42$ at $t \sim 5.56$. When the fifth dimension KK modes become kinematically accessible, there are large changes in the Weinberg angle up until we reach the cut-off scale. We have chosen the cut-off for our effective theory as $g_1 = g_2$, as shown in Table 6.1.

In this chapter we have introduced the evolution of the gauge coupling for a G_2 gauge group, and it was used to test the impact on lower energy observables, in particular the evolution of the Weinberg angle. The other possible rank 2 gauge groups that contain the $SU(2) \times U(1)$ EW gauge group is $U(1) \times U(1)$, and $SO(4)$. The group $U(1) \times U(1)$ is not large enough to include the SM group, and it only contains two gauge bosons. While $SO(4) \sim SU(2) \times SU(2)/\mathbb{Z}_2$ group contains the SM group when one of the $SU(2)$ components is broken, where the adjoint representation $(3, 1) \times (1, 3)$ does not contain enough generators, thus this group must be disregarded.

We have discussed models of GHU in previous chapters, where these kinds of models ensure the existence of a DM candidate. Recall that in the extra-dimension models we have many additional lightest KK particles, and these can be identified as DM candidates if they are stable. As such, in the next two chapters we shall start looking

into the spin-3/2 fermionic DM candidate interacting with SM fermions through a vector mediator in the *s*-channel, as well as interacting with the SM quarks through the exchange of a charged and coloured scalar or vector mediator in a simple *t*-channel model.

Note that the spin-3/2 particles exist in several models beyond the SM, namely in models of supergravity, where the graviton is accompanied by spin-3/2 gravitino superpartner. Spin-3/2 fermions also exist in KK models, in string theory, and in models of composite fermions [143, 144, 145, 146, 147]. Recently spin-3/2 CDM has been studied in EFT models, and constraints from direct and indirect observations have been obtained [26, 27, 28, 29].

Chapter 7

Minimal Spin-3/2 Dark Matter in a simple *s*-channel model

In this chapter we shall address a spin-3/2 fermionic DM candidate interacting with SM fermions through a vector mediator in the *s*-channel, where we will consider a minimal SM singlet spin-3/2 vector-like fermion χ , interacting with the SM particles through the exchange of a spin-1 mediator, Z' , in a minimal flavour violation (MFV) *s*-channel model. This chapter is heavily based on our paper [64].

A large number of cosmological and astrophysical observations provide strong evidence for the existence of DM in the universe. The amount of CDM has been precisely estimated from the measurements of the Planck satellite to be $\Omega_{\text{DM}}h^2 = 0.1198 \pm 0.0015$ [18]. The nature of DM particles and their properties is the subject of intense investigation. One of the main physics programmes at the LHC is devoted to the detection of DM, where there is the real possibility of the production of DM particles of any spin at 13 TeV centre-of-mass energy. As such, the ATLAS and the CMS collaborations are closely examining several DM signatures involving missing energy, \cancel{E}_T , accompanied by a single or two jet events [19]. In addition there are direct detection experiments, which measure the nuclear-recoil energy and its spectrum in DM-nucleon elastic scattering. The indirect detection experiments look for signals of DM annihilation into SM particles in cosmic rays, and have detection instruments mounted on satellites and ground based telescopes [148, 149].

EFTs in which the DM-SM interactions are mediated by heavy particles, which are not accessible at the LHC energies, have been analysed in detail with limits from direct and indirect searches. Recently the need to go beyond these EFT models has been pointed out, in light of the large energy accessible at the LHC [150].

Simplified models of DM with interactions to SM particles have emerged as attractive alternatives to EFT models. In these models the interaction between the DM and SM particles are mediated by spin-0 and spin-1 particles in the s -channel, which is the focus of this chapter; whereas in the t -channel models the mediator can be a scalar, a fermion or a vector particle, which will typically also carry colour or lepton number, as discussed in chapter 8 [65].

As such we shall now consider a minimal SM singlet spin-3/2 fermion, χ , as a DM candidate, interacting with the SM particles through the exchange of a spin-1 mediator, Z' , in a MFV s -channel model. We shall begin by introducing the spin-3/2 CDM in an MFV s -channel model in section 7.1. Whilst in section 7.2 we discuss all relevant experimental constraints including the relic density and the signatures of these DM particles at the LHC. In section 7.3 we summarise our main results.

7.1 Spin-3/2 Singlet DM Model

In this section we extend the SM by including a spin-3/2 particle χ . We further let χ be a SM singlet which interacts with the SM particles through the exchange of a vector particle Z' in the s -channel. Note that this can be done, for example, by extending the SM gauge symmetry with a new $U(1)'$ gauge symmetry which is spontaneously broken, such that the mediator obtains a mass $m_{Z'}$. We also invoke a discrete \mathbb{Z}_2 symmetry under which the spin-3/2 DM particle χ is odd, whereas all other SM particles, including the vector mediator Z' , are even. The spin-3/2 free Lagrangian is given by [151]:

$$\mathcal{L} = \bar{\chi}_\mu \Lambda^{\mu\nu} \chi_\nu, \quad (7.1.1)$$

with

$$\Lambda^{\mu\nu} = (i\partial^\mu - m_\chi)g^{\mu\nu} - i(\gamma^\mu \partial^\nu + \gamma^\nu \partial^\mu) + i\gamma^\mu \partial^\nu \gamma^\nu + m_\chi \gamma^\mu \gamma^\nu. \quad (7.1.2)$$

Note that χ_μ satisfies $\Lambda^{\mu\nu} \chi_\nu = 0$, and with χ_μ being on mass-shell we have

$$(i\partial^\mu - m_\chi) \chi_\mu = \partial^\mu \chi_\mu = \gamma^\mu \chi_\mu = 0. \quad (7.1.3)$$

The spin sum for spin-3/2 fermions

$$S_{\mu\nu}^+(p) = \sum_{i=-3/2}^{3/2} u_\mu^i(p) \bar{u}_\nu^i(p) \quad (7.1.4)$$

and

$$S_{\mu\nu}^-(p) = \sum_{i=-3/2}^{3/2} v_\mu^i(p) \bar{v}_\nu^i(p), \quad (7.1.5)$$

are given by [151]:

$$S_{\mu\nu}^{\pm}(p) = -(\not{p} \pm m_{\chi}) \left[g_{\mu\nu} - \frac{1}{3} \gamma_{\mu} \gamma_{\nu} - \frac{2}{3m_{\chi}^2} \not{p}_{\mu} \not{p}_{\nu} \mp \frac{1}{3m_{\chi}} (\gamma_{\mu} p_{\nu} - \gamma_{\nu} p_{\mu}) \right]. \quad (7.1.6)$$

In view of the non-renormalisable nature of interacting spin-3/2 theories, we can only write a generic set of interactions respecting the SM gauge symmetry between the singlet Dirac-vector spinor, χ_{μ} , with SM fermions mediated by a vector particle Z'_{μ} as (see for example [152])

$$\mathcal{L}_{\chi, Z'} + \mathcal{L}_{f, Z'} \supset \bar{\chi}_{\alpha} \gamma^{\mu} (g_{\chi}^V - \gamma^5 g_{\chi}^A) \chi_{\beta} Z'_{\mu} g^{\alpha\beta} + \sum_{f=q,l,\nu} \bar{f} \gamma^{\mu} (g_f^V - \gamma^5 g_f^A) f Z'_{\mu}, \quad (7.1.7)$$

where the sum is over all quarks, charged leptons and neutrinos. The interaction is not restricted by MFV to be either a pure vector or axial vector. Although the form of the low energy interactions of spin-3/2 particles should arise from an underlying theory at high energies, we follow the approach of simplified model theories. The purpose of a simplified model approach is to characterise the DM production present in a complete theory, without having to specify the complete theory. In these theories the mediator provides the link between the SM and DM candidate. In general this interaction will induce flavour-changing neutral currents (FCNC), which are strongly constrained by low energy phenomenology. The constraints can be avoided by imposing a MFV structure on the couplings, or by restricting the interactions to one generation.

There exists an extensive range of models with an extra $U(1)'$ symmetry (for a review see [153]). The most stringent indirect constraints on $m_{Z'}$ arise from the effect of a Z' coupling to SM fermions in precision electro-weak observables from low energy weak neutral current experiments [154, 155], and gives a lower limit on $m_{Z'}$ of $\mathcal{O}(1)$ TeV; where LHC experiments set strong bounds on the Z' mass. For a Z' coupling with SM particles to be of the order of SM- Z electro-weak coupling this bound is typically $m'_{Z'} \geq 2$ TeV [150]. This bound is somewhat relaxed (depending on the model) when Z' is allowed to decay into DM candidates [154, 156].

The decay width $\Gamma(Z' \rightarrow f\bar{f} + \chi_\alpha\bar{\chi}_\alpha)$ is given by ¹

$$\begin{aligned} \Gamma(Z' \rightarrow f\bar{f} + \chi_\alpha\bar{\chi}_\alpha) = \sum_f \frac{N_c}{12\pi} m_{Z'} \sqrt{1 - \frac{4m_f^2}{m_{Z'}^2}} & \left[((g_f^V)^2 + (g_f^A)^2) \right. \\ & + \frac{2m_f^2}{m_{Z'}^2} ((g_f^V)^2 - 2(g_f^A)^2) \left. \right] + \frac{m_{Z'}}{108\pi} \left(\frac{m_\chi^2}{m_{Z'}^2} \right) \sqrt{1 - \frac{4m_\chi^2}{m_{Z'}^2}} \\ & \times \left[(g_\chi^V)^2 \left(36 - 2\frac{m_{Z'}^2}{m_\chi^2} - 2\frac{m_{Z'}^4}{m_\chi^4} + \frac{m_{Z'}^6}{m_\chi^6} \right) \right. \\ & \left. + (g_\chi^A)^2 \left(-40 + 26\frac{m_{Z'}^2}{m_\chi^2} - 8\frac{m_{Z'}^4}{m_\chi^4} + \frac{m_{Z'}^6}{m_\chi^6} \right) \right]. \end{aligned} \quad (7.1.8)$$

The sum extends over all SM fermions f that are above the threshold, $N_c = 3$ for quarks and 1 for leptons. There are several interesting consequences on the DM mass and couplings arising from the above decay width expressions. If the DM mass $m_\chi > m_{Z'}/2$, the only decay channel available to the mediator Z' is into SM fermions. Since $\Gamma(Z') < m_{Z'}$ is required for the mediator description to be perturbatively valid, the vector coupling, for example, should satisfy

$$\frac{8m_{Z'}}{12\pi} (g_f^V)^2 < m_{Z'} \quad \Rightarrow \quad (g_f^V)^2 < \frac{3\pi}{2}. \quad (7.1.9)$$

Here we consider the coupling to be only to one generation for the purposes of illustration. The qualitative result remains essentially unchanged if all three generations are taken, except that the top quark mass may not be neglected in comparison to the mediator mass. This gives $\Gamma_{Z'}/m_{Z'} \simeq 2(g_f^V)^2/3\pi$, and we have the narrow width approximation being applicable for $g_f^V \leq 1$. However, if the DM mass $m_\chi < m_{Z'}/2$, the mediator can decay into DM pairs, and there exists a minimum limit on the DM mass χ for a given value of the mediator mass with the coupling given roughly by

$$\frac{1}{108\pi} \left(\frac{m_{Z'}}{m_\chi} \right)^4 (g_\chi^{V,A})^2 < 1. \quad (7.1.10)$$

If the DM mass is below this value, the decay width would exceed the mediator mass.

In what follows we consider universal couplings for simplicity, $g_\chi^V = g_f^V$ and $g_\chi^A = g_f^A$, and restrict ourselves to one generation of SM fermions. In Figure 7.1 we have plotted the mediator Z' decay width as a function of m_χ for some benchmark values of pure vector couplings $g_{\chi,f}^V$, chiral couplings $g_{\chi,f}^V = \pm g_{\chi,f}^A$ and pure axial couplings $g_{\chi,f}^A$. It can be seen from Figure 7.1 that there exists a minimum m_χ for a given coupling, where a mass of χ less than the limit given in Equation (7.1.10) results in a value of the decay width more than the value of m_χ . This feature is peculiar to the spin-3/2 nature of the DM.

¹The decay widths for the mediator Z'_μ decay into $\chi\bar{\chi}$ and into $f\bar{f}$ are given in Appendix D.

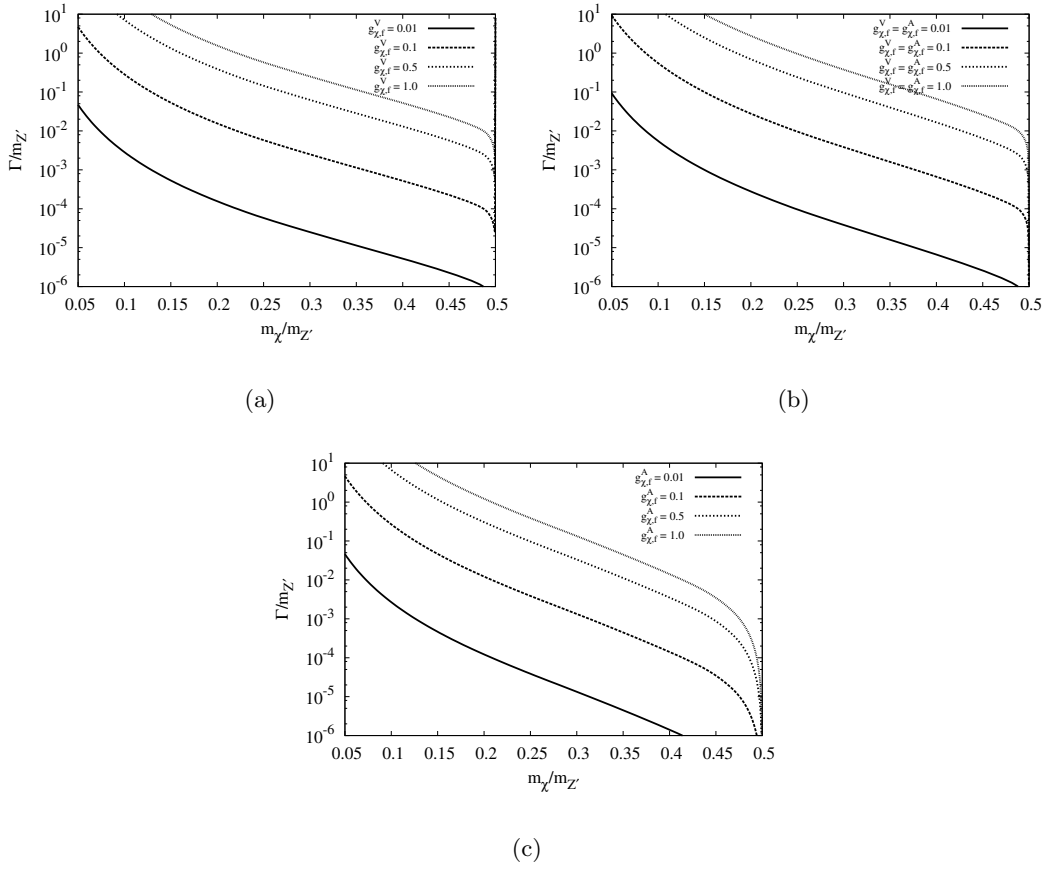


Figure 7.1: *Ratio of the mediator decay width to its mass $\Gamma/m_{Z'}$ as a functions of $m_\chi/m_{Z'}$ for a few benchmark values of the couplings: 0.1, 0.5 and 1.0. The (a) panel is for the vector couplings $g_{\chi,f}^V$, and the (b) panel is for the chiral couplings ($g_{\chi,f}^V = \pm g_{\chi,f}^A$). The (c) panel is for the axial-vector couplings $g_{\chi,f}^A$.*

7.2 Constraints for the spin-3/2 singlet DM model

7.2.1 Relic Density.

In the early universe the DM particles were kept in thermal equilibrium with the rest of the plasma through the creation and annihilation of χ 's. The cross-section of the annihilation process $\chi\bar{\chi} \rightarrow f\bar{f}$ proceeds through Z' , and the spin averaged

cross-section is given by ²

$$\begin{aligned}
\sigma(\chi\bar{\chi} \rightarrow f\bar{f}) = & \sum_f \frac{N_c \sqrt{s - 4m_f^2}}{432 \pi m_\chi^4 m_{Z'}^4 s} \frac{1}{\sqrt{s - 4m_\chi^2}} \left[\frac{1}{(s - m_{Z'}^2)^2 + \Gamma^2 m_{Z'}^2} \right] \\
& \times \left[(g_f^A)^2 \left\{ (g_\chi^A)^2 \left\{ 4m_f^2 \left\{ 10m_\chi^6 (7m_{Z'}^4 - 6m_{Z'}^2 s + 3s^2) \right. \right. \right. \right. \right. \\
& \left. \left. \left. \left. \left. \left. - 2m_\chi^4 s (16m_{Z'}^4 - 6m_{Z'}^2 s + 3s^2) + m_\chi^2 s^2 (11m_{Z'}^4 \right. \right. \right. \right. \right. \\
& \left. \left. \left. \left. \left. \left. - 6m_{Z'}^2 s + 3s^2 \right) - m_{Z'}^4 s^3 \right\} + m_{Z'}^4 s (-40m_\chi^6 + 26m_\chi^4 s \right. \right. \right. \right. \right. \\
& \left. \left. \left. \left. \left. \left. - 8m_\chi^2 s^2 + s^3 \right) \right\} - (g_\chi^V)^2 m_{Z'}^4 (4m_f^2 - s) (36m_\chi^6 \right. \right. \right. \right. \right. \\
& \left. \left. \left. \left. \left. \left. - 2m_\chi^4 s - 2m_\chi^2 s^2 + s^3 \right) \right\} + (g_f^V)^2 m_{Z'}^4 (2m_f^2 + s) \right. \right. \right. \right. \right. \\
& \times \left\{ (g_\chi^A)^2 (-40m_\chi^6 + 26m_\chi^4 s - 8m_\chi^2 s^2 + s^3) \right. \right. \right. \right. \right. \\
& \left. \left. \left. \left. \left. \left. + (g_\chi^V)^2 (36m_\chi^6 - 2m_\chi^4 s - 2m_\chi^2 s^2 + s^3) \right) \right\} \right]. \tag{7.2.1}
\end{aligned}$$

Freeze out occurs when the χ 's are non-relativistic ($v \ll c$). We then have

$$s \simeq 4m_\chi^2 + m_\chi^2 v^2 + \mathcal{O}(v^4) \tag{7.2.2}$$

in the lab frame. The cross-section can be expanded in powers of v^2 as ³

$$\sigma v = a + b v^2 + \mathcal{O}(v^4). \tag{7.2.3}$$

The relic density contributions of the DM particles can be obtained by numerically solving the Boltzmann equation:

$$\frac{dn_\chi}{dt} + 3Hn_\chi = -\langle\sigma|v|\rangle (n_\chi^2 - (n_\chi^{eq})^2), \tag{7.2.4}$$

where $\langle\sigma|v|\rangle$ is the thermally averaged χ -annihilation cross-section $\langle\sigma(\chi\bar{\chi} \rightarrow f\bar{f})|v\rangle$, and n_χ is the number density of the χ 's. When we are in thermal equilibrium the number density is given by

$$n_\chi^{eq} = 4 \left(\frac{m_\chi T}{2\pi} \right)^{3/2} \exp\left(-\frac{m_\chi}{T}\right). \tag{7.2.5}$$

The Hubble expansion rate is given by

$$H = \sqrt{\frac{8\pi\rho}{3M_{pl}^2}}, \tag{7.2.6}$$

where $M_{pl} = 1.22 \times 10^{19}$ GeV is the Planck mass. The Boltzmann equation is solved numerically to yield [157]

$$\Omega_{DM} h^2 \simeq \frac{2 \times 1.07 \times 10^9 X_F}{M_{pl} \sqrt{g_*} \left(a + \frac{3b}{X_F} \right)}, \tag{7.2.7}$$

²The full expressions of the annihilation cross-section of spin-3/2 DM into SM fermions as a function of v are given in the Appendix D.

³The expressions for a and b are given in the Appendix D.

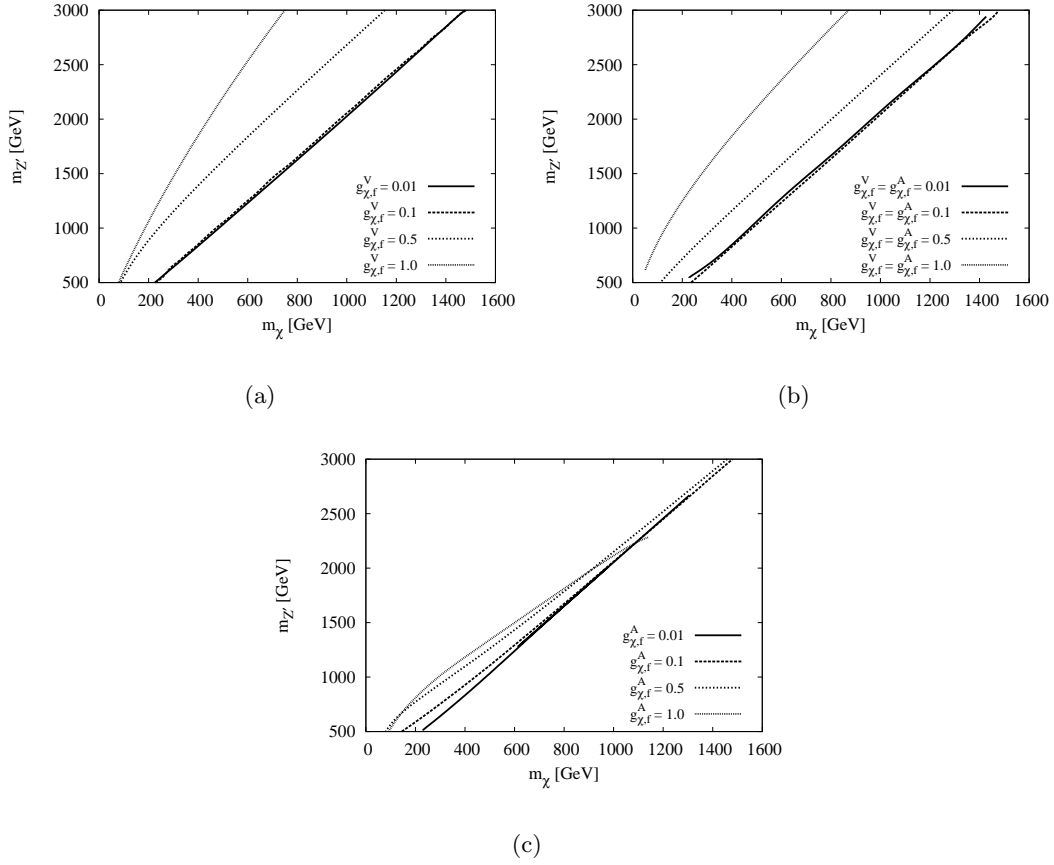


Figure 7.2: The contour plots between the $m_{Z'}$ and m_χ , where we have assumed that the DM χ saturates the observed DM density. The (a) and the (c) panels are for benchmark values of vector and axial-vector couplings respectively. The (b) panel is for the chiral coupling.

where g_* is the number of degrees of freedom at freeze-out temperature T_F , and is taken to be 92 for $m_b < T_F < m_{Z'}$, $X_F = m_\chi/T_F$. The freeze-out temperature is obtained by solving

$$X_F = \ln \left[c(c+2) \sqrt{\frac{45}{8}} \frac{g M_{pl} m_\chi \left(a + \frac{6b}{X_F} \right)}{2\pi^3 \sqrt{g_*(X_F)} \sqrt{X_F}} \right], \quad (7.2.8)$$

where c is taken to be 1/2. For spin-3/2 DM $g = 4$.

In Figure 7.2 we show the contour graphs between the mass of the mediator $m_{Z'}$ and the DM mass m_χ , by assuming that the DM χ saturates the observed DM density. From the graphs we see that for small couplings $g \leq 0.1$, the parameter space $(m_\chi, m_{Z'})$ is consistent with the observed relic density and is thus independent of the coupling. This can be understood by noting that the leading term in the

thermally averaged DM annihilation cross-section into SM fermions is given by

$$\begin{aligned} \langle\sigma(\chi\bar{\chi} \rightarrow f\bar{f})|v\rangle &\simeq \frac{20g^4}{9\pi m_{Z'}^2 m_{Z'}^2} \frac{1}{\left(1 - \frac{4m_\chi^2}{m_{Z'}^2}\right)^2 + \left(\frac{\Gamma^2}{m_{Z'}^2}\right)} \\ &\simeq \frac{8 \times 10^{-24}}{(m_{Z'}/1\text{TeV})^2} \frac{g^4}{\left(1 - \frac{4m_\chi^2}{m_{Z'}^2}\right)^2 + \left(\frac{\Gamma^2}{m_{Z'}^2}\right)} \left(\frac{m_\chi}{m_{Z'}}\right)^2 \text{cm}^3 \text{s}^{-1}. \end{aligned} \quad (7.2.9)$$

The annihilation cross-section, being proportional to the fourth power in coupling, falls rapidly for couplings ≤ 0.1 , and the freeze out occurs early when the temperature is high. This will result in the relic density falling below the observed value. The annihilation rate, however, receives resonant enhancement at $m_\chi \simeq \frac{1}{2}m_{Z'}$, in which case the $\Gamma/m_{Z'}$ term dominates over the pole term in the denominator. Thus near resonance the annihilation cross-section becomes independent of the coupling and we get the relic density contour curves almost independent of coupling. In this situation the observed relic density is obtained for $m_\chi \simeq \frac{1}{2}m_{Z'}$ as is evident from the graphs.

7.2.2 Direct Detection.

Constraints from DM detection experiments can be obtained from the elastic DM-nucleon cross-section. In the present case, owing to the presence of both vector and axial-vector couplings, the DM-nucleon scattering has both spin-independent and spin-dependent components. The corresponding cross-section at zero momentum transfer can be easily computed [158, 159, 160]. The spin-independent and spin-dependent sub-dominant cross-sections are given by [161]:

$$\begin{aligned} \sigma_{\chi N}^{\text{SI}} &= \frac{\mu^2 f_N^2}{\pi m_{Z'}^4} = \frac{9\mu^2 (g_f^V g_\chi^V)^2}{\pi m_{Z'}^4} \\ &\simeq 1.4 \times 10^{-37} (g_f^V g_\chi^V)^2 \left(\frac{\mu}{1\text{GeV}}\right)^2 \left(\frac{300\text{GeV}}{m_{Z'}}\right)^4 \text{cm}^2, \end{aligned} \quad (7.2.10)$$

and

$$\begin{aligned} \sigma_{\chi N}^{\text{SD}} &= \frac{5\mu^2}{3\pi m_{Z'}^4} a_N^2 = \frac{5\mu^2 (g_f^A g_\chi^A)^2}{3\pi m_{Z'}^4} (\Delta u^N + \Delta d^N + \Delta s^N)^2 \\ &\simeq 4.7 \times 10^{-39} (g_\chi^A g_f^A)^2 \left(\frac{\mu}{1\text{GeV}}\right)^2 \left(\frac{300\text{GeV}}{m_{Z'}}\right)^4 \text{cm}^2, \end{aligned} \quad (7.2.11)$$

where

$$\mu = \frac{m_\chi m_N}{m_\chi + m_N} \quad (7.2.12)$$

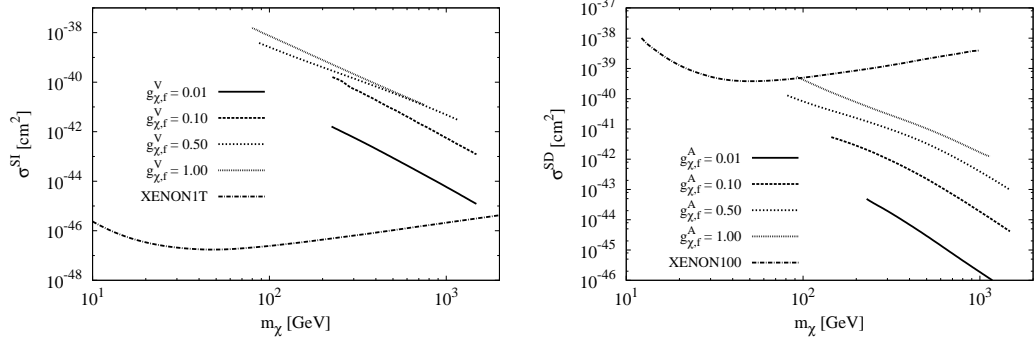


Figure 7.3: The spin-independent nucleon-DM cross-section σ^{SI} (left panel) and spin-dependent nucleon-DM cross-section σ^{SD} (right panel). The predicted cross-section is shown here for different values of the coupling, and are in agreement with the relic density constraints. In the plots we show the recent XENON1T data for σ^{SI} , and the XENON 100 neutron bounds for σ^{SD} .

is the reduced mass. $m_N = (m_p + m_n)/2 \simeq 0.939$ GeV is the nucleon-mass for direct detection, with f_p , f_n and $a_{p,n}$ being given by:

$$f_p = g_\chi^V (2g_u^V + g_d^V), \quad f_n = g_\chi^V (2g_d^V + g_u^V) \quad (7.2.13)$$

and

$$a_{p,n} = \sum_{q=u,d,s} g_\chi^A \Delta q^{p,n} g_q^A. \quad (7.2.14)$$

The coefficients $\Delta q^{p,n}$ depend on the light quark contributions to the nucleon spin [161]:

$$\begin{aligned} \Delta u^p &= \Delta d^n = 0.84 \pm 0.02, \\ \Delta d^p &= \Delta u^n = -0.43 \pm 0.02, \\ \Delta s^p &= \Delta s^n = -0.09 \pm 0.02. \end{aligned} \quad (7.2.15)$$

The axial-vector term is suppressed by the momentum transfer, or by the DM velocity, and has been neglected. In Figure 7.3 we show the predictions for the spin-independent σ^{SI} and spin-dependent σ^{SD} cross-sections for benchmark values of the vector and axial-vector couplings, as a function of DM mass m_χ . The corresponding experimental bounds from XENON1T [23] and XENON100 [162] are also displayed. The mediator mass $m_{Z'}$ is set to give the observed relic density for all values of m_χ and the couplings. We find that for the vector coupling almost the entire parameter space $(m_\chi, m_{Z'})$ is consistent with the observed relic density, and is ruled out from the XENON1T bound on spin-independent nucleon-DM elastic scattering cross-sections. The XENON-100 data on the spin-dependent cross-section, on the other hand, does not place severe constraints on the parameter space, and as such the allowed parameter space is consistent with the observed relic density.

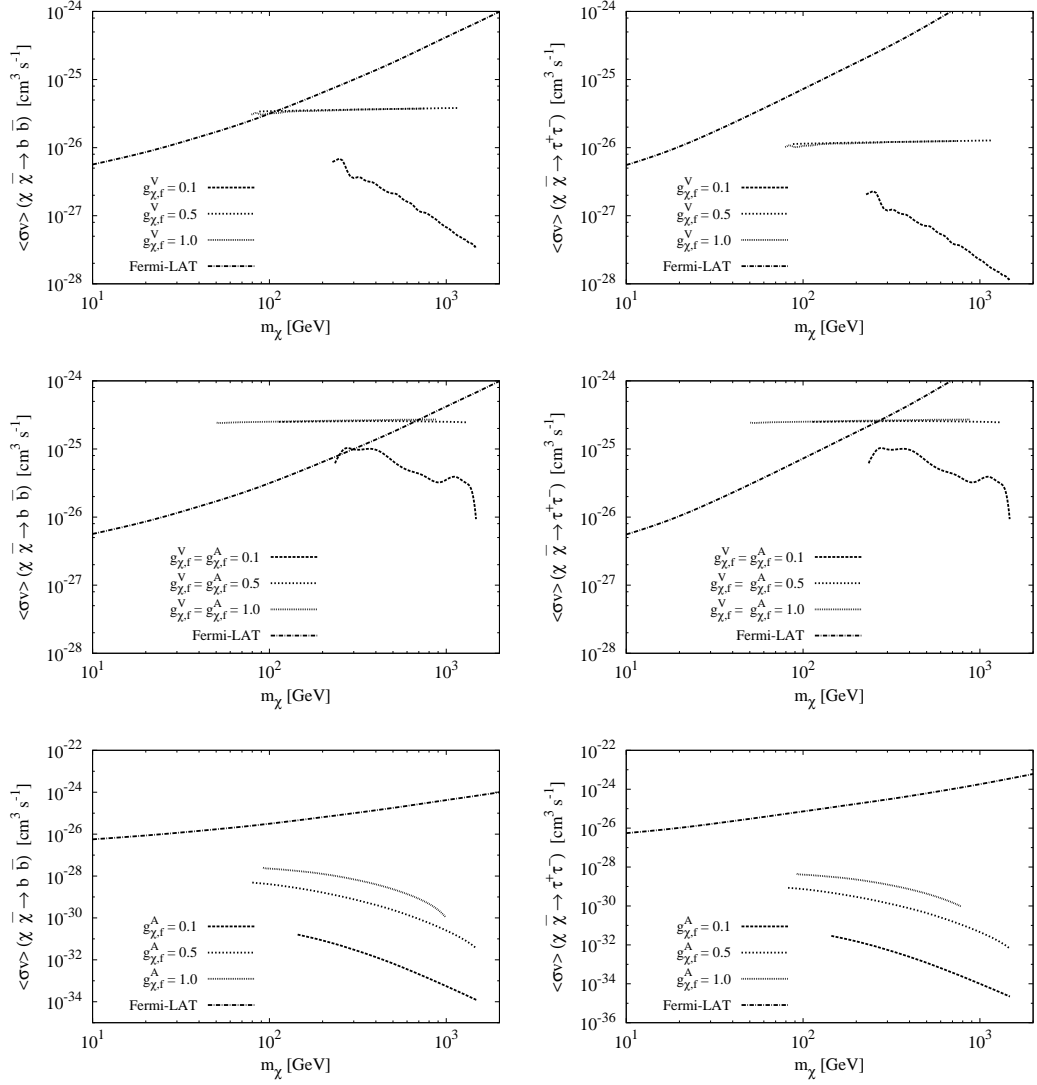


Figure 7.4: The prediction for the DM χ annihilation rate into $b\bar{b}$ and $\tau^+\tau^-$ for benchmark values of couplings. The top, middle and bottom panels are for pure vector, chiral and axial couplings respectively. The cross-sections are obtained for $(m_\chi, m_{Z'})$ values consistent with the observed relic density. Bounds from the Fermi-LAT experiments are also shown.

7.2.3 Indirect Detection.

DM annihilation in the universe would result in cosmic ray fluxes which can be observed by dedicated detectors. The Fermi Large Area Telescope (LAT) collaboration [163, 164] has produced constraints on the DM annihilation cross-section into some final states, namely e^+e^- , $\mu^+\mu^-$, $\tau^+\tau^-$, $b\bar{b}$, $u\bar{u}$, W^+W^- etc. [163, 165].

In Figure 7.4 we show the prediction for the DM annihilation into $b\bar{b}$ and $\tau^+\tau^-$ for vector, axial-vector and chiral couplings, as a function of m_χ . The predictions shown here are for benchmark values of couplings and for the DM mass m_χ consistent with the observed relic density. We have also shown the bounds from the Fermi-LAT experiments. It can be seen from these figures that the Fermi-LAT data on the DM annihilation cross-section, $\langle\sigma(\chi\bar{\chi} \rightarrow b\bar{b}, \tau^+\tau^-)|v\rangle$, is consistent with the benchmark vector and axial-vector couplings, and for $(m_\chi, m_{Z'})$ parameters obtained from the observed relic density. However, for the chiral couplings considered in this work there is only a narrow window in the high DM mass ($m_\chi \geq 400$ GeV) range for the coupling $g \simeq 1$. For small values of the coupling ($g \leq 0.1$) Fermi-LAT data does not provide any stringent bounds on the $(m_\chi, m_{Z'})$ parameter space.

7.2.4 Collider Constraints.

Monojet searches at the LHC with missing transverse energy, \cancel{E}_T , have been used by CMS at 8 TeV, based on an integrated luminosity of 19.7 fb^{-1} [166], to put constraints on the interaction of quarks and DM particles. In the context of a spin-1/2 DM particle interacting through a vector mediator, with vector and axial-vector couplings, constraints on the DM mass m_χ and the mediator mass $m_{Z'}$ for some representative values of the coupling have been obtained in the literature [167, 168, 169, 170, 171, 172].

For monojet constraints at the LHC, we use the parameter space $(m_\chi, m_{Z'})$ for the spin-3/2 DM, consistent with the observed DM density for benchmark couplings. To obtain the cross-section for monojets we generate parton level events of the process $pp \rightarrow \chi\bar{\chi} + 1j$ using `MadGraph5` [173], where the required model file for the Lagrangian (7.1.7) is obtained from `FeynRules` [174]. The cross-sections are calculated here to obtain bounds by requiring $\cancel{E}_T > 450$ GeV, for which the CMS results exclude new contributions to the monojet cross-section exceeding 7.8 fb at 95% CL. The resulting monojet cross-section for the vector, axial-vector and chiral couplings are shown in Figure 7.5, where we find that the vector coupling results are in agreement with the bounds from the direct detection experiments. In the case of axial-vector couplings, the monojet search places stronger constraints on the parameters, in comparison to the constraints from direct and indirect searches, albeit for $g_{\chi,f}^A \sim 1$.

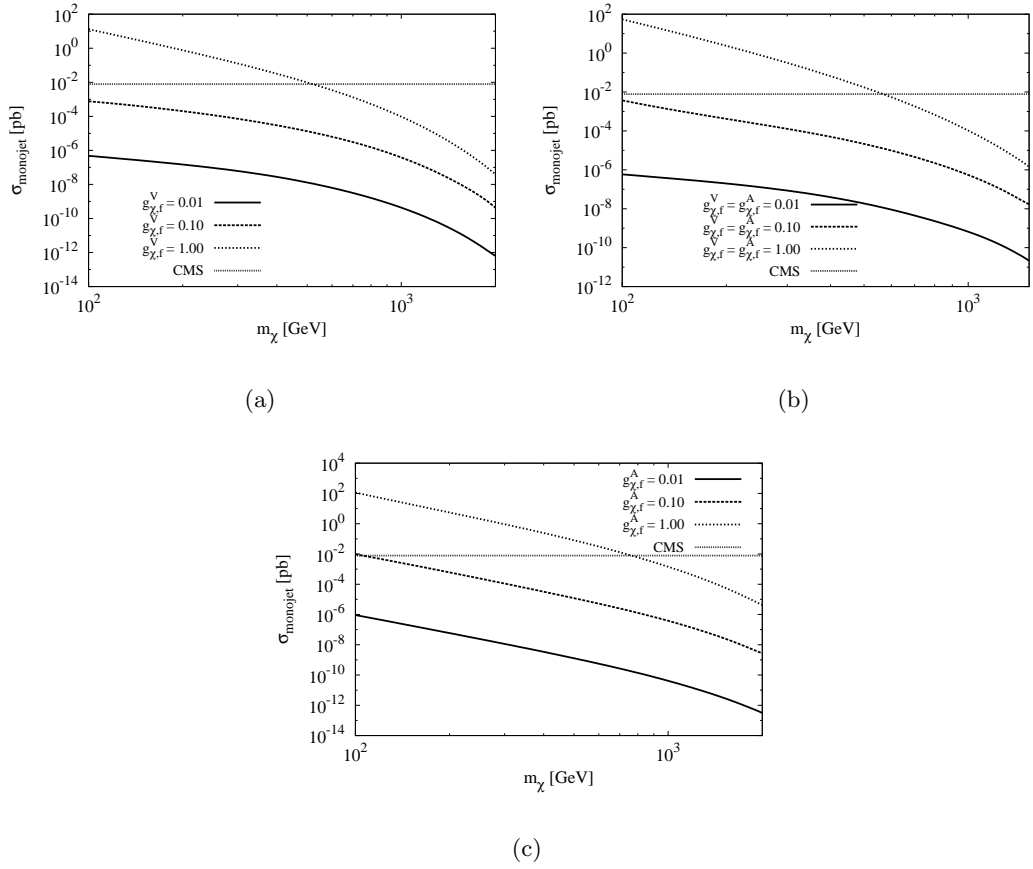


Figure 7.5: The monojet cross-section in [pb] at the LHC with missing transverse energy $\cancel{E}_T + 1$ jet signal, through $pp \rightarrow Z' \rightarrow \chi\bar{\chi} + 1j$. The cross-sections are obtained by considering values of $(m_{Z'}, m_\chi)$ consistent with the observed relic density for the benchmark couplings. The allowed parameter space for spin-3/2 DM candidates lies below the CMS bound of $\sigma_{\text{monojet}} = 7.8$ fb. The (a), (b) and (c) panels are for pure vector, chiral and axial-vector couplings respectively.

7.3 Summary and discussion

Presuming a spin-3/2 nature of DM, in addition to the restriction on the coupling arising from the decay width, there exists a minimum value of the DM mass for a given coupling and mediator mass. In the case of vector and chiral couplings, almost the entire parameter space $(m_\chi, m_{Z'})$ is consistent with the observed relic density, and is ruled out by direct detection through nucleon-DM elastic scattering bounds given by XENON1T data. While for the case of a vector mediator with pure axial-vector coupling there is, in contrast, a different result with respect to the vector coupling. In this case the parameter space is consistent with the observed relic density, and is also allowed by the indirect and direct (XENON100 neutron)

observations.

For the benchmark couplings considered here there are no strong bounds on vector and chiral couplings from the monojet searches at the LHC, and the results are in broad agreement with the direct detection experiments. The case of pure axial coupling is, however, different. Here the monojet search places stronger constraints on the parameters in comparison to the constraints obtained from the XENON100 neutron observations.

The Fermi-LAT data on the DM annihilation cross-section is consistent with the vector and axial-vector couplings considered here, and for the $(m_\chi, m_{Z'})$ parameter values obtained from the relic density. For couplings $g \leq 0.1$ the Fermi-LAT data does not provide stringent bounds on the $(m_\chi, m_{Z'})$ parameters. For chiral couplings the data allows only a narrow window in the DM mass ($m_\chi \geq 400$ GeV) and $g \simeq 1$. In the EFT frame work for pure vector couplings [26, 27] the entire parameter space 10 GeV $< m_\chi < 1$ TeV, and an effective interaction scale of the order of a few tens of TeV, though consistent with the observed relic density, is ruled out from the direct detection observations. For the case of pure axial coupling, bounds from direct detection do not forbid the DM mass lying in this range. This is in agreement with our study in a simple s -channel mediator model, except that in the mediator model the minimum allowed DM mass is consistent with the observed relic density, and is of order of 100 GeV. In the case of couplings with chiral SM fermions ($g_f^V = g_f^A$) it was found that for a spin-3/2 DM mass up to 1 TeV [28], the entire parameter space is ruled out from direct detection. The monojet + \cancel{E}_T searches at ATLAS rules out DM masses up to 200 GeV. In contrast the s -channel mediator model monojet searches at ATLAS are more stringent, and the allowed DM mass limit is raised to greater than 500 GeV. For DM masses exceeding 1 TeV, there are no direct detection constraints, but collider and indirect observation constraints still exist.

We will extend our discussion to the simple t -channel model in the next chapter by looking into the spin-3/2 fermionic DM interacting with the SM quarks through the exchange of a charged and colour scalar or vector mediator.

Chapter 8

Spin-3/2 Dark Matter in a simple *t*-channel model

We will now consider a spin-3/2 fermionic DM particle interacting with the SM quarks through the exchange of a charged and coloured scalar or vector mediator in a simple *t*-channel model. The DM particle in this case is a *t*-channel annihilator, and it interacts with the SM particles through the exchange of a scalar (S) or vector (V) particle. This is in contrast to the *s*-channel model considered in chapter 7, where a class of such *t*-channel models for scalar and vector mediator couplings with a spin-1/2 DM candidate has been considered in Refs. [175, 176, 177, 178]. The mediators in these *t*-channel models carry colour or leptonic index.

As such we shall describe the model for this study in section 8.1, and in section 8.2 all the relevant experimental constraints. The relic density contributions of the DM particles is calculated, and assuming that the contribution by these spin-3/2 DM particles does not exceed the observed relic density, constraints on the parameters of the model are obtained in section 8.2.1. With these constraints in place we discuss the compatibility of these constraints from the direct and indirect detection experiments in section 8.2.2 and section 8.2.3 respectively. In section 8.3 we examine the signature of these DM particles at the LHC, where a monojet signal with missing energy is investigated. Section 8.4 is devoted to the summary and discussion of our main results.

8.1 The simple t -channel model

The model consists of a SM singlet spin-3/2 particle interacting through the mediation of a scalar (S) or a vector (V^μ) which carries a baryonic (colour) or lepton index. In general the mediator couples to right-handed up-type quarks (or leptons), right-handed down-type quarks (or leptons) or left-handed quark (or lepton) doublets. We consider here the right-handed up-type quark case for simplicity and the other cases are similar. The spin-3/2 free Lagrangian is given by Equations (7.1.1) to (7.1.6).

In view of the non-renormalisable nature of interacting spin-3/2 theories, we can only write generic interactions which respect to the SM gauge symmetry between the singlet, χ , with SM fermions mediated by a scalar or a vector [179]. We will consider the vector and scalar mediator case separately:

1. Scalar mediator S : For the scalar mediator case, we can write the SM gauge invariant interaction as:

$$\mathcal{L}_{int} \supset -\frac{(g_\chi^S)^i}{\Lambda} \bar{\chi}_\mu g^{\mu\nu} u_R^i D_\nu S_i^* + \text{h.c.}, \quad (8.1.1)$$

where i is a generation index and $u_R^i \equiv (u_R, c_R, t_R)$. In this case we do not have a dimension-4 interaction term. This is because of the nature of the vector-spinor χ_μ , which on mass-shell satisfies $\gamma^\mu \chi_\mu = 0$, and thus it is not possible to construct a Lorentz-invariant dimension-4 interaction term involving χ_μ , S and the Dirac field u_R .

2. Vector mediator V_μ : In this case we can write a dimension-4 term, as well as a dimension-5 interaction term, namely,

$$\mathcal{L}_{int} \supset i (c_\chi^V)^i \bar{\chi}_\mu u_R^i (V_i^\mu)^* + \text{h.c.}, \quad (8.1.2)$$

and

$$\mathcal{L}_{int} \supset i \frac{(g_\chi^V)^i}{\Lambda} \bar{\chi}_\mu g^{\mu\alpha} \gamma^\beta u_R^i V_{\alpha\beta}^{*i} + \text{h.c.} \quad (8.1.3)$$

For all calculations we set $\Lambda = 1$ TeV. The interaction Lagrangian for the scalar and vector can be written as:

$$\mathcal{L}_{scalar} = (D_\mu S_i)^\dagger (D^\mu S_i) - m_{S_i}^2 S_i^\dagger S_i, \quad (8.1.4)$$

and

$$\mathcal{L}_{vector} = -\frac{1}{4} V_{\mu\nu}^i V_i^{\mu\nu} + m_V^2 V_{\mu i}^\dagger V^{\mu i} + i g_s V_{\mu i}^\dagger t^a V_\mu^i G_a^{\mu\nu}, \quad (8.1.5)$$

where $V_{\mu\nu}^i = D_\mu V_\nu^i - D_\nu V_\mu^i$. Therefore, the covariant derivative is given by

$$D_\mu = \partial_\mu + i g_s t_a G_\mu^a + i g \frac{1}{2} \vec{\tau} \cdot \vec{W}_\mu + i g' \frac{1}{2} Y B_\mu, \quad (8.1.6)$$

where g_s is the QCD strong coupling constant. Unlike the s -channel mediator, where a single mediator is required, in the t -channel model we require a different mediator for each generation. In general, the interaction given in Lagrangian (8.1.1), (8.1.2) and (8.1.3) induce FCNC, which are strongly constrained by low energy phenomenology. The FCNC constraints can be avoided by imposing a MFV structure on the Yukawa couplings. The parameter space will be consist with the DM candidate mass m_χ , the scalar (vector) couplings $(g_\chi^S)^i \left((c_\chi^V)^i, (g_\chi^V)^i \right)$, and the mediator masses m_S^i (m_V^i), for each generation. For simplicity we will set the couplings and mediator masses for all the generations to be equal. If the mediator mass is in the kinematically accessible region of the LHC, the decay of the mediator and the ensuing signal will become important. The decay width of the scalar and vector mediators $\Gamma(S^i/V^i \rightarrow \chi \bar{u}_i)$, dropping the generation index, are given by:

$$\begin{aligned} \Gamma(S \rightarrow \chi \bar{u}) &= \frac{(g_\chi^S)^2 m_S^5}{96 \pi \Lambda^2 m_\chi^2} \left[1 - \left(\frac{m_\chi}{m_S} + \frac{m_u}{m_S} \right)^2 \right] \left[1 - \left(\frac{m_\chi}{m_S} - \frac{m_u}{m_S} \right)^2 \right] \\ &\quad \times \left[1 - \frac{m_\chi^2}{m_S^2} - \frac{m_u^2}{m_S^2} \right] \lambda^{1/2} \left(1, \frac{m_\chi^2}{m_S^2}, \frac{m_u^2}{m_S^2} \right) \\ &\simeq \frac{(g_\chi^S)^2 m_S^5}{96 \pi \Lambda^2 m_\chi^2} \left(1 - \frac{m_\chi^2}{m_S^2} \right)^4, \end{aligned} \quad (8.1.7)$$

since $m_S^i, m_\chi \gg m_u$ is true for all quarks, except the top quark, and $\lambda(a, b, c) \equiv a^2 + b^2 + c^2 - 2ab - 2ac - 2bc$;

$$\begin{aligned} \Gamma(V \rightarrow \chi \bar{u}) &= \frac{(c_\chi^V)^2 m_V}{288 \pi} \left(1 - \frac{m_\chi^2}{m_V^2} - \frac{m_u^2}{m_V^2} \right) \left[5 + \frac{m_V^2}{m_\chi^2} + \frac{m_\chi^2}{4m_V^2} - \frac{m_u^2}{m_\chi^2} \right. \\ &\quad \left. - \frac{m_u^2}{2m_V^2} + \frac{m_u^4}{4m_V^2 m_\chi^2} \right] \lambda^{1/2} \left(1, \frac{m_\chi^2}{m_V^2}, \frac{m_u^2}{m_V^2} \right) \\ &\simeq \frac{(c_\chi^V)^2 m_V}{288 \pi} \left(1 - \frac{m_\chi^2}{m_V^2} \right)^2 \left(5 + \frac{m_V^2}{m_\chi^2} + \frac{m_\chi^2}{4m_V^2} \right), \end{aligned} \quad (8.1.8)$$

and

$$\begin{aligned} \Gamma(V \rightarrow \chi \bar{u}) &= \frac{(g_\chi^V)^2 m_V^5}{288 \pi \Lambda^2 m_\chi^2} \left[\frac{m_\chi^2}{m_V^2} + \frac{m_\chi^4}{m_V^4} - \frac{3m_\chi^6}{m_V^6} + \left(1 - \frac{m_u^2}{m_V^2} \right)^3 \right. \\ &\quad \left. + \frac{5m_\chi^4 m_u^2}{m_V^6} - \frac{m_\chi^2 m_u^4}{m_V^6} \right] \lambda^{1/2} \left(1, \frac{m_\chi^2}{m_V^2}, \frac{m_u^2}{m_V^2} \right) \\ &\simeq \frac{(g_\chi^V)^2 m_V^5}{288 \pi \Lambda^2 m_\chi^2} \left[1 + \frac{m_\chi^2}{m_V^2} + \frac{m_\chi^4}{m_V^4} - \frac{3m_\chi^6}{m_V^6} \right] \left(1 - \frac{m_\chi^2}{m_V^2} \right), \end{aligned} \quad (8.1.9)$$

for dimension-4 and dimension-5 interaction Lagrangians given in Equations (8.1.2) and (8.1.3) respectively.

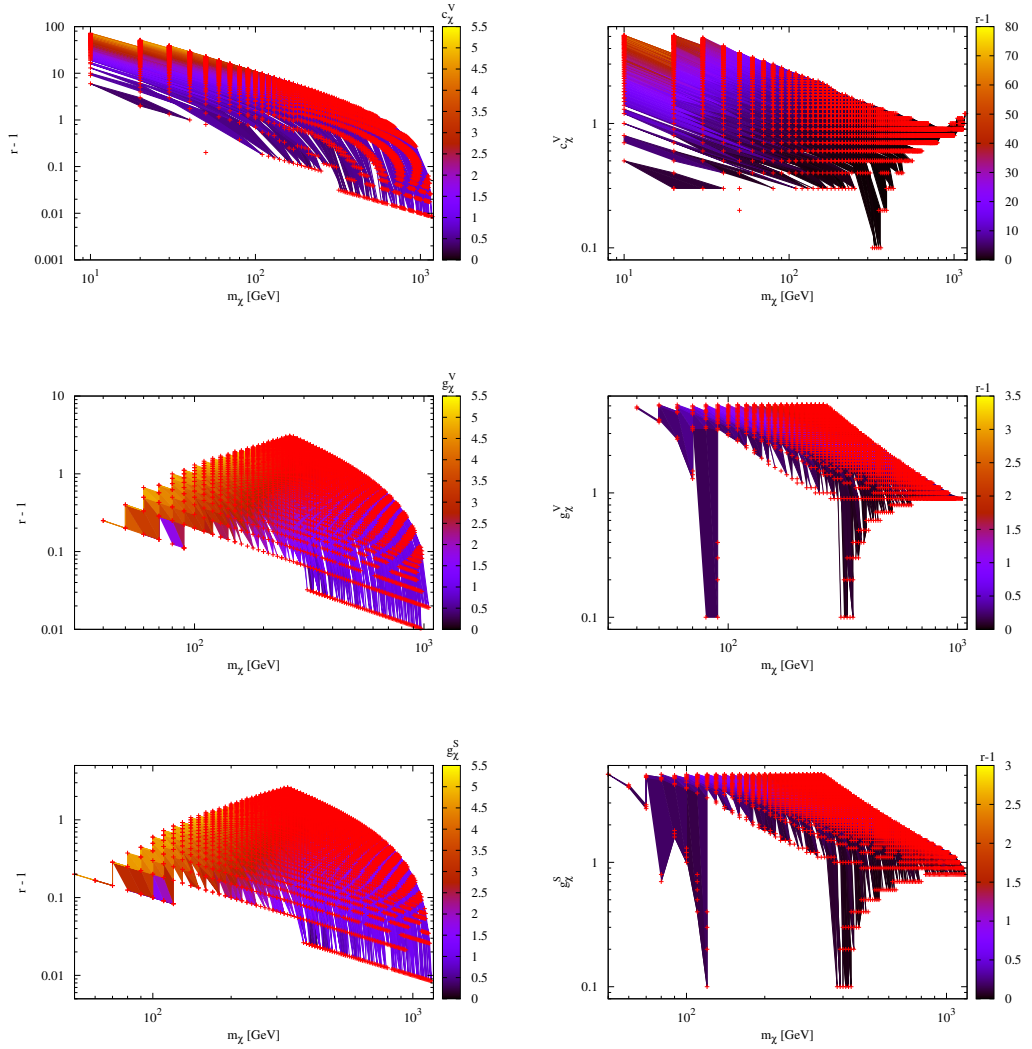


Figure 8.1: *Contour plots in the allowed DM mass m_χ and the mass splitting ratio $r - 1$ (with $r = m_S(m_V)/m_\chi$) in the left panels, and in the DM mass m_χ and the couplings in the right panels. We have assumed that the DM χ saturates the observed relic density. The top panels are for the dimension-4 interaction term for the vector mediator case. The middle and the bottom panels are for dimension-5 vector and scalar mediator cases respectively. In the left panels the colour gradient corresponds to the Yukawa couplings required to give the observed relic density, which in the right panels, the colour gradient corresponds to the mass splitting consistent with the observed relic density.*

8.2 The constraints for the simple t -channel model

In this section we examine the constraints on the model parameters m_χ, m_S, m_V and the coupling constants from the relic density, direct and indirect observations.¹

8.2.1 Relic density.

In the early Universe the DM relic density is determined by the dominant DM annihilation processes $\chi \bar{\chi} \rightarrow u \bar{u}$ mediated by the t -channel exchange of scalar/vector mediators. Since the mediators in this model carry colour and charge co-annihilation processes like $\chi S(V) \rightarrow u g$ and $SS^*(VV^*) \rightarrow gg$, even though exponentially suppressed when mass splitting $(m_{S/V} - m_\chi) >$ freeze-out temperature T_F , will play an important role if the DM mass gets closer to the mediator mass. The co-annihilation processes $\chi S(V) \rightarrow u g$ are mediated by t -channel exchange of mediators as well as by s -channel exchange of gluons and through the four-point interaction involving the DM, mediator, u -quark and the gluon vertex. These processes will reduce the Yukawa coupling needed to generate the required thermal relic abundance. Self annihilation mediator processes $SS^*(VV^*) \rightarrow gg$ are generated by purly gauge interactions and are independent of the Yukawa couplings and have the potential to suppress the relic density below the observed value.

At freeze-out the DM and mediator particles are non-relativistic. In the non-degenerate parameter space, the channel $\chi \bar{\chi} \xrightarrow{S/V} u \bar{u}$ cross-section can be easily evaluated, and in the limit $m_\chi, m_S, m_V \gg m_u$ are given by

$$\langle \sigma(\chi \bar{\chi} \xrightarrow{S} u \bar{u}) | v \rangle \simeq \frac{(g_\chi^S)^4 m_\chi^2}{768 \pi \Lambda^4} \frac{1}{(1 + r^2)^2}, \quad (8.2.1)$$

$$\langle \sigma(\chi \bar{\chi} \xrightarrow{V} u \bar{u}) | v \rangle \simeq \frac{(c_\chi^V)^4}{1536 \pi m_\chi^2} \frac{1}{(1 + r^2)^2} \left[5 - \frac{4}{r^2} + \frac{2}{r^4} \right], \quad (8.2.2)$$

and

$$\langle \sigma(\chi \bar{\chi} \xrightarrow{V} u \bar{u}) | v \rangle \simeq \frac{(g_\chi^V)^4 m_\chi^2}{768 \pi \Lambda^4} \frac{1}{(1 + r^2)^2} \left[5 + \frac{1}{24} \frac{1}{(1 + r^2)^2} \right], \quad (8.2.3)$$

for the scalar-mediator and the vector-mediator dimension-4 and dimension-5 interaction Lagrangians (8.1.1), (8.1.2) and (8.1.3) respectively, and the mass ratio $r = (m_{S/V})/m_\chi$. The thermal relic density of χ 's is obtained by solving the Boltzmann equation (7.2.4).

The annihilation cross-section for the co-annihilation processes $\chi S(V) \rightarrow u g$ in this

¹The work of this chapter is based on our paper [65].

limit are give by ²

$$\langle\sigma(\chi S \rightarrow u g)|v\rangle \simeq \frac{(g_\chi^S)^2 g_s^2}{64\pi\Lambda^2} \frac{(1+r)}{r^3} \left[1 + \frac{14}{9}r + \frac{13}{27}r^2 \right], \quad (8.2.4)$$

$$\begin{aligned} \langle\sigma(\chi V \rightarrow u g)|v\rangle \simeq & \frac{(c_\chi^V)^2 g_s^2}{165888\pi m_\chi^2} \frac{1}{r^6(1+r)} \left[1164 + 5628r + 11403r^2 + 12568r^3 \right. \\ & \left. + 8242r^4 + 2452r^5 + 319r^6 \right], \end{aligned} \quad (8.2.5)$$

and

$$\begin{aligned} \langle\sigma(\chi V \rightarrow u g)|v\rangle \simeq & \frac{(g_\chi^V)^2 g_s^2}{497664\pi\Lambda^2} \frac{1}{r^5(1+r)} \left[372 + 2724r + 6537r^2 + 8742r^3 \right. \\ & \left. + 7072r^4 + 5222r^5 + 307r^6 \right]. \end{aligned} \quad (8.2.6)$$

To calculate the relic density we have implemented the t -channel scalar and vector interactions with SM quarks and spin-3/2 DM including the relevant co-annihilation processes in `micrOMEGAS` [180], which numerically solves the Boltzmann equation by taking the full expressions of the annihilation cross-section.³ We have checked the relic abundance in the non-degenerate parameter space for some representative values of the parameters, and found them to be in agreement with the numerical calculations done by `micrOMEGAS`. The necessary model files for `micrOMEGAS` were built using `FeynRules` [174]. In Figure 8.1 we show the contour graphs in the DM mass and the mass splitting ratio $r - 1$. The colour gradients correspond to the Yukawa couplings in the right panels and to the mass splitting ratio in the left panels to conform to the observed relic density $\Omega_{\text{DM}}h^2 \simeq 0.12$. In the parameter space in which co-annihilation is not important, comparatively large Yukawa couplings are required to obtain the required relic density. In the co-annihilation region on the other hand, we find the couplings to be reduced for almost all DM masses both for the scalar and vector mediator cases. We find that with the increase in DM masses, the co-annihilation channels take over the DM self annihilation processes and the co-annihilation channels involving gauge interactions alone are able to depress the relic density below the observed value. We see from the left-hand panels that there are two regions in the DM mass, one around $80 \text{ GeV} \leq m_\chi \leq 100 \text{ GeV}$ and another one around $300 \text{ GeV} \leq m_\chi \leq 400 \text{ GeV}$, where the co-annihilation processes result in a sharp drop in the couplings, required for the requisite relic density.

²In Appendix E we show the annihilation thermal cross section, in the case where the mediator mass is getting closer to the DM mass.

³The relic density contributed by the DM particles is calculated by taking into account the co-annihilation processes.

8.2.2 Direct detection.

Direct detection experiments [22, 23, 24, 25] on elastic nucleon-DM scattering have provided the most stringent bounds on DM mass and interactions in a large number of conventional DM models. In the t -channel spin-3/2 DM model considered here, the cross-sections at zero momentum transfer can be easily calculated [158, 159, 181]. The dominant contribution to the spin-independent cross-section for the vector mediator case is given by

$$\sigma^{\text{SI}} \simeq \frac{1}{64\pi} \frac{(c_\chi^V)^2 \mu^2}{m_\chi^4 \left[\left(1 + \frac{m_N}{m_\chi}\right)^2 - r^2 \right]^2} f_N, \quad (8.2.7)$$

and

$$\sigma^{\text{SI}} \simeq \frac{1}{64\pi} \left(\frac{g_\chi^V}{\Lambda} \right)^4 \frac{\mu^2}{\left[\left(1 + \frac{m_N}{m_\chi}\right)^2 - r^2 \right]^2} f_N, \quad (8.2.8)$$

where $\mu = (m_\chi m_N) / (m_\chi + m_N)$, $f_N = 4$ for protons and 1 for the neutrons, and we have dropped the terms proportional to the quark mass and momenta in comparison to the leading term. The cross-section given in Equations (8.2.7) and (8.2.8) correspond to the dimension-4 and dimension-5 interaction Lagrangians. The elastic nucleon-DM cross section for the case of scalar mediator is suppressed by terms proportional to quark momenta, and have not been considered here.

In Figure 8.2 we show the predictions for the spin-independent DM-proton scattering cross-sections, σ^{SI} , for the vector mediator case. In the left panels the colour gradient corresponds to the coupling and in the right panels to the mass splitting $r - 1$. In the left panels for every DM mass and mass splitting, the Yukawa coupling is obtained such that the parameters conform to the observed relic density, whereas in the right panels the required mass splitting is obtained for a given Yukawa coupling. We find that for any DM mass, the scattering cross-section generally increases as the degenerate parameter region is approached. This happens because of resonant enhancement of σ^{SI} near $r = 1$. For the case of dimension-5 vector interaction (bottom panels), we see a drop of several orders of magnitude in the scattering cross-section around the same DM mass regions, where the co-annihilation results in a sharp drop in the couplings. In Figure 8.2 we have also shown the current upper limits from LUX [25], PandaX-II [24] and the projected upper limit for the XENON1T experiment [23].

8.2.3 Indirect detection.

The Fermi-LAT collaborations [164] have dedicated detectors to measure cosmic ray fluxes arising from DM annihilation in the Universe. In Figure 8.3 we show the

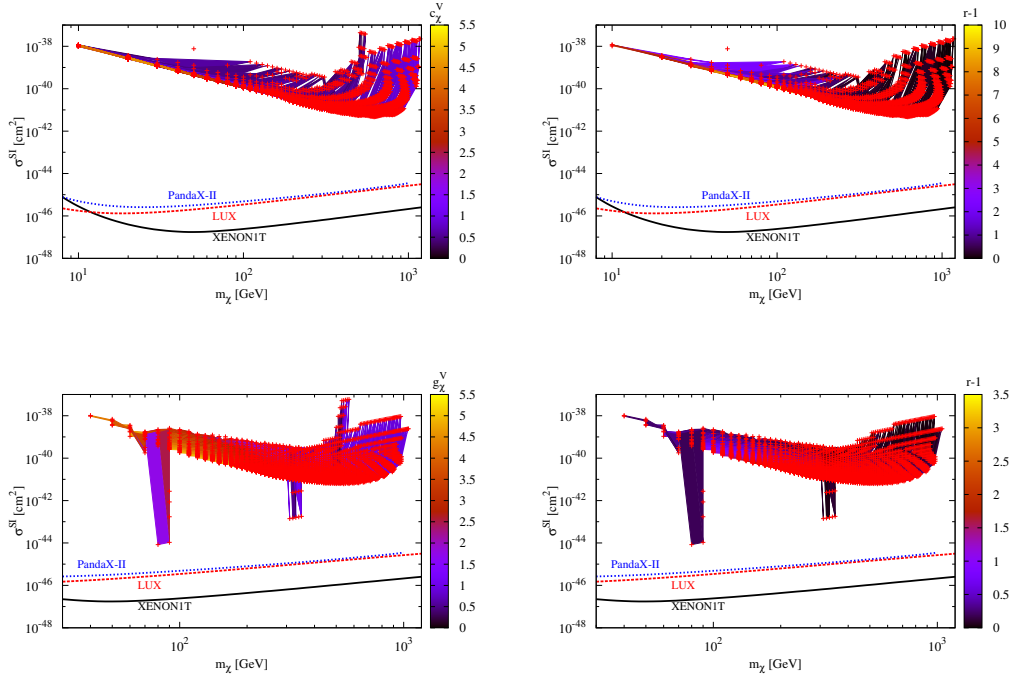


Figure 8.2: The spin-independent proton-DM cross-section σ^{SI} . The top and the bottom panels correspond to dimension-4 and dimension-5 vector interactions. In the left and right panel the colour gradients correspond to the Yukawa couplings and mass splittings respectively. All parameters are consistent with the observed relic density. We have also shown the graphs from the observed current upper limits from LUX [25] and PANDAX-II [24] experiments. The projected upper limit for XENON1T [23] has also been shown. Almost the entire parameter space (m_χ, m_V) for the vector mediator case considered here is already ruled out from the LUX data.

prediction for the total DM annihilation into $u\bar{u}$ for the vector/scalar mediated t -channel model. The predictions shown here are for the DM mass, mediator mass and the couplings consistent with the observed relic density. We have also shown the bounds from the 95% CL upper limits on the thermally-averaged cross-section for DM particles annihilating into $u\bar{u}$ Fermi-LAT observations. As expected in the parameter region where co-annihilation is important ($r \simeq 1$) the $\chi\bar{\chi}$ annihilation cross-section in the $u\bar{u}$ channel is greatly suppressed. Even in the region away from resonance ($r \gg 1$), the Fermi-LAT data does not provide strong bounds on the mass and coupling parameters in the entire range consistent with $\Omega_{\text{DM}}h^2 = 0.12$.

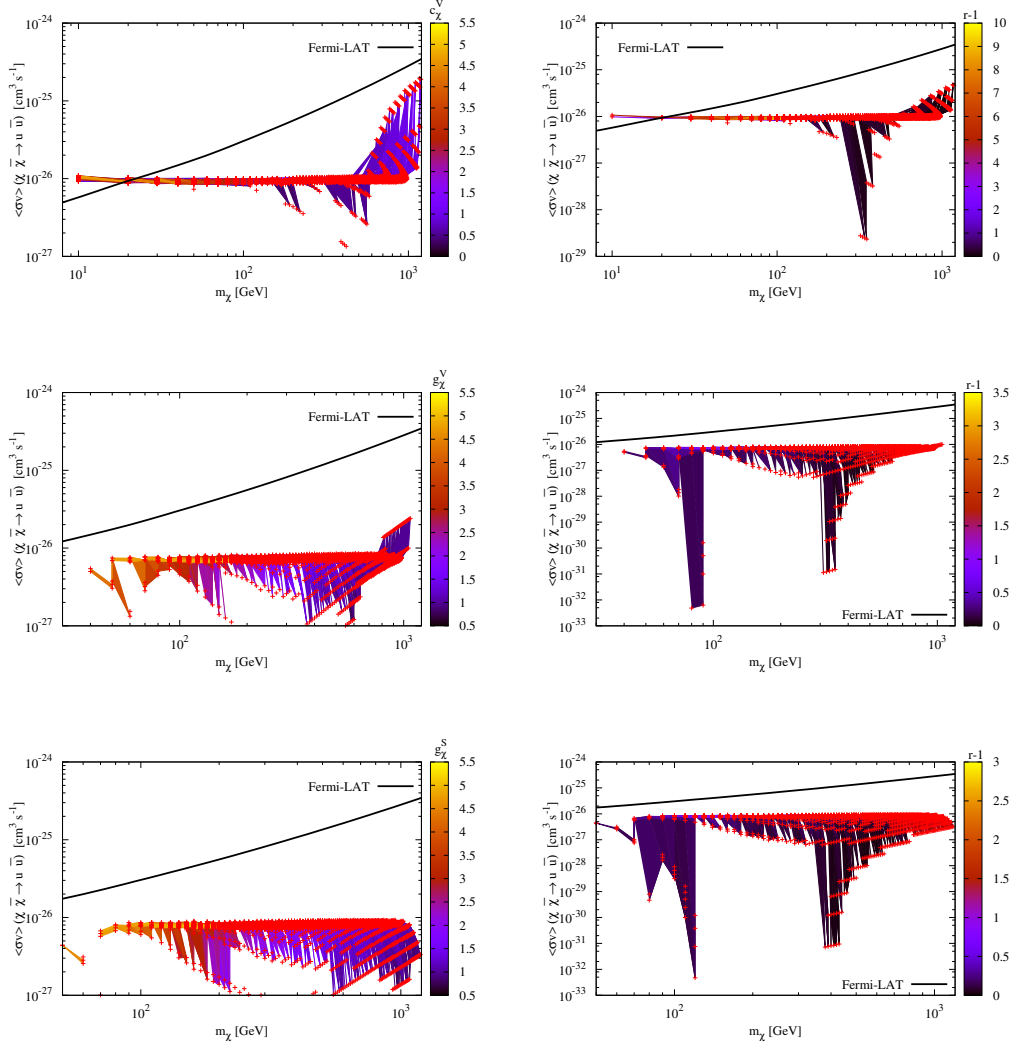


Figure 8.3: The prediction for the DM $\chi\bar{\chi}$ annihilation rate into $u\bar{u}$, as a function of the DM mass m_χ . All the parameters are chosen to be consistent with the observed relic density. The top and the middle panels are for dimension-4 and dimension-5 vector interactions respectively. The bottom panels are for the scalar interaction. The colour gradient in the left and right panels correspond to the coupling and mass splitting respectively. Bounds from the Fermi-LAT experiments are also shown [164].

8.3 Collider bounds

The t -channel mediator model considered here has scalar and vector mediators which carry colour, $SU(2)_L$ and $U(1)$ charges. They can thus be singly produced in association with DM particles, or pair produced if they are light enough at the LHC. These processes will contribute to the monojet and dijet signals with missing energy, with distinct signatures that can be searched for in dedicated searches. For monojet events $qg \rightarrow q\chi\bar{\chi}$, these are dominant processes in comparison to $q\bar{q} \rightarrow g\chi\bar{\chi}$, because of the large parton distribution probability of the gluon, as compared to quark and antiquark in the proton. The authors of the simplified DM model document [161] have emphasised that the dominance of the associated production channels is a distinct feature of t -channel models. The 8 TeV CMS collaboration data based on an integrated luminosity 19.7 fb^{-1} [19, 166] has been used by the authors of Refs. [177, 182] to put bounds on the coupling of fermionic DM as a function of the mediator and DM mass for the case of scalar and vector mediators. In the present study we confine ourselves to constraints arising from the monojet signals using the parameter space $(m_\chi, m_{S/V})$ for different values of the couplings $(g_\chi^S)^i / (g_\chi^V)^i / (c_\chi^V)^i$ consistent with the observed relic density. The cross-section for monojet events is obtained by generating parton level events for the process $pp \rightarrow \chi\bar{\chi}j$ using `MadGraph` [173], where the model file for the Lagrangian is obtained from `FeynRules`, and we use `CTEQ611` parton distribution function for five flavour quarks in the initial state. We employ the usual cuts, and the cross-sections are calculated to put bounds on the parameters of the model by requiring (i) $E_T^{miss} > 250 \text{ GeV}$ and (ii) $E_T^{miss} > 450 \text{ GeV}$, for which the CMS result excludes new contributions to the monojet cross-section for the scalar and vector mediators as shown in Figure 8.4 as function of m_χ , for the values of mediator mass m_S/m_V consistent with the relic density. The results are displayed for some representative values of the couplings. From Figure 8.4 we find that the collider bounds are much weaker compared to the bounds from the direct detection experiments for the vector mediator case. The scalar mediator case is interesting in this case as the collider bound rules out low mass DM particles. The bounds from the monojet + missing energy cross section puts a lower limit on the DM particle mass, where the limit depends on the coupling, and increases with the coupling.

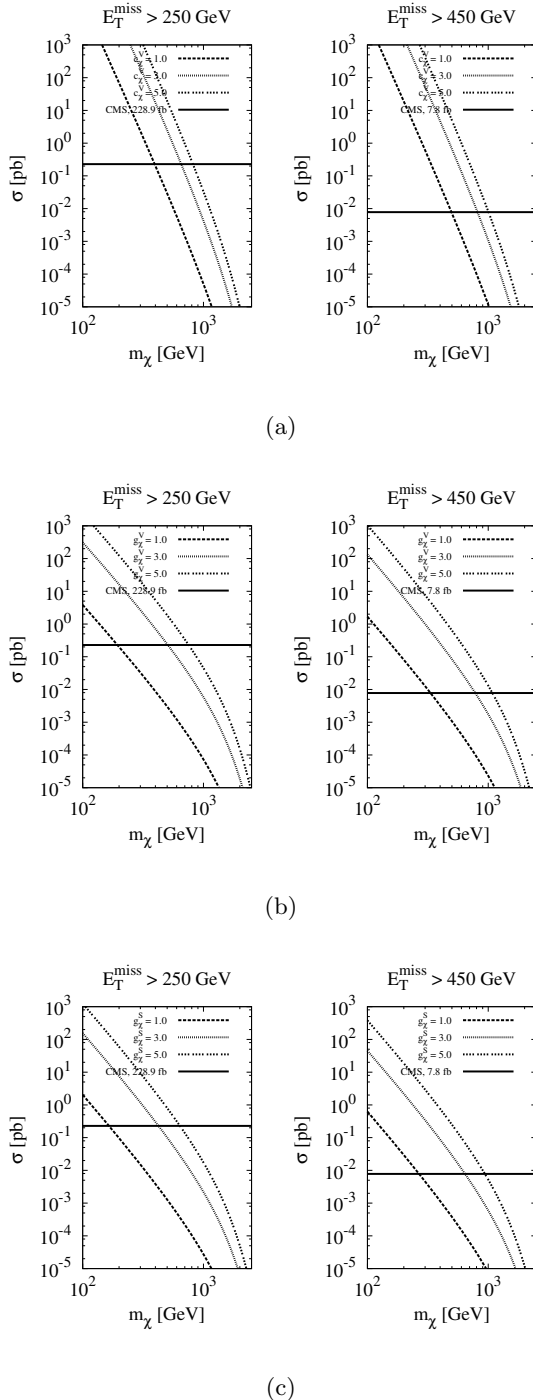


Figure 8.4: The monojet cross-section in [pb] at the LHC with missing energy for two cases (i) $E_T^{\text{miss}} > 250 \text{ GeV}$ and (ii) $E_T^{\text{miss}} > 450 \text{ GeV}$. The cross-sections are obtained for all masses and couplings consistent with the observed relic density. (a) and (b) correspond to the dimension-4 and dimension-5 vector interactions terms respectively and (c) for the dimension-5 interaction term for the scalar mediator. The monojet cross-section from 8 TeV CMS collaboration data [166] based on an integrated luminosity 19.7 fb^{-1} is shown.

8.4 Summary and discussion

The direct detection experiments, through DM-nucleon elastic scattering data, provide the most stringent bounds for the case of a vector mediator. In this case the entire parameter space allowed by the relic density is already ruled out by the LUX data. This result is consistent with the earlier studies of spin-3/2 DM in the EFT [26] frame work for pure vector couplings, as well as in a simplified *s*-channel model [64]. The co-annihilation is unable to ameliorate this situation.

There are no strong bounds from the the direct detection experiments on the scalar mediated interactions due to the velocity suppression of σ^{SI} . In contrast, in the EFT frame work, both the scalar as well as vector interactions give rise to dominant spin-independent nucleon-DM scattering cross-sections and direct detection rules out scalar interactions for spin-3/2 DM particles of masses lying between 10 GeV and 1 TeV [26]. The current constraints from indirect searches, like the Fermi-LAT data, are not sensitive enough to put any meaningful constraints on the parameters.

Monojet searches at the LHC do not provide strong bounds on the vector couplings in comparison to the bounds from direct detection experiments. However, for the case of the scalar mediator, where we do not get any strong bounds from the direct detection experiment, collider bounds put a lower limit on the DM mass which is $m_\chi \geq 300$ GeV. This limit rises with the increase in coupling. Finally, it may be mentioned that bounds from direct detection experiments can, however, be evaded by foregoing the universal coupling between DM mediators and quarks, and letting the DM particles interact with only one generation, say with the third generation quarks (top-philic DM).

Chapter 9

Conclusion

9.1 Summary of key results

In this thesis we show that the running of couplings from the EW scale to the extra-dimension scale needs to be taken into account in order to obtain reliable results. When included, it allows us to obtain simple models of GHU where both the EW gauge couplings and the top Yukawa unify. We have studied a toy model in five-dimensions, compactified on an interval S^1/\mathbb{Z}_2 , with bulk gauge groups $SU(3)_c \times SU(3)_W$ and a bulk fermion transforming as a bi-fundamental. This simple structure is enough to describe the EW gauge sector unified in $SU(3)_W$. The fermions contained in the bulk fermion match a down-type quark, yet the effective Yukawa coupling is enhanced at low energies thanks to the running. We show that the running allows us to match the value of the Weinberg angle at the EW scale, as well as larger than expected Yukawa couplings. Unified values of the couplings appear as an attractor in the UV, providing an example of asymptotic unification. The QCD gauge coupling also unifies, suggesting that the double- $SU(3)$ structure may be symmetric and may be embedded in a larger algebra.

We also derived in this thesis the one-loop RGEs in a five-dimensional GHU model for an $SU(3)$ gauge group by assuming that the fermion doublet and the two singlets are located at the fixed points of the fifth dimension. We tested the evolution of the mass ratios m_u/m_t , m_c/m_t , the CKM elements $|V_{cb}|$, $|V_{ts}|$, the Jarlskog rephasing-invariant, the renormalisation group invariant R_{23} and the evolution of the mixing angle $\sin \theta_{23}$ and $\sin \theta_{12}$. We observed that when the fifth dimension KK-modes became kinematically accessible all the previous physical observables evolution changed rapidly. These physical observables evolutions m_u/m_t , m_c/m_t , $|V_{cb}|$, $|V_{ts}|$, J , R_{23} ,

$\sin \theta_{23}$ and $\sin \theta_{12}$ all over-shot by approximately 14%, 3%, 25%, 26%, 7%, 6%, 12% and 20% respectively.

The one-loop RGEs in five-dimensions for an $SU(5)$ and $SU(5) \times U(1)'$ gauge group compactified on an S_1/\mathbb{Z}_2 have also been derived. We observed that when the fifth dimension KK-modes became kinematically accessible the evolution of the Weinberg angle rapidly increased by approximately 20% for $SU(5)$ and 7% for $SU(5) \times U(1)'$. We also explicitly tested, in a simplified 5-dimensional model with a G_2 gauge symmetry, the evolution of the gauge couplings and Weinberg angle. In this case we observed that when the fifth dimension KK-modes switch on all the previous physical observables evolution changed rapidly. The Weinberg angle rapidly increased by approximately 6% for G_2 gauge group.

As we know, there is no direct evidence in the SM which explains DM, however, in the GHU models we can obtain many additional particles. Note that we can seek these out to use as candidates for DM. Accordingly, we have considered a spin-3/2 DM particle interacting with SM fermions through a vector mediator in the s -channel. Assuming MFV we used universal vector and axial-vector couplings and restricted ourselves to one generation. We also considered a spin-3/2 DM particle interacting with the SM fermions through the exchange of a scalar or a vector mediator in the t -channel. Invoking MFV we restricted ourselves to the coupling of DM candidates with SM singlet right-handed quarks with universal coupling. The thermal relic DM abundance has been computed by taking into account the co-annihilation processes. Co-annihilation has the effect of reducing the Yukawa couplings needed to generate the required DM density. The co-annihilation effects are more pronounced in the large m_χ regime, where mediator self annihilation into gauge bosons has the potential to suppress the relic density below the observed value. Similar behaviour was observed in the t -channel model for spin-1/2 and scalar DM particles [182]. In both s -channel and t -channel models, spin independent cross section bounds from direct detection experiments rule out the parameter space which yields the observed DM abundance, while other experiments yield typically weaker bounds.

9.2 Aspects for future work

Further study is really crucial in order to see whether the phenomenology will change or not when we change the gauge group, by focussing on a more pragmatic or realistic model, such as $SO(5) \times U(1)$. In the case of the $SO(5)$ gauge group, it contains $SU(2) \times U(1)$ into two different ways: firstly, we can have a subgroup which is not a subgroup of $SO(4)$, therefore, in this situation the adjoint representation of $SO(5)$

decomposes as $\mathbf{10} = (3, 0) + (1, 0) + (3, \pm 1)$, thus there is no doublet which can play the role of a SM-like Higgs. As such, this choice is not viable. The other possibility is $\text{SO}(5) \rightarrow \text{SU}(2) \times \text{U}(1) \subset \text{SO}(4)$, where in this case the adjoint representation decomposes into $\mathbf{10} = (3, 0) + (1, 0) + (1, \pm 1) + (2, \pm 1/2)$. In this case there is a complex doublet which can play the role of the Higgs, and furthermore the three singlets and the doublet form the adjoint representation of the $\text{SO}(4)$ subgroup. The other gauge group is F_4 , where this gauge group is rank 4 and contains as maximal subgroups $\text{SU}(3) \times \text{SU}(3)$, $\text{SU}(2) \times \text{Sp}_6$ as well as $\text{SO}(9)$. For instance, the $\text{SO}(5)$ gauge group can decompose under the adjoint representation of $\text{SU}(3) \times \text{SU}(3)$ as $52 \rightarrow (8, 1) + (1, 8) + (6, \bar{3}) + (\bar{6}, 3)$, where in this case the Higgs doublet candidate can be in the adjoint of both the $\text{SU}(3)$ gauge groups. Given these preliminary possible higher rank, more realistic, GHU models which can be studied, further investigations are required.

Furthermore we can test GHU models in 6 dimensions by changing the geometry of the extra-dimensional space. Extensions of our studies to two-loop corrections can also be made.

With larger gauge groups comes the possibility of more additional particles, which when viewed from an effective interacting DM perspective can lead to more intricate phenomenologies. One such further study is to extend the DM into a Higgs portal model, but instead of looking into thermal spin-3/2 DM it will be interesting to look into non-thermal spin-3/2 creation, and then see the phenomenological changes, this creates. We can also study the Sommerfeld enhancement for this spin-3/2 DM, all of which we hope to pursue in up coming works.

Appendix **A**

One-loop correction for gauge coupling coefficients in the SM

In this appendix we shall derive the numerical coefficients of the gauge couplings in the SM. One-loop corrections for gauge coupling coefficients in the SM are given by [70]:

$$16\pi^2 \frac{d g_i}{d t} = b_i^{SM} g_i^3, \quad (\text{A.0.1})$$

where the SM numerical coefficients b_i^{SM} are given by

$$b_i^{SM} = \left(\frac{11}{3} T_{GB}(R) - \frac{4}{3} n_G T_F(R) - \frac{1}{3} n_H T_H(R) \right). \quad (\text{A.0.2})$$

The coefficients in this expression are

$$T(R) \delta_{ab} = \text{Tr} (T_a T_b), \quad (\text{A.0.3})$$

where n_H refers to the number of Higgs scalars in the theory and n_G is the number of generations. $T_H(R)$, $T_F(R)$ and $T_{GB}(R)$ are the Higgs scalar, fermionic and bosonic contributions respectively. As we know, the gauge bosons are in the adjoint representation of the group G , which mean that for $G = \text{SU}(N)$: $T_{GB}(\text{SU}(N)) = N$. Hence, the SM numerical coefficients b_i^{SM} are determined as follows:

A.1 The strong interactions: $\text{SU}(3)_C$

1. $T_{GB}(R)$: The gluons belong to the adjoint representation of $\text{SU}(3)$, which means that $T_{GB}(\text{SU}(3)) = 3$.

2. $T_F(R)$: For one fermionic generation, the contribution is coming from u_α and d_α , hence

$$T_F(1 \text{ generation}) = T_F(3) + T_F(3) = \frac{1}{2} + \frac{1}{2} = 1. \quad (\text{A.1.1})$$

Recall that if we are dealing with Weyl fermions (u_L, u_R, d_L, d_R), then we must include a $1/2$ factor for each helicity, this coming from the fact that $TrL(R) = 1/2$, with $L(R) = (1 \pm \gamma_5)/2$. Thus

$$T_F(1 \text{ generation}) = 4 \cdot \frac{1}{2} \cdot \frac{1}{2} = 1. \quad (\text{A.1.2})$$

3. $T_H(R)$: In the SM gauge group there are no coloured scalars, which means $T_H = 0$.

Finally, we have the numerical coefficient for the strong interaction as:

$$b_3 = \frac{33}{3} - \frac{4}{3} n_G, \quad \text{since we have 3 generations} \Rightarrow b_3 = 7. \quad (\text{A.1.3})$$

A.2 The weak interactions: $SU(2)_L$

$T_{GB}(SU(2)) = 2$, $T_F(1 \text{ generation}) = 4 \cdot \frac{1}{2} \cdot \frac{1}{2} = 1$ (the factor $1/2$ is due to the helicity), and since in the SM we have the standard Higgs doublet, $T_H = 1/2$. Finally, we have the numerical coefficient for the weak interaction as:

$$b_2 = \frac{22}{3} - \frac{4}{3} n_G - \frac{1}{6}, \quad \text{since we have 3 generations} \Rightarrow b_2 = \frac{19}{6}. \quad (\text{A.2.1})$$

A.3 Electromagnetic interactions: $U(1)_{\text{em}}$

Since there are no boson contributions in the hypercharge coefficient b_Y , therefore $T_{GB} = 0$.

$$T_F(1 \text{ generation}) = \sum Q_{em}^2 = 3(Q_u^2 + Q_d^2) + 2(Q_Q^2 + Q_L^2) + Q_e^2 = \frac{10}{3}. \quad (\text{A.3.1})$$

T_H for the SM Higgs is $1/2$, therefore

$$b_1 = \left[-3 \times \frac{4}{3} \times \frac{10}{3} \times \frac{1}{2} - \frac{1}{6} \right] = -\frac{41}{6}. \quad (\text{A.3.2})$$

By using the $SU(5)$ normalisation: $g' = \sqrt{3/5} g_1$. Thus

$$b_1 = -\frac{41}{6} \times \frac{3}{5} = -\frac{41}{10}. \quad (\text{A.3.3})$$

Appendix B

Running of gauge and gauge-scalar couplings in 5D

In this appendix let us consider a theory based on the gauge group

$$\mathcal{G}_{\text{bulk}} = \text{SU}(N)_W \times \text{SU}(N)_c, \quad (\text{B.0.1})$$

where $\text{SU}(N)_W$ contains the EW sector and $\text{SU}(N)_c$ contains QCD colour. In our model we also add a single bulk fermion in the irreducible representation

$$\psi = (R_W, R_c). \quad (\text{B.0.2})$$

Accordingly, the one-loop beta-function for the vector couplings can be easily obtained by using the standard formulas for the running of gauge couplings as:

$$\beta_W = -\frac{11}{3}C(G)_W + \frac{1}{6}C(G)_W + \frac{4}{3}T(R_W)d(R_c), \quad (\text{B.0.3})$$

$$\beta_c = -\frac{11}{3}C(G)_c + \frac{1}{6}C(G)_c + \frac{4}{3}T(R_c)d(R_W). \quad (\text{B.0.4})$$

Note that the formula applies for Dirac fermions and real scalars. The group theory factors are defined as follows:

$$f^{abc}f^{bcd} = C(G)\delta^{ad}, \quad \text{Tr}[T_R^a T_R^b] = T(R)\delta^{ab}, \quad T_R^a T_R^b = C_2(R), \quad (\text{B.0.5})$$

and $d(R)$ is the dimension of the irreducible representation R .

B.1 Running of the gauge-scalar couplings

The running of the gauge-scalars is similar to the one for Yukawa couplings, which receives contributions from the diagrams in Figure B.1. The result of the calculation

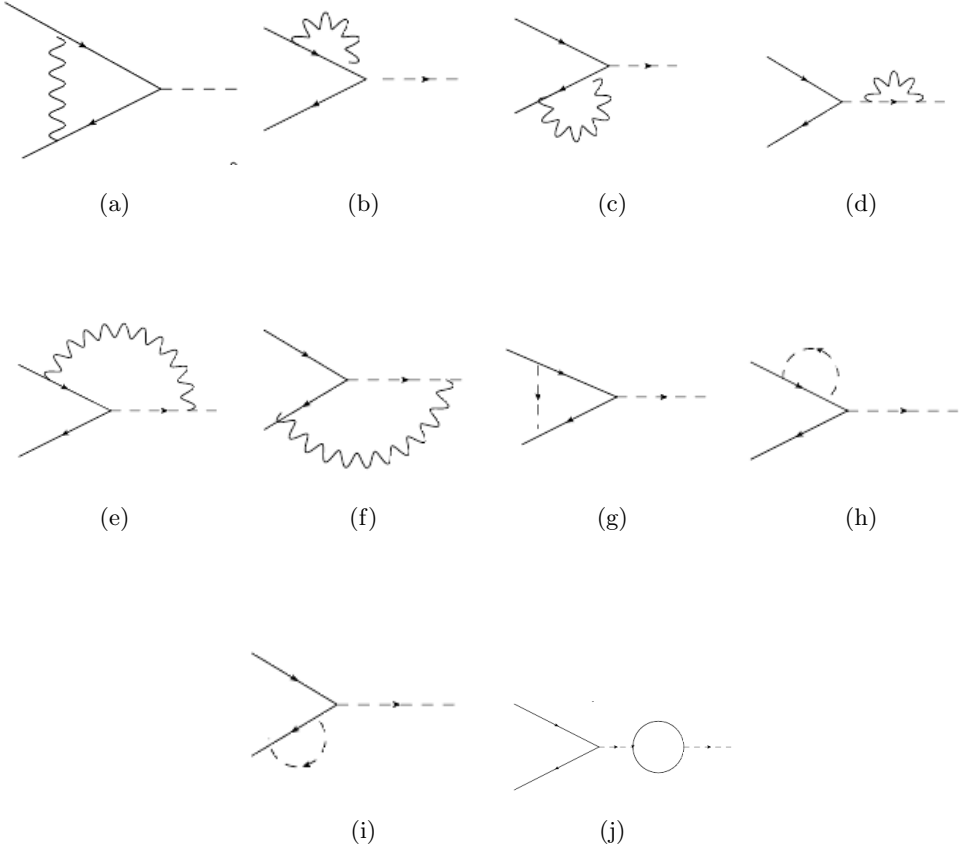


Figure B.1: The diagrams contributing to the running of the gauge-scalar couplings.

can be expressed in a very compact form as follows: We define $T_{L/R}^a$ as the couplings of the gauge vectors to fermions, h^a the couplings of gauge scalars to fermions, and κ_{ij}^a the couplings of the gauge scalars $i-j$ to the gauge bosons a (note that the gauge indices cover all the gauge generators of the two groups in the model). Thus, the contribution of each diagram to the beta function can be written as:

$$\text{Diagram (a)} \Rightarrow gh^i \beta = -8T_L^a \cdot h^i \cdot T_R^a, \quad (\text{B.1.1})$$

$$\text{Diagram (b+c)} \Rightarrow gh^i \beta = T_L^a \cdot T_L^a \cdot h^i + H^i \cdot T_R^a \cdot T_R^a, \quad (\text{B.1.2})$$

$$\text{Diagram (d)} \Rightarrow gh^i \beta = -2h^k \kappa_{kl}^a \kappa_{li}^a, \quad (\text{B.1.3})$$

$$\text{Diagram (e+f)} \Rightarrow gh^i \beta = 2(T_L^a \cdot h^k - h^k \cdot T_R^a) \kappa_{ki}^a, \quad (\text{B.1.4})$$

$$\text{Diagram (g)} \Rightarrow gh^i \beta = 2h^m \cdot h^i \cdot h^m, \quad (\text{B.1.5})$$

$$\text{Diagram (h+i)} \Rightarrow gh^i \beta = \frac{1}{2}(h^m \cdot h^m \cdot h^i + h^i \cdot h^m \cdot h^m), \quad (\text{B.1.6})$$

$$\text{Diagram (j)} \Rightarrow gh^i \beta = 2\text{Tr}[h^i \cdot h^m] h^m \left(\times \frac{1}{2} \text{ for Weyl} \right). \quad (\text{B.1.7})$$

In the model under study: $T_{L/R}^a = gT^a$, $h^i = gT^i$, $\kappa_{ij}^a - igf^{aij}$, where the contribution of each diagram to the beta function of the gauge scalar coupling for $SU(N)_W$

diagram	$SU(N)_W$		$SU(N)_c$	
	g_W^2	g_c^2	g_c^2	g_W^2
a	$-8C_2(R_W) + 4C(G)_W$	$-8C_2(R_c)$	$-8C_2(R_c) + 4C(G)_c$	$-8C_2(R_W)$
b+c	$2C_2(R_W)$	$2C_2(R_c)$	$2C_2(R_c)$	$2C_2(R_W)$
d	$-2C(G)_W$	-	$-2C(G)_c$	-
e+f	$-2C(G)_W$	-	$-2C(G)_c$	-
g	$2C_2(R_W) - C(G)_W$	$2C_2(R_c)$	$2C_2(R_c) - C(G)_c$	$2C_2(R_W)$
h+i	$C_2(R_W)$	$C_2(R_c)$	$C_2(R_c)$	$C_2(R_W)$
j	$2d(R_c) T(R_W)$	-	$2d(R_W) T(R_c)$	-

Table B.1: *The contribution of each diagram to the beta-function.*

and $SU(N)_c$ can be computed in a straightforward manner. The results of these calculations are given in Table B.1.

Therefore, by summing all the contributions from Table B.1, the one-loop beta functions can be written as:

$$\beta_{sW} = (-3C_2(R_W) - C(G)_W + 2d(R_c) T(R_W))g_W^2 - 3C_2(R_c)g_c^2, \quad (\text{B.1.8})$$

$$\beta_{sc} = (-3C_2(R_c) - C(G)_c + 2d(R_W) T(R_c))g_c^2 - 3C_2(R_W)g_W^2. \quad (\text{B.1.9})$$

B.2 $SU(3)_W$ GHU model with bulk triplet

In this section let us consider the case where $N_W = N_c = 3$ and also $R_W = R_c = 3$. Therefore, in this scenario, $C(G) = 3$, $C_2(R) = 4/3$ and $T(R) = 1/2$, and we find

$$\beta_W = \beta_c = -\frac{17}{2}g_{W/c}^2 \quad (\text{B.2.1})$$

$$\beta_{sW} = \beta_{sc} = -4g_W^2 - 4g_c^2. \quad (\text{B.2.2})$$

To compute the running of the SM gauge couplings and Yukawas, which are embedded in $SU(3)_W$, we can use the formulas developed in the previous section. However, we assign different values to the gauge couplings depending on the generator they are associated to. The rules are straightforward for the fermions, where the coupling is g_2 for the 3 generators in $SU(2)$, $g_1 = g'/\sqrt{3}$ for the generator of $U(1)$, and $g_y = \sqrt{2}y$ for the generators belonging to the doublet. The coupling y will be associated to the Yukawa (for the bottom, in this specific toy model).

However, an ambiguity arises when considering the scalar couplings. As we are interested in the running of the coupling of the doublet, the relevant vertices will

always contain 2 doublets (either 2 scalars or one scalar and one vector) and one in the $SU(2) \times U(2)$ group (either vector or scalar). There are two useful choices:

- A) Assign the coupling following the generator associated to the vector in the vertex. This choice allows for a nice limit: the contribution of the first 4 diagrams can be associated to the SM contribution to the running of the SM Yukawa, while the last 3 diagrams to the Yukawa contribution to the running of the Yukawa itself. This fact allows us to cross check the calculation against the SM results.
- B) Assign the coupling to the generators in $SU(2)$ or $U(1)$, i.e. always to the SM gauge coupling. This choice is more physical: In fact, in models where there are more than one coupling of the doublet to the fermions (like in the case $R_W = 6$), there is an ambiguity to what Yukawa to use in the scalar couplings. Thus, this choice is the most physically motivated one.

Thus, choice A will be used as a check, choice B for the physical results.

B.2.1 Choice A.

The beta functions for the couplings of the doublet scalar (i.e. a bottom-like Yukawa) can be extracted by the general formulas by choosing the external generator aligned with the doublet. The results with coupling assignment A are summarised in Table B.2. In bold we indicate the numbers that match to the SM calculation of the bottom Yukawa coupling.

diagram	g'^2	g_2^2	g_c^2	y^2	$g'y$	g_2y
a	4/9		-32/3			
b+c	5/36	3/4	8/3	3		
d	-1/2	-3/2		-6		
e+f	-1/2	-3/2			$-\sqrt{6}/2$	$-3\sqrt{2}$
g	$-1/9$		$8/3$			
h+i	$5/72$	$3/8$	$4/3$	3/2		
j				6		
tot	$-11/24$	$-15/8$	-4	$9/2$	$-\sqrt{6}/2$	$-3/\sqrt{2}$

Table B.2: *Coefficients of the beta-function in case A. In bold are the values corresponding to SM values (for diagram j an extra factor of 1/2 should be taken as the SM is chiral).*

Therefore,

$$\beta_y(SM) = -\frac{5}{12}g'^2 - \frac{9}{4}g_2^2 - 8g_c^2 + \frac{9}{2}y^2. \quad (\text{B.2.3})$$

B.2.2 Choice B.

The results with coupling assignment B are summarised in Table B.3.

diagram	g'^2	g_2^2	g_c^2	y^2
a	4/9		-32/3	
b+c	5/36	3/4	8/3	3
d	-1	-3		
e+f	-1	-3		
g	-1/9		8/3	
h+i	5/72	3/8	4/3	3/2
j				6
tot	-35/24	-39/8	-4	21/2

Table B.3: *Coefficients of the beta-function in case B.*

Therefore,

$$\beta_y(KK) = -\frac{35}{24}g'^2 - \frac{39}{8}g_2^2 - 4g_c^2 + \frac{21}{2}y^2. \quad (\text{B.2.4})$$

B.3 $SU(3)_W$ GHU model with bulk sextet

Consider $N_W = N_c = 3$ with $R_c = 3$ and $R_W = \bar{6}$. In this case the group factors that need to be changed are: $C_2(R_W) = 10/3$ and $T(R_W) = 5/2$. Therefore we find:

$$\beta_W = -\frac{1}{2}g_W^2, \quad (\text{B.3.1})$$

$$\beta_c = -\frac{13}{2}g_c^2, \quad (\text{B.3.2})$$

$$\beta_{sW} = 2g_W^2 - 4g_c^2, \quad (\text{B.3.3})$$

$$\beta_{sc} = -g_c^2 - 10g_W^2. \quad (\text{B.3.4})$$

In this model there are 2 couplings of the Higgs doublets to the components of the sextet:

$$\bar{6}_{SU(3)_W} = 3_{-1/3} \oplus 2_{1/6} \oplus 1_{2/3}. \quad (\text{B.3.5})$$

If we denote ψ_i ($i = 1, 2, 3$) with the singlet, doublet and triplet respectively, the gauge scalar transforming as a doublet (Higgs) couples to the following combinations of fermions:

$$-gH\bar{\psi}_1\psi_2 - \frac{g}{\sqrt{2}}H\bar{\psi}_2\psi_3 + \text{h.c.} = -y_t H\bar{\psi}_1\psi_2 - y_T H\bar{\psi}_2\psi_3 + \text{h.c.} \quad (\text{B.3.6})$$

where y_t will play the role of the top Yukawa coupling. Note also that $y_t = g$ and $y_T = g/\sqrt{2}$ at unification.

As there are two couplings of the scalar to fermions, the coupling assignment A defined in section B.2 is not physical in this case, but simply allows us to calculate the SM running of the couplings y_t and y_T .

Note also that the bulk sextet will have a massless chiral colour triplet: to give it mass and to cancel gauge anomalies, where an opposite chirality partner will need to be added to one of the extra-dimension boundaries and coupled to give it a mass M_T . Thus the SM running of the gauge couplings when $M_T < m_{KK}$, is modified by:

$$\delta\beta_{g'} = \frac{4}{3}, \quad \delta\beta_{g_2} = 8, \quad \delta\beta_{g_c} = 2. \quad (\text{B.3.7})$$

Putting all this together, the beta functions for the SM gauge couplings below and above M_T are given by:

$$\beta_{g'} = \begin{cases} 41/6 \\ 49/6 \end{cases}, \quad \beta_{g_2} = \begin{cases} -19/6 \\ 29/6 \end{cases}, \quad \beta_{g_c} = \begin{cases} -7 \\ -5 \end{cases}. \quad (\text{B.3.8})$$

B.3.1 Choice A.

The coefficients, relative to the SM running of the two Yukawa couplings are reported in Table B.4 (we omitted the coefficients that are not physical). Thus the running of the two Yukawas below the first KK threshold follow is:

$$\beta_{y_t}(SM + T) = -\frac{17}{12}g'^2 - \frac{9}{4}g_2^2 - 8g_c^2 + \frac{9}{2}y_t^2 + \frac{33}{2}y_T^2, \quad (\text{B.3.9})$$

$$\beta_{y_T}(SM + T) = -\frac{5}{12}g'^2 - \frac{33}{4}g_2^2 - 8g_c^2 + \frac{11}{2}y_t^2 + \frac{23}{2}y_T^2. \quad (\text{B.3.10})$$

These equations are valid down to M_T , below which one can integrate out the triplet and the running goes back to the SM:

$$\beta_{y_t}(SM) = -\frac{17}{12}g'^2 - \frac{9}{4}g_2^2 - 8g_c^2 + \frac{9}{2}y_t^2. \quad (\text{B.3.11})$$

B.3.2 Choice B.

The results with coupling assignment B are summarised in Table B.5. They contribute to the running above the first KK threshold.

$$\beta_{y_t}(KK) = -\frac{47}{24}g'^2 - \frac{39}{8}g_2^2 - 4g_c^2 + \frac{21}{2}y_t^2 + \frac{9}{2}y_T^2, \quad (\text{B.3.12})$$

$$\beta_{y_T}(KK) = -\frac{35}{24}g'^2 - \frac{63}{8}g_2^2 - 4g_c^2 + \frac{3}{2}y_t^2 + \frac{51}{2}y_T^2. \quad (\text{B.3.13})$$

running of y_t	g'^2	g_2^2	g_c^2	y_t^2	y_T^2
a	$-8/9$		$-32/3$		
b+c	$17/36$	$3/4$	$8/3$		
d	$-1/2$	$-3/2$			
e+f	$-1/2$	$-3/2$			
g					6
h+i				$3/2$	$3/2$
j				3	9
tot	$-17/12$	$-9/4$	-8	$9/2$	$33/2$

running of y_T	g'^2	g_2^2	g_c^2	y_t^2	y_T^2
a	$4/9$	-8	$-32/3$		
b+c	$5/36$	$11/4$	$8/3$		
d	$-1/2$	$-3/2$			
e+f	$-1/2$	$-3/2$			
g					2
h+i				$1/2$	$5/2$
j				3	9
tot	$-5/12$	$-33/4$	-8	$11/2$	$23/2$

Table B.4: *Coefficients of the beta-function in case A, keeping only the values corresponding to SM running below m_{KK} (for diagram j, an extra factor of 1/2 should be taken as the SM is chiral).*

running y_t	g'^2	g_2^2	g_c^2	y_t^2	y_T^2
a	$-8/9$		$-32/3$		-24
b+c	$17/36$	$3/4$	$8/3$	3	3
d	-1	-3			
e+f	-1	-3			
g	$2/9$		$8/3$		6
h+i	$17/72$	$3/8$	$4/3$	$3/2$	$3/2$
j				6	18
tot	$-47/24$	$-39/8$	-4	$21/2$	$9/2$
running y_T	g'^2	g_2^2	g_c^2	y^2	
a	$4/9$	-8	$-32/3$	-8	
b+c	$5/36$	$11/4$	$8/3$	1	5
d	-1	-3			
e+f	-1	-3			
g	$-1/9$	2	$8/3$	2	
h+i	$5/72$	$11/8$	$4/3$	$1/2$	$5/2$
j				6	18
tot	$-35/24$	$-63/8$	-4	$3/2$	$51/2$

Table B.5: Coefficients of the beta-functions for y_t and y_T in case B.

Appendix **C**

Some calculations for one-loop β -functions

We present in this appendix some examples of the one-loop calculation for the top Yukawa couplings for an $SU(3)$ gauge group.

Our fields in the GHU models have KK modes, and they contribute to the RGEs at the energy scale $E = 1/R$. Up to this scale the evolution is logarithmic and is controlled by the evolution of the SM. The contributions of the KK states should be taken into account beyond this state.

When we calculate the renormalisation constants, we usually ignore the mass terms in the propagators, since they have nothing to do with the divergent part of the one-loop diagrams. We therefore focus on the UV regime, where we can neglect the m/μ dependence of β . We use the dimensional regularisation scheme, in order to calculate the contribution from Figure C.1.(a):

$$\begin{aligned} \Pi_1^{\mu\nu}(p, k) &= \int \frac{d^D k}{(2\pi)^D} y_t^2 \text{Tr} [T^a T^b] \text{Tr} \left[\frac{\gamma^5 (p+k)_\mu \gamma^\mu \gamma^5 k_\nu \gamma^\nu}{(p+k)^2 k^2} \right] \\ &= -y_t^2 \text{Tr} [T^a T^b] \int \frac{d^D k}{(2\pi)^D} (p+k)_\mu k_\nu \text{Tr} [\gamma^\mu \gamma^\nu]. \end{aligned} \quad (\text{C.0.1})$$

By using the relations $\text{Tr} [T^a T^b] = \delta^{ab} C(f) n_f$, and $\text{Tr} [\gamma^\mu \gamma^\nu] = D g^{\mu\nu}$, the above integral can be written as:

$$\Pi_1^{\mu\nu}(p, k) = -y_t^2 \delta^{ab} C(f) n_f D \int \frac{d^D k}{(2\pi)^D} \frac{1}{k^2}, \quad (\text{C.0.2})$$

where n_f is the number of generations, and $C(f)$ refers to the fermion contributions. By multiplying the above integral by $(q+k)^2/(q+k)^2$, we get:

$$\Pi_1^{\mu\nu}(p, k) = -y_t^2 \delta^{ab} C(f) n_f D \int \frac{d^D k}{(2\pi)^D} \frac{(q+k)^2}{k^2 (q+k)^2}. \quad (\text{C.0.3})$$

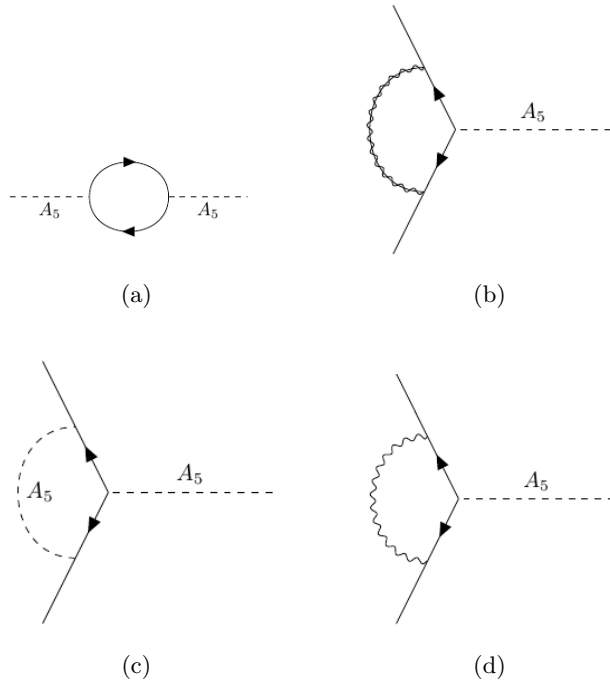


Figure C.1: Contributions to the top Yukawa coupling's RGEs in GHU models in the Landau gauge. The solid lines correspond to the top quarks, the broken lines correspond to A_5 , the wavy lines correspond to the ordinary gauge bosons, while the wavy lines with a line through them correspond to the higher mode components of gauge bosons.

Using the Feynman parametrisation

$$\frac{1}{AB} = \int_0^1 dx \frac{1}{[B + (A - B)x]^2}, \quad (\text{C.0.4})$$

we get

$$\Pi_1 = -y_t^2 \delta^{ab} C(f) n_f D \int \frac{d^D k}{(2\pi)^D} \int_0^1 dx \frac{(q + k)^2}{[k^2 + (q^2 + 2qk)x]^2}. \quad (\text{C.0.5})$$

Now let us introduce a new variable $l = k + qx$. Thus

$$\Pi_1 = -y_t^2 \delta^{ab} C(f) n_f D \int_0^1 dx \int \frac{d^D l}{(2\pi)^D} \frac{\left(l^2 + q^2(1-x)^2\right)}{[l^2 + q^2 x(1-x)]^2}. \quad (\text{C.0.6})$$

Using the following standard integrals:

$$\int d^D l \frac{l^2}{[l^2 + q^2 x(1-x)]^2} = \frac{i \pi^{D/2} \Gamma(1 - D/2) D}{2 [q^2 x (1-x)]^{(1-D/2)}}, \quad (\text{C.0.7})$$

and

$$\int d^D l \frac{1}{[l^2 + q^2 x(1-x)]^2} = \frac{i \pi^{D/2} \Gamma(2 - D/2)}{[q^2 x (1-x)]^{(2-D/2)}}, \quad (\text{C.0.8})$$

Equation (C.0.6) become:

$$\begin{aligned} \Pi_1 = -y_t^2 \delta^{ab} C(f) n_f D \int_0^1 \frac{dx}{(2\pi)^D} & \left[\frac{i \pi^{D/2} \Gamma(1 - D/2) D}{2 [q^2 x (1 - x)]^{(1-D/2)}} \right. \\ & \left. + \frac{i q^2 (1 - x)^2 \pi^{D/2} \Gamma(2 - D/2)}{[q^2 x (1 - x)]^{(2-D/2)}} \right]. \end{aligned} \quad (\text{C.0.9})$$

By integrating over x and substituting $D = 4 - \epsilon$, we get:

$$\Pi_1 = -i y_t^2 \delta^{ab} \frac{4}{3} C(f) n_f P^2 \frac{1}{\epsilon} \frac{1}{16 \pi^2}. \quad (\text{C.0.10})$$

Again, let us use the dimensional regularisation scheme, to calculate the contribution from Figure C.1.(b). Using the same technique to calculate the contributions of Figure C.1.(c) and (d):

$$\begin{aligned} \Pi_2 = 2 y_t g^2 & \left[T^a T^b T^c \right] \int \frac{d^D p}{(2\pi)^D} \left[\gamma^5 \frac{i}{p' + k'} \gamma^\nu \frac{i}{p' - k'} \gamma^\mu \right] \left[\frac{-i g_{\mu\nu}}{p^2 - \left(\frac{n}{R}\right)^2} \right] \\ = 2 i y_t g^2 & \left[T^a T^b T^c \right] \gamma^5 \int \frac{d^D p}{(2\pi)^D} \left[\frac{(p' + k') \gamma^\nu (p' - k') \gamma^\mu g_{\mu\nu}}{(p + k)^2 (p - k)^2 \left(p^2 - \left(\frac{n}{R}\right)^2\right)} \right]. \end{aligned} \quad (\text{C.0.11})$$

By using the relation $T^a T^b T^c = [C(f) - \frac{1}{2} C_2(G)] T^a$, where $C(f)$ and $C_2(G)$ refer to fermion and the gauge bosons respectively, Equation (C.0.11) can be written as:

$$\Pi_2 = 2 \left[C(f) - \frac{1}{2} C_2(G) \right] T^a y_t g^2 \int \frac{d^D p}{(2\pi)^D} \left[\frac{i \gamma^5 (p' + k') \gamma^\nu (p' - k') \gamma^\mu g_{\mu\nu}}{(p + k)^2 (p - k)^2 \left(p^2 - \left(\frac{n}{R}\right)^2\right)} \right]. \quad (\text{C.0.12})$$

Let us simplify the following term:

$$\gamma^5 (p' + k') \gamma^\nu (p' - k') \gamma^\mu g_{\mu\nu} = -\gamma^5 (p + k)_\rho (p - k)_\sigma \gamma^\nu \gamma^\rho \gamma^\sigma \gamma_\nu, \quad (\text{C.0.13})$$

where

$$\gamma^\nu \gamma^\rho \gamma^\sigma \gamma_\nu = 4 g^{\rho\sigma}. \quad (\text{C.0.14})$$

Then, we can rewrite Equation (C.0.13) as follows:

$$\gamma^5 (p' + k') \gamma^\nu (p' - k') \gamma^\mu g_{\mu\nu} = -4 \gamma^5 p_\rho p_\sigma g^{\rho\sigma} + \text{linear term in } p. \quad (\text{C.0.15})$$

Replacing $p_\rho p_\sigma$ by $(p^2 g_{\rho\sigma}/D)$,

$$\gamma^5 (p' + k') \gamma^\nu (p' - k') \gamma^\mu g_{\mu\nu} = -4 \gamma^5 p^2, \quad (\text{C.0.16})$$

and the linear term in p_μ vanishes (because of the angular integral). We can then rewrite Equation (C.0.12) as follows:

$$\Pi_2 = -8i \left[C(f) - \frac{1}{2} C_2(G) \right] \gamma^5 T^a y_t g^2 \int \frac{d^D p}{(2\pi)^D} \frac{p^2}{\left[(p^2)^2 \left(p^2 - \left(\frac{n}{R} \right)^2 \right) \right]}, \quad (\text{C.0.17})$$

by expanding $\frac{1}{p^2 - \left(\frac{n}{R} \right)^2}$ for $p^2 \gg \left(\frac{n}{R} \right)^2$. This will lead to:

$$\frac{1}{p^2 - \left(\frac{n}{R} \right)^2} \simeq \frac{1}{p^2} + \frac{(n/R)^2}{p^4} + \mathcal{O}(p^{-6}), \quad (\text{C.0.18})$$

and by using this approximation, one can rewrite Equation (C.0.17) as:

$$\begin{aligned} \Pi_2 &= -8i \left[C(f) - \frac{1}{2} C_2(G) \right] \gamma^5 T^a y_t g^2 \int \frac{d^D p}{(2\pi)^D} \left[\frac{1}{(p^2)^2} + \frac{(n/R)^2}{(p^2)^3} \right] \\ &= -8i^2 \left[C(f) - \frac{1}{2} C_2(G) \right] \gamma^5 T^a y_t g^2 \frac{\pi^{D/2}}{(2\pi)^D} \left[\Gamma \left(2 - \frac{D}{2} \right) \right. \\ &\quad \left. + \left(\frac{n}{R} \right)^2 \frac{1}{2} \Gamma \left(3 - \frac{D}{2} \right) \right]. \end{aligned} \quad (\text{C.0.19})$$

Now by using the fact that $x\Gamma(x) = \Gamma(1+x)$

$$\begin{aligned} \Pi_2 &= -8i \left[C(f) - \frac{1}{2} C_2(G) \right] \gamma^5 T^a y_t g^2 \int \frac{d^D p}{(2\pi)^D} \left[\frac{1}{(p^2)^2} + \frac{(n/R)^2}{(p^2)^3} \right] \\ &= -8i^2 \left[C(f) - \frac{1}{2} C_2(G) \right] \gamma^5 T^a y_t g^2 \frac{\pi^{D/2}}{(2\pi)^D} \Gamma \left(2 - \frac{D}{2} \right) \\ &\quad \times \left[1 + \left(\frac{n}{R} \right)^2 \frac{1}{2} \left(2 - \frac{D}{2} \right) \right]. \end{aligned} \quad (\text{C.0.20})$$

Let us define $\epsilon = 4 - D$, having cancelled out the singular term, we may let $\epsilon \rightarrow 0$, and the finite renormalised result will be:

$$\Pi_2 = 8 \left[C(f) - \frac{1}{2} C_2(G) \right] \gamma^5 T^a y_t g^2 \frac{1}{16\pi^2} \frac{2}{\epsilon}. \quad (\text{C.0.21})$$

Thus

$$Z_1 = 1 - 8 \left[C(f) - \frac{1}{2} C_2(G) \right] \gamma^5 T^a y_t g^2 \frac{1}{16\pi^2} \frac{2}{\epsilon} \mu^{\epsilon/2}, \quad (\text{C.0.22})$$

where μ is an arbitrary quantity called the renormalisation scale, then

$$-\mu \frac{\partial}{\partial \mu} Z_1 = 8 \left[C(f) - \frac{1}{2} C_2(G) \right] \gamma^5 T^a y_t g^2 \frac{1}{16\pi^2}. \quad (\text{C.0.23})$$

Appendix **D**

Full expression for the decay widths and cross-section

In this appendix we will determine the decay widths of $Z' \rightarrow \chi\bar{\chi}, f\bar{f}$ and the cross-sections for the spin-3/2 DM annihilation into SM fermions $\chi\bar{\chi} \rightarrow f\bar{f}$.

D.1 Decay widths

The squared matrix element for the mediator Z'_μ decay into $\chi\bar{\chi}$ and into $f\bar{f}$ in the limit when $s \rightarrow m_{Z'}^2$, are given by:

$$|\mathcal{M}(Z' \rightarrow \chi\bar{\chi})|^2 = \frac{1}{9m_\chi^4} \left[16m_\chi^6 \left(10(g_\chi^A)^2 - 9(g_\chi^V)^2 \right) + 8m_\chi^4 m_{Z'}^2 \right. \\ \times \left((g_\chi^V)^2 - 13(g_\chi^A)^2 \right) + 8m_\chi^2 m_{Z'}^4 \left(4(g_\chi^A)^2 + (g_\chi^V)^2 \right) \\ \left. - 4m_{Z'}^6 \left((g_\chi^A)^2 + (g_\chi^V)^2 \right) \right], \quad (\text{D.1.1})$$

and

$$|\mathcal{M}(Z' \rightarrow f\bar{f})|^2 = \left[8m_f^2 \left(2(g_f^A)^2 - (g_f^V)^2 \right) - 4m_{Z'}^2 \left((g_f^A)^2 + (g_f^V)^2 \right) \right]. \quad (\text{D.1.2})$$

Therefore, the decay widths for the mediator Z'_μ decay into $\chi\bar{\chi}$ and into $f\bar{f}$ are given by:

$$\Gamma(Z' \rightarrow \chi\bar{\chi}) = \frac{1}{108\pi m_\chi^4 m_{Z'}} \sqrt{1 - \frac{4m_\chi^2}{m_{Z'}^2}} \left[(g_\chi^A)^2 (-40m_\chi^6 + 26m_\chi^4 m_{Z'}^2 - 8m_\chi^2 m_{Z'}^4 + m_{Z'}^6) \right. \\ \left. + (g_\chi^V)^2 (36m_\chi^6 - 2m_\chi^4 m_{Z'}^2 - 2m_\chi^2 m_{Z'}^4 + m_{Z'}^6) \right], \quad (\text{D.1.3})$$

and

$$\Gamma(Z' \rightarrow f\bar{f}) = \frac{1}{12\pi m_{Z'}} \sqrt{1 - \frac{4m_f^2}{m_{Z'}^2}} \left[2m_f^2 \left((g_f^V)^2 - 2(g_f^A)^2 \right) + m_{Z'}^2 \left((g_f^A)^2 + (g_f^V)^2 \right) \right]. \quad (\text{D.1.4})$$

D.2 Cross-section

From the Feynman diagram in Figure D.1 we have the amplitude is given as follows

$$i\mathcal{M} = \left\{ \bar{v}_\chi^\alpha(p_2) \gamma^\mu (g_\chi^V - \gamma^5 g_\chi^A) u_\chi^\alpha(p_1) \right\} \left[-g_{\mu\nu} + \frac{p_\mu p_\nu}{m_{Z'}^2} \right] \times \left\{ \bar{u}_f^\beta(p_3) \gamma^\nu (g_f^V - \gamma^5 g_f^A) v_f^\beta(p_4) \right\}. \quad (\text{D.2.1})$$

Therefore, we have

$$|\mathcal{M}|^2 = \left\{ \bar{v}_\chi^\alpha(p_2) \gamma^\mu (g_\chi^V - \gamma^5 g_\chi^A) u_\chi^\alpha(p_1) \right\} \left[-g_{\mu\nu} + \frac{p_\mu p_\nu}{m_{Z'}^2} \right] \times \left\{ \bar{u}_f^\beta(p_3) \gamma^\nu (g_f^V - \gamma^5 g_f^A) v_f^\beta(p_4) \right\} \times \left\{ \bar{v}_f^b(p_4) \gamma^{\nu'} (g_f^V - \gamma^5 g_f^A) u_f^b(p_3) \right\} \left[-g_{\mu'\nu'} + \frac{p_{\mu'} p_{\nu'}}{m_{Z'}^2} \right] \times \left\{ \bar{u}_\chi^a(p_1) \gamma^{\mu'} (g_\chi^V - \gamma^5 g_\chi^A) v_\chi^a(p_2) \right\}. \quad (\text{D.2.2})$$

Thus, we have the spin-3/2 polarisation sums are given as:

$$\sum_{i=-3/2}^{3/2} u_\mu^i(p) \bar{u}_\nu^i(p) = -(p' + m_\chi) \left[g_{\mu\nu} - \frac{1}{3} \gamma_\mu \gamma_\nu - \frac{2}{3m_\chi^2} p_\mu p_\nu - \frac{1}{3m_\chi} (\gamma_\mu p_\nu - \gamma_\nu p_\mu) \right], \quad (\text{D.2.3})$$

$$\sum_{i=-3/2}^{3/2} v_\mu^i(p) \bar{v}_\nu^i(p) = -(p' - m_\chi) \left[g_{\mu\nu} - \frac{1}{3} \gamma_\mu \gamma_\nu - \frac{2}{3m_\chi^2} p_\mu p_\nu + \frac{1}{3m_\chi} (\gamma_\mu p_\nu - \gamma_\nu p_\mu) \right]. \quad (\text{D.2.4})$$

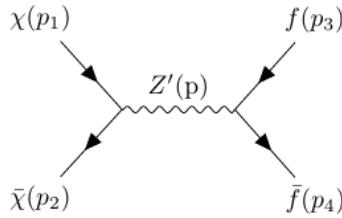


Figure D.1: The Feynman diagram for the spin-3/2 DM annihilation into SM fermions $\chi\bar{\chi} \rightarrow Z' \rightarrow f\bar{f}$.

For the fermion the polarisation sums are given as:

$$\sum_{i=-1/2}^{1/2} u_f^i(p) \bar{u}_f^i(p) = p' + m_f; \quad \sum_{i=-1/2}^{1/2} v_f^i(p) \bar{v}_f^i(p) = p' - m_f. \quad (\text{D.2.5})$$

The squared matrix element for the spin-3/2 DM annihilating into SM fermions are given by

$$\begin{aligned} |\mathcal{M}(\chi\bar{\chi} \rightarrow f\bar{f})|^2 &= \frac{1}{27 m_\chi^4 m_{Z'}^4 (m_{Z'}^4 + m_{Z'}^2 (\Gamma^2 - 2s) + s^2)} \\ &\times 32 \left[(g_f^A)^2 \left\{ (g_\chi^A)^2 \left\{ 4m_f^2 \left((10m_\chi^6 (7m_{Z'}^4 - 6m_{Z'}^2 s + 3s^2)) \right. \right. \right. \right. \\ &\quad - 2m_\chi^4 s (16m_{Z'}^4 - 6m_{Z'}^2 s + 3s^2) - m_{Z'}^4 s^3 \\ &\quad \left. \left. \left. \left. + m_\chi^2 s^2 (11m_{Z'}^4 - 6m_{Z'}^2 s + 3s^2) \right) + m_{Z'}^4 s \right\} \right. \\ &\quad \times \left(-40m_\chi^6 + 26m_\chi^4 s - 8m_\chi^2 s^2 + s^3 \right) \left. \right\} - (g_\chi^V)^2 m_{Z'}^4 \\ &\quad \times (4m_f^2 - s) (36m_\chi^6 - 2m_\chi^4 s - 2m_\chi^2 s^2 + s^3) \left. \right\} \\ &\quad + (g_f^V)^2 m_{Z'}^4 (2m_f^2 + s) \left\{ (g_\chi^A)^2 \left(-40m_\chi^6 + 26m_\chi^4 s \right. \right. \\ &\quad \left. \left. - 8m_\chi^2 s^2 + s^3 \right) + (g_\chi^V)^2 \left(36m_\chi^6 - 2m_\chi^4 s - 2m_\chi^2 s^2 + s^3 \right) \right\} \right]. \end{aligned} \quad (\text{D.2.6})$$

The full expressions of the annihilation cross-section of spin-3/2 DM into SM fermions, in the non-relativistic approximation ($s \simeq 4m_\chi^2 + m_\chi^2 v^2$) are given by the following expression:

$$\begin{aligned} \langle \sigma(\chi\bar{\chi} \rightarrow f\bar{f}) v \rangle &= \sum_f N_f \left[\frac{m_\chi \sqrt{1 - \frac{4m_f^2}{m_\chi^2(v^2+4)}}}{432\pi m_{Z'}^4 \sqrt{m_\chi^2(v^2+4)}} \right] \left[\frac{1}{(m_{Z'}^2 - m_\chi^2(v^2+4))^2 + \Gamma^2 m_{Z'}^2} \right] \\ &\times \left[(g_f^A)^2 \left\{ (g_\chi^A)^2 \left\{ 4m_f^2 \left\{ 3m_\chi^4(v^2+4)^2(v^4+6v^2+18) \right. \right. \right. \right. \right. \\ &\quad - 6m_\chi^2 m_{Z'}^2(v^2+4)(v^4+6v^2+18) - m_{Z'}^4(v^6+v^4-8v^2-54) \right\} \\ &\quad + m_\chi^2 m_{Z'}^4 v^2(v^2+4)(v^4+4v^2+10) \left. \right\} \\ &\quad + (g_\chi^V)^2 m_{Z'}^4 (v^6+10v^4+30v^2+60)(m_\chi^2(v^2+4) - 4m_f^2) \left. \right\} \\ &\quad + (g_f^V)^2 m_{Z'}^4 \left\{ (g_\chi^A)^2 v^2(v^4+4v^2+10) \right. \\ &\quad + (g_\chi^V)^2 (v^6+10v^4+30v^2+60) \left. \right\} (2m_f^2 + m_\chi^2(v^2+4)) \right]. \end{aligned} \quad (\text{D.2.7})$$

The expressions for a and b are given by:

$$a = \frac{2\sqrt{1 - \frac{m_f^2}{m_\chi^2}}}{9\pi m_{Z'}^4 \left((m_{Z'}^2 - 4m_\chi^2)^2 + \Gamma^2 m_{Z'}^2 \right)} \left[9(g_f^A)^2 (g_\chi^A)^2 m_f^2 (m_{Z'}^2 - 4m_\chi^2)^2 + 10(g_\chi^V)^2 (g_f^A)^2 m_{Z'}^4 (m_\chi^2 - m_f^2) + 5(g_f^V)^2 (g_\chi^V)^2 m_{Z'}^4 (m_f^2 + 2m_\chi^2) \right], \quad (\text{D.2.8})$$

and

$$b = \frac{1}{108\pi m_\chi^2 m_{Z'}^4 \sqrt{1 - \frac{m_f^2}{m_\chi^2} \left((m_{Z'}^2 - 4m_\chi^2)^2 + \Gamma^2 m_{Z'}^2 \right)^2}} \left[\begin{aligned} & \times \left[(g_f^A)^2 \left\{ (g_\chi^A)^2 \left\{ (m_{Z'}^2 - 4m_\chi^2)^2 \right. \right. \right. \right. \\ & \times \left. \left. \left. \left. m_f^4 (-288m_\chi^4 + 144m_\chi^2 m_{Z'}^2 + 22m_{Z'}^4) + 5m_f^2 m_\chi^2 \right. \right. \right. \\ & \times \left. \left. \left. (12m_\chi^2 - 7m_{Z'}^2) (12m_\chi^2 + m_{Z'}^2) + 40m_\chi^4 m_{Z'}^4 \right. \right. \right. \\ & + \left. \left. \left. \Gamma^2 m_{Z'}^2 \left\{ m_f^4 (-2016m_\chi^4 + 576m_\chi^2 m_{Z'}^2 + 22m_{Z'}^4) \right. \right. \right. \\ & + m_f^2 (2448m_\chi^6 - 792m_\chi^4 m_{Z'}^2 - 35m_\chi^2 m_{Z'}^4) \\ & + 40m_\chi^4 m_{Z'}^4 \right. \right. \right. \\ & \times \left. \left. \left. m_f^2 (32m_\chi^4 - 2m_{Z'}^2 (\Gamma^2 + m_{Z'}^2)) \right. \right. \right. \\ & + m_\chi^2 (16m_\chi^4 - 24m_\chi^2 m_{Z'}^2 + 5m_{Z'}^2 (\Gamma^2 + m_{Z'}^2)) \right\} \right] \\ & - 5(g_f^V)^2 m_{Z'}^4 \left\{ 4(g_\chi^A)^2 (m_f^4 + m_f^2 m_\chi^2 - 2m_\chi^4) \right. \\ & \times \left. \left((m_{Z'}^2 - 4m_\chi^2)^2 + \Gamma^2 m_{Z'}^2 \right) + 3(g_\chi^V)^2 \left\{ \Gamma^2 m_{Z'}^2 \right. \right. \\ & \times \left. \left. (2m_f^4 + 5m_f^2 m_\chi^2 - 10m_\chi^4) - (4m_\chi^2 - m_{Z'}^2) \right. \right. \\ & \times \left. \left. \left. 8m_f^4 m_\chi^2 - 4m_f^2 m_\chi^4 + m_{Z'}^2 (2m_f^4 + 5m_f^2 m_\chi^2 - 10m_\chi^4) \right. \right. \right. \\ & + 8m_\chi^6 \right\} \right\} \right]. \quad (\text{D.2.9}) \end{aligned}$$

Appendix **E**

The thermal cross-section for $\chi S \rightarrow u g$

In this appendix we will derive the annihilation thermal cross section in the case where the mediator mass is approaching the DM mass. For example, we will take only the case when the mediator is a scalar $\chi(p_1) S(p_2) \rightarrow u(p_3) g(p_4)$, with $p_1^2 = m_\chi^2$, $p_2^2 = m_S^2$, $p_3^2 = 0$, $p_4^2 = 0$, $s = (p_1 + p_2)^2$ and $t = (p_1 - p_3)^2$. Actually the contributions largely come from six diagrams, and have the following propagators $\frac{1}{(t - m_S^2)^2}$, $\frac{1}{(t - m_S^2)}$, $\frac{1}{(t - m_S^2)s}$, $\frac{1}{s^2}$, $\frac{1}{s}$, 1. In the propagators we replace s and t by their non-relativistic approximations, namely,

$$s \simeq (m_\chi + m_S)^2, \quad t \simeq -(m_\chi m_S), \quad (\text{E.0.1})$$

such that

$$t - m_S^2 \simeq -m_S(m_\chi + m_S). \quad (\text{E.0.2})$$

In which case we can express the differential cross-section as:

$$\frac{d\sigma}{d\cos\theta} = \left(\frac{1}{3}\right) \left(\frac{1}{4}\right) \left(\frac{1}{32\pi}\right) \left(\frac{\sum |\mathcal{M}|^2 d \cos\theta}{\lambda^{1/2}(s, m_\chi^2, m_S^2)}\right), \quad (\text{E.0.3})$$

where

$$\lambda^{1/2}(s, m_\chi^2, m_S^2) = [s^2 + m_\chi^4 + m_S^4 - 2s m_\chi^2 - 2s m_S^2 - 2m_\chi^2 m_S^2]^{1/2}. \quad (\text{E.0.4})$$

In the non-relativistic approximation we only keep the terms proportional to v^2 , where v is the relative velocity between the DM χ and the mediator S . As such

$$s = \left(M + \frac{1}{2}\mu v^2\right)^2 \simeq M^2 + \mu M v^2, \quad (\text{E.0.5})$$

where $M = m_\chi + m_S$, and $\mu = m_\chi m_S / (m_\chi + m_S)$, by substituting we get

$$\lambda^{1/2} (s, m_\chi^2, m_S^2) \rightarrow 2 m_\chi m_S v. \quad (\text{E.0.6})$$

Therefore

$$\langle \sigma(\chi S \rightarrow u g) | v \rangle = \left(\frac{1}{3} \right) \left(\frac{1}{4} \right) \left(\frac{1}{32\pi} \right) \left(\frac{1}{2m_\chi m_S} \right) \int \sum |\mathcal{M}|^2 d \cos \theta. \quad (\text{E.0.7})$$

We now replace s by $s \rightarrow (m_\chi + m_S)^2$ in the expression of $\sum |\mathcal{M}|^2$, by neglecting the terms proportional to v^2 . Similarly, we can follow the same strategy for the case of the dimension-4 and dimension-5 vector mediators. Finally, the annihilation cross-section for the co-annihilation processes $\chi S(V) \rightarrow u g$ in this limit are give by:

- For the scalar case

$$\langle \sigma(\chi S \rightarrow u g) | v \rangle = \frac{(g_\chi^S)^2 g_s^2}{1728 \pi \Lambda^2 m_S^3} \left[(m_S + m_\chi) (13 m_S^2 + 42 m_S m_\chi + 27 m_\chi^2) \right]. \quad (\text{E.0.8})$$

- For the 5-dimension vector case

$$\begin{aligned} \langle \sigma(\chi V \rightarrow u g) | v \rangle = & \frac{(g_\chi^V)^2 g_s^2}{497664 \pi \Lambda^2 m_V^5 (m_V + m_\chi)} \left[307 m_V^6 + 5222 m_V^5 m_\chi + 372 m_\chi^6 \right. \\ & \left. + 7072 m_V^4 m_\chi^2 + 8742 m_V^3 m_\chi^3 + 6537 m_V^2 m_\chi^4 + 2724 m_V m_\chi^5 \right]. \end{aligned} \quad (\text{E.0.9})$$

- Finally, the 4-dimension vector case

$$\begin{aligned} \langle \sigma(\chi V \rightarrow u g) | v \rangle = & \frac{(c_\chi^V)^2 g_s^2}{165888 \pi m_V^7 (m_V + m_\chi)} \left[319 m_V^6 + 2452 m_V^5 m_\chi + 1164 m_\chi^6 \right. \\ & \left. + 8242 m_V^4 m_\chi^2 + 12568 m_V^3 m_\chi^3 + 11403 m_V^2 m_\chi^4 + 5628 m_V m_\chi^5 \right]. \end{aligned} \quad (\text{E.0.10})$$

References

- [1] Cacciapaglia, Giacomo and Kubik, Bogna, “Even tiers and resonances on the real projective plane,” *JHEP*, vol. 2013, no. 2, p. 52, 2013.
- [2] G. Aad *et al.*, “Observation of a new particle in the search for the Standard Model Higgs boson with the ATLAS detector at the LHC,” *Phys. Lett.*, vol. B716, pp. 1–29, 2012.
- [3] S. Chatrchyan *et al.*, “Observation of a new boson at a mass of 125 GeV with the CMS experiment at the LHC,” *Phys. Lett.*, vol. B716, pp. 30–61, 2012.
- [4] G. Aad *et al.*, “Measurement of the Higgs boson mass from the $H \rightarrow \gamma\gamma$ and $H \rightarrow ZZ^* \rightarrow 4\ell$ channels with the ATLAS detector using 25 fb^{-1} of pp collision data,” *Phys. Rev.*, vol. D90, no. 5, p. 052004, 2014.
- [5] Abdalgabar, Ammar and Cornell, A. S. and Deandrea, Aldo and Tarhini, Ahmad, “Evolution of Yukawa couplings and quark flavor mixings in two universal extra dimension models,” *Phys. Rev.*, vol. D88, no. 5, p. 056006, 2013.
- [6] G. Bhattacharyya, A. Datta, S. K. Majee, and A. Raychaudhuri, “Power law blitzkrieg in universal extra dimension scenarios,” *Nucl. Phys.*, vol. B760, pp. 117–127, 2007.
- [7] M. Masip and A. Pomarol, “Effects of SM Kaluza-Klein excitations on electroweak observables,” *Phys. Rev.*, vol. D60, p. 096005, 1999.
- [8] G. Burdman and Y. Nomura, “Unification of Higgs and gauge fields in five-dimensions,” *Nucl. Phys.*, vol. B656, pp. 3–22, 2003.
- [9] G. Bertone, D. Hooper, and J. Silk, “Particle dark matter: Evidence, candidates and constraints,” *Phys. Rept.*, vol. 405, pp. 279–390, 2005.

- [10] Csaki, Csaba and Grojean, Christophe and Murayama, Hitoshi, “Standard model Higgs boson from higher dimensional gauge fields,” *Physical Review D*, vol. 67, no. 8, p. 085012, 2003.
- [11] Jungman, Gerard and Kamionkowski, Marc and Griest, Kim, “Supersymmetric dark matter,” *Physics Reports*, vol. 267, no. 5-6, pp. 195–373, 1996.
- [12] G. Servant and T. M. P. Tait, “Is the lightest Kaluza-Klein particle a viable dark matter candidate?,” *Nucl. Phys.*, vol. B650, pp. 391–419, 2003.
- [13] H.-C. Cheng, J. L. Feng, and K. T. Matchev, “Kaluza-Klein dark matter,” *Phys. Rev. Lett.*, vol. 89, p. 211301, 2002.
- [14] Foadi, Roshan and Frandsen, Mads T and Sannino, Francesco, “Technicolor dark matter,” *Physical Review D*, vol. 80, no. 3, p. 037702, 2009.
- [15] Gudnason, Sven Bjarke and Kouvaris, Chris and Sannino, Francesco, “Dark matter from new technicolor theories,” *Physical Review D*, vol. 74, no. 9, p. 095008, 2006.
- [16] R. A. Lineros and F. A. Pereira dos Santos, “Inert scalar dark matter in an extra dimension inspired model,” *JCAP*, vol. 1410, no. 10, p. 059, 2014.
- [17] J. H. Kuhn and P. M. Zerwas, “Excited Quarks and Leptons,” *Phys. Lett.*, vol. 147B, pp. 189–196, 1984.
- [18] P. A. R. Ade *et al.*, “Planck 2015 results. XIII. Cosmological parameters,” *Astron. Astrophys.*, vol. 594, p. A13, 2016.
- [19] A. Askew, S. Chauhan, B. Penning, W. Shepherd, and M. Tripathi, “Searching for Dark Matter at Hadron Colliders,” *Int. J. Mod. Phys.*, vol. A29, p. 1430041, 2014.
- [20] A. Basalaev, “Search for WIMP dark matter produced in association with a Z boson with the ATLAS detector,” *EPJ Web Conf.*, vol. 164, p. 08008, 2017.
- [21] M. Aaboud *et al.*, “Search for dark matter and other new phenomena in events with an energetic jet and large missing transverse momentum using the ATLAS detector,” *JHEP*, vol. 01, p. 126, 2018.
- [22] Akerib, DS and Akerlof, CW and Akimov, D Yu and Alsum, SK and Araújo, HM and Bai, X and Bailey, AJ and Balajthy, J and Balashov, S and Barry, MJ and others, “LUX-ZEPLIN (LZ) conceptual design report,” *arXiv preprint arXiv:1509.02910*, 2015.

- [23] E. Aprile *et al.*, “Physics reach of the XENON1T dark matter experiment,” *JCAP*, vol. 1604, no. 04, p. 027, 2016.
- [24] A. Tan *et al.*, “Dark Matter Results from First 98.7 Days of Data from the PandaX-II Experiment,” *Phys. Rev. Lett.*, vol. 117, no. 12, p. 121303, 2016.
- [25] D. S. Akerib *et al.*, “Results from a search for dark matter in the complete LUX exposure,” *Phys. Rev. Lett.*, vol. 118, no. 2, p. 021303, 2017.
- [26] Z.-H. Yu, J.-M. Zheng, X.-J. Bi, Z. Li, D.-X. Yao, and H.-H. Zhang, “Constraining the interaction strength between dark matter and visible matter: II. scalar, vector and spin-3/2 dark matter,” *Nucl. Phys.*, vol. B860, pp. 115–151, 2012.
- [27] R. Ding and Y. Liao, “Spin 3/2 Particle as a Dark Matter Candidate: an Effective Field Theory Approach,” *JHEP*, vol. 04, p. 054, 2012.
- [28] R. Ding, Y. Liao, J.-Y. Liu, and K. Wang, “Comprehensive Constraints on a Spin-3/2 Singlet Particle as a Dark Matter Candidate,” *JCAP*, vol. 1305, p. 028, 2013.
- [29] K. G. Savvidy and J. D. Vergados, “Direct dark matter detection: A spin 3/2 WIMP candidate,” *Phys. Rev.*, vol. D87, no. 7, p. 075013, 2013.
- [30] S. Dutta, A. Goyal, and S. Kumar, “Anomalous X-ray galactic signal from 7.1 keV spin-3/2 dark matter decay,” *JCAP*, vol. 1602, no. 02, p. 016, 2016.
- [31] C.-F. Chang, X.-G. He, and J. Tandean, “Exploring Spin-3/2 Dark Matter with Effective Higgs Couplings,” *Phys. Rev.*, vol. D96, no. 7, p. 075026, 2017.
- [32] Donoghue, John F. and Golowich, Eugene and Holstein, Barry R, *Dynamics of the standard model*, vol. 35. Cambridge university press, 2014.
- [33] S. Weinberg, “Elementary particle theory of composite particles,” *Phys. Rev.*, vol. 130, pp. 776–783, 1963.
- [34] S. Weinberg, “A New Light Boson?,” *Phys. Rev. Lett.*, vol. 40, pp. 223–226, 1978.
- [35] Shifman, Mikhail A. and Vainshtein, Arkady I. and Zakharov, Valentin I., “QCD and resonance physics. Theoretical foundations,” *Nuclear Physics B*, vol. 147, no. 5, pp. 385–447, 1979.
- [36] S. L. Glashow, “Partial Symmetries of Weak Interactions,” *Nucl. Phys.*, vol. 22, pp. 579–588, 1961.

- [37] S. Weinberg, “A. Salam Phys. Rev. Letters, 19 (1967),” in *Proc. 8th Nobel Symp.: Elementary Particle Theory, Almqvist and Wiksell, Stockholm*, p. 1264, 1968.
- [38] S. Weinberg, “A Model of Leptons,” *Phys. Rev. Lett.*, vol. 19, pp. 1264–1266, 1967.
- [39] F. Englert and R. Brout, “Broken Symmetry and the Mass of Gauge Vector Mesons,” *Phys. Rev. Lett.*, vol. 13, pp. 321–323, 1964.
- [40] G. S. Guralnik, C. R. Hagen, and T. W. B. Kibble, “Global Conservation Laws and Massless Particles,” *Phys. Rev. Lett.*, vol. 13, pp. 585–587, 1964.
- [41] Goldstone, J. and Salam, Abdus and Weinberg, Steven, “Broken symmetries,” *Physical Review*, vol. 127, no. 3, p. 965, 1962.
- [42] Goldstone, J., “Nuovo Cim. 19 (1961) 154; J. Goldstone, A. Salam and S. Weinberg,” *Phys. Rev.*, vol. 127, no. 965, p. 2, 1962.
- [43] Goldstone, J., “Nuovo Cim. 19 (1961), 154. Y. Nambu and G. Jona-Lasinio,” *Phys. Rev.*, vol. 122, no. 345, p. 124, 1961.
- [44] Higgs, P. W., “Phys. Letters 12 (1964) 132,” *Phys. Rev. Letters*, vol. 13, no. 508, p. 1174, 1964.
- [45] Higgs, P. W., “Broken symmetries, massless particles and gauge fields,” *Physics Letters*, vol. 12, no. 2, pp. 132–133, 1964.
- [46] Branco, G.C. and Senjanović, G., “The question of neutrino mass,” *Phys. Rev.*, vol. D18, no. 5, p. 1621, 1978.
- [47] Senjanović, G., “Spontaneous breakdown of parity in a class of gauge theories,” *Nuclear Physics B*, vol. 153, pp. 334–364, 1979.
- [48] Mohapatra, Rabindra N. and Senjanović, G., “Neutrino masses and mixings in gauge models with spontaneous parity violation,” *Phys. Rev.*, vol. D23, no. 1, p. 165, 1981.
- [49] T. Kajita, “Nobel Lecture: Discovery of atmospheric neutrino oscillations,” *Rev. Mod. Phys.*, vol. 88, no. 3, p. 030501, 2016.
- [50] Fukuda, Y and Hayakawa, T and Ichihara, E and Inoue, K and Ishihara, K and Ishino, H and Itow, Y and Kajita, T and Kameda, J and Kasuga, S and others, “Evidence for oscillation of atmospheric neutrinos,” *Physical Review Letters*, vol. 81, no. 8, p. 1562, 1998.

- [51] B. C. Allanach, *Beyond the Standard Model Lectures for the 2016 European School of High-Energy Physics*. PhD thesis, Cambridge U., DAMTP, 2016.
- [52] Krippendorf, Sven and Quevedo, Fernando and Schlotterer, Oliver, “Cambridge Lectures on Supersymmetry and Extra Dimensions,” *arXiv preprint arXiv:1011.1491*, 2010.
- [53] Arkani–Hamed, Nima and Dimopoulos, Savas and Dvali, Gia, “The hierarchy problem and new dimensions at a millimeter,” *Physics Letters B*, vol. 429, no. 3, pp. 263–272, 1998.
- [54] C. Csáki and P. Tanedo, “Beyond the Standard Model,” in *Proceedings, 2013 European School of High-Energy Physics (ESHEP 2013): Paradfurdo, Hungary, June 5-18, 2013*, pp. 169–268, 2015.
- [55] West, Peter, *Introduction to supersymmetry and supergravity*. World Scientific Publishing Co Inc, 1990.
- [56] A. Masiero, S. K. Vempati, and O. Vives, “Flavour physics and grand unification,” in *Particle physics beyond the standard model. Proceedings, Summer School on Theoretical Physics, 84th Session, Les Houches, France, August 1-26, 2005*, pp. 1–78, 2005.
- [57] S. F. King, A. Merle, S. Morisi, Y. Shimizu, and M. Tanimoto, “Neutrino Mass and Mixing: from Theory to Experiment,” *New J. Phys.*, vol. 16, p. 045018, 2014.
- [58] M. Trodden, “Electroweak baryogenesis: A Brief review,” in *Proceedings, 33rd Rencontres de Moriond 98 electroweak interactions and unified theories: Les Arcs, France, Mar 14-21, 1998*, pp. 471–480, 1998.
- [59] G. C. Branco, P. M. Ferreira, L. Lavoura, M. N. Rebelo, M. Sher, and J. P. Silva, “Theory and phenomenology of two-Higgs-doublet models,” *Phys. Rept.*, vol. 516, pp. 1–102, 2012.
- [60] K. R. Dienes, E. Dudas, and T. Gherghetta, “Extra space-time dimensions and unification,” *Phys. Lett.*, vol. B436, pp. 55–65, 1998.
- [61] Bertolini, Matteo, “Lectures on supersymmetry,” *Lecture notes given at SISSA*, 2015.
- [62] K. R. Dienes, E. Dudas, and T. Gherghetta, “Grand unification at intermediate mass scales through extra dimensions,” *Nucl. Phys.*, vol. B537, pp. 47–108, 1999.

- [63] M. Blennow, H. Melbeus, T. Ohlsson, and H. Zhang, “RG running in a minimal UED model in light of recent LHC Higgs mass bounds,” *Phys. Lett.*, vol. B712, pp. 419–424, 2012.
- [64] M. O. Khojali, A. Goyal, M. Kumar, and A. S. Cornell, “Minimal Spin-3/2 Dark Matter in a simple *s*-channel model,” *Eur. Phys. J.*, vol. C77, no. 1, p. 25, 2017.
- [65] Khojali, Mohammed Omer and Goyal, Ashok and Kumar, Mukesh and Cornell, Alan S, “Spin-3/2 Dark Matter in a simple *t*-channel model,” *arXiv preprint arXiv:1705.05149*, 2017.
- [66] A. Cordero-Cid, H. Novales-Sanchez, and J. J. Toscano, “The Standard Model with one universal extra dimension,” *Pramana*, vol. 80, pp. 369–412, 2013.
- [67] A. Zee, “Study of the renormalization group for small coupling constants,” *Phys. Rev.*, vol. D7, pp. 3630–3636, 1973.
- [68] A. A. Vladimirov, “Renormalization Group Equations in Different Approaches,” *Theor. Math. Phys.*, vol. 25, p. 1170, 1976. [Teor. Mat. Fiz.25,335(1975)].
- [69] H. D. Politzer, “Reliable Perturbative Results for Strong Interactions?,” *Phys. Rev. Lett.*, vol. 30, pp. 1346–1349, 1973.
- [70] N. N. Bogolyubov and D. V. Shirkov, “INTRODUCTION TO THE THEORY OF QUANTIZED FIELDS,” *Intersci. Monogr. Phys. Astron.*, vol. 3, pp. 1–720, 1959.
- [71] M. E. Peskin and D. V. Schroeder, *An Introduction to quantum field theory*. Reading, USA: Addison-Wesley, 1995.
- [72] T. P. Cheng, E. Eichten, and L.-F. Li, “Higgs Phenomena in Asymptotically Free Gauge Theories,” *Phys. Rev.*, vol. D9, p. 2259, 1974.
- [73] M. E. Machacek and M. T. Vaughn, “Two Loop Renormalization Group Equations in a General Quantum Field Theory (II). Yukawa Couplings,” *Nucl. Phys.*, vol. B236, pp. 221–232, 1984.
- [74] L. Randall and M. D. Schwartz, “Quantum field theory and unification in AdS5,” *JHEP*, vol. 11, p. 003, 2001.
- [75] H. Georgi and S. L. Glashow, “Unity of All Elementary Particle Forces,” *Phys. Rev. Lett.*, vol. 32, pp. 438–441, 1974.

- [76] E. Byckling and K. Kajantie, “Kinematic separation of three-particle channels in counter experiments,” *Nucl. Phys.*, vol. B14, pp. 355–365, 1969.
- [77] Maggiore, Michele, *A modern introduction to quantum field theory*, vol. 12. Oxford University Press, 2005.
- [78] O. F. Piattella, “Lecture Notes in Cosmology,” 2018.
- [79] P. Gondolo and G. Gelmini, “Cosmic abundances of stable particles: Improved analysis,” *Nucl. Phys.*, vol. B360, pp. 145–179, 1991.
- [80] P. S. Bhupal Dev, A. Mazumdar, and S. Qutub, “Constraining Non-thermal and Thermal properties of Dark Matter,” *Front.in Phys.*, vol. 2, p. 26, 2014.
- [81] H. Baer, K.-Y. Choi, J. E. Kim, and L. Roszkowski, “Dark matter production in the early Universe: beyond the thermal WIMP paradigm,” *Phys. Rept.*, vol. 555, pp. 1–60, 2015.
- [82] J. Beringer *et al.*, “Review of Particle Physics (RPP),” *Phys. Rev.*, vol. D86, p. 010001, 2012.
- [83] W. Buchmuller, R. D. Peccei, and T. Yanagida, “Leptogenesis as the origin of matter,” *Ann. Rev. Nucl. Part. Sci.*, vol. 55, pp. 311–355, 2005.
- [84] A. Abdalgabar, M. O. Khojali, A. S. Cornell, G. Cacciapaglia, and A. Deandrea, “Unification of gauge and Yukawa couplings,” *Phys. Lett.*, vol. B776, pp. 231–235, 2018.
- [85] I. Antoniadis, “A Possible new dimension at a few TeV,” *Phys. Lett.*, vol. B246, pp. 377–384, 1990.
- [86] I. Antoniadis, N. Arkani-Hamed, S. Dimopoulos, and G. R. Dvali, “New dimensions at a millimeter to a Fermi and superstrings at a TeV,” *Phys. Lett.*, vol. B436, pp. 257–263, 1998.
- [87] N. Arkani-Hamed, S. Dimopoulos, and G. R. Dvali, “The Hierarchy problem and new dimensions at a millimeter,” *Phys. Lett.*, vol. B429, pp. 263–272, 1998.
- [88] G. Dvali, G. Gabadadze, and M. Shifman, “Diluting cosmological constant in infinite volume extra dimensions,” *Phys. Rev.*, vol. D67, p. 044020, 2003.
- [89] Y. Hosotani, “Dynamical Mass Generation by Compact Extra Dimensions,” *Phys. Lett.*, vol. 126B, pp. 309–313, 1983.

- [90] H. Hatanaka, T. Inami, and C. S. Lim, “The Gauge hierarchy problem and higher dimensional gauge theories,” *Mod. Phys. Lett.*, vol. A13, pp. 2601–2612, 1998.
- [91] G. R. Dvali, S. Randjbar-Daemi, and R. Tabbash, “The Origin of spontaneous symmetry breaking in theories with large extra dimensions,” *Phys. Rev.*, vol. D65, p. 064021, 2002.
- [92] A. Masiero, C. A. Scrucca, M. Serone, and L. Silvestrini, “Nonlocal symmetry breaking in Kaluza-Klein theories,” *Phys. Rev. Lett.*, vol. 87, p. 251601, 2001.
- [93] I. Antoniadis, K. Benakli, and M. Quiros, “Finite Higgs mass without supersymmetry,” *New J. Phys.*, vol. 3, p. 20, 2001.
- [94] C. Csaki, C. Grojean, and H. Murayama, “Standard model Higgs from higher dimensional gauge fields,” *Phys. Rev.*, vol. D67, p. 085012, 2003.
- [95] D. Ghilencea and G. G. Ross, “Unification and extra space-time dimensions,” *Phys. Lett.*, vol. B442, pp. 165–172, 1998.
- [96] D. M. Ghilencea, “Regularization techniques for the radiative corrections of the Kaluza-Klein states,” *Phys. Rev.*, vol. D70, p. 045011, 2004.
- [97] T. Varin, J. Welzel, A. Deandrea, and D. Davesne, “Power law in a gauge-invariant cut-off regularisation,” *Phys. Rev.*, vol. D74, p. 121702, 2006.
- [98] C. A. Scrucca, M. Serone, and L. Silvestrini, “Electroweak symmetry breaking and fermion masses from extra dimensions,” *Nucl. Phys.*, vol. B669, pp. 128–158, 2003.
- [99] N. Yamatsu, “Gauge coupling unification in gauge–Higgs grand unification,” *PTEP*, vol. 2016, no. 4, p. 043B02, 2016.
- [100] S. Weinberg, “Phenomenological Lagrangians,” *Physica*, vol. A96, pp. 327–340, 1979.
- [101] A. Manohar and H. Georgi, “Chiral Quarks and the Nonrelativistic Quark Model,” *Nucl. Phys.*, vol. B234, pp. 189–212, 1984.
- [102] A. S. Cornell, A. Deandrea, L.-X. Liu, and A. Tarhini, “Renormalisation running of masses and mixings in UED models,” *Mod. Phys. Lett.*, vol. A28, no. 11, p. 1330007, 2013.
- [103] H. Gies, “Renormalizability of gauge theories in extra dimensions,” *Phys. Rev.*, vol. D68, p. 085015, 2003.

- [104] T. R. Morris, “Renormalizable extra-dimensional models,” *JHEP*, vol. 01, p. 002, 2005.
- [105] R. Contino, L. Pilo, R. Rattazzi, and E. Trincherini, “Running and matching from five-dimensions to four-dimensions,” *Nucl. Phys.*, vol. B622, pp. 227–239, 2002.
- [106] S. Funatsu, H. Hatanaka, Y. Hosotani, Y. Orikasa, and T. Shimotani, “Novel universality and Higgs decay $H \rightarrow \gamma\gamma$, gg in the $SO(5) \times U(1)$ gauge-Higgs unification,” *Phys. Lett.*, vol. B722, pp. 94–99, 2013.
- [107] S. Funatsu, H. Hatanaka, Y. Hosotani, Y. Orikasa, and T. Shimotani, “LHC signals of the $SO(5) \times U(1)$ gauge-Higgs unification,” *Phys. Rev.*, vol. D89, no. 9, p. 095019, 2014.
- [108] S. Funatsu, H. Hatanaka, Y. Hosotani, and Y. Orikasa, “Collider signals of W' and Z' bosons in the gauge-Higgs unification,” *Phys. Rev.*, vol. D95, no. 3, p. 035032, 2017.
- [109] M. Carena, T. M. P. Tait, and C. E. M. Wagner, “Branes and orbifolds are opaque,” *Acta Phys. Polon.*, vol. B33, p. 2355, 2002.
- [110] G. Cacciapaglia, C. Csaki, and S. C. Park, “Fully radiative electroweak symmetry breaking,” *JHEP*, vol. 03, p. 099, 2006.
- [111] R. Contino, Y. Nomura, and A. Pomarol, “Higgs as a holographic pseudo-Goldstone boson,” *Nucl. Phys.*, vol. B671, pp. 148–174, 2003.
- [112] Y. Hosotani and M. Mabe, “Higgs boson mass and electroweak-gravity hierarchy from dynamical gauge-Higgs unification in the warped spacetime,” *Phys. Lett.*, vol. B615, pp. 257–265, 2005.
- [113] Y. Grossman and M. Neubert, “Neutrino masses and mixings in nonfactorizable geometry,” *Phys. Lett.*, vol. B474, pp. 361–371, 2000.
- [114] M. O. Khojali and A. S. Cornell, “Evolution of Quark Masses and Flavour Mixings in 5D for an $SU(5)$ gauge group,” in *Proceedings, 61th Annual Conference of the South African Institute of Physics (SAIP2016): Cape Town, South Africa, July 4-8, 2016*, pp. 495–500, 2016.
- [115] M. O. Khojali, A. S. Cornell, and A. Deandrea, “The evolution of gauge couplings and the Weinberg angle in 5 dimensions for an $SU(3)$ gauge group,” *J. Phys. Conf. Ser.*, vol. 802, no. 1, p. 012005, 2017.

- [116] D. Falcone, “Fermion masses and mixings in gauge theories,” *Int. J. Mod. Phys.*, vol. A17, pp. 3981–4006, 2002.
- [117] H. Fritzsch and Z.-z. Xing, “Mass and flavor mixing schemes of quarks and leptons,” *Prog. Part. Nucl. Phys.*, vol. 45, pp. 1–81, 2000.
- [118] Z.-z. Xing, H. Zhang, and S. Zhou, “Updated Values of Running Quark and Lepton Masses,” *Phys. Rev.*, vol. D77, p. 113016, 2008.
- [119] A. S. Cornell, A. Deandrea, L.-X. Liu, and A. Tarhini, “Scaling of the CKM Matrix in the 5D MSSM,” *Phys. Rev.*, vol. D85, p. 056001, 2012.
- [120] P. H. Chankowski and S. Pokorski, “Quantum corrections to neutrino masses and mixing angles,” *Int. J. Mod. Phys.*, vol. A17, pp. 575–614, 2002.
- [121] A. S. Cornell and L.-X. Liu, “Evolution of the CKM Matrix in the Universal Extra Dimension Model,” *Phys. Rev.*, vol. D83, p. 033005, 2011.
- [122] Cabibbo, Nicola, “Unitary symmetry and leptonic decays,” *Physical Review Letters*, vol. 10, no. 12, p. 531, 1963.
- [123] Kobayashi, Makoto and Maskawa, Toshihide, “CP-violation in the renormalizable theory of weak interaction,” *Progress of Theoretical Physics*, vol. 49, no. 2, pp. 652–657, 1973.
- [124] Chau, Ling-Lie and Keung, Wai-Yee, “Comments on the parametrization of the Kobayashi-Maskawa matrix,” *Physical Review Letters*, vol. 53, no. 19, p. 1802, 1984.
- [125] Wolfenstein, Lincoln, “Parametrization of the Kobayashi-Maskawa matrix,” *Physical Review Letters*, vol. 51, no. 21, p. 1945, 1983.
- [126] Babu, K.S., “Renormalization-Group analysis of the Kobayashi-Maskawa matrix,” *Zeitschrift für Physik C Particles and Fields*, vol. 35, no. 1, pp. 69–75, 1987.
- [127] L.-X. Liu and A. S. Cornell, “Scaling of Yukawa Couplings and Quark Flavor Mixings in the UED Model,” *PoS*, vol. KRUGER2010, p. 045, 2010.
- [128] M. O. Khojali, A. S. Cornell, A. Deandrea, and G. Cacciapaglia, “Evolution of the gauge couplings and Weinberg angle in 5-dimensions for an SU(5) and flipped SU(5) gauge group,” *J. Phys. Conf. Ser.*, vol. 878, no. 1, p. 012024, 2017.

- [129] T. Appelquist, H.-C. Cheng, and B. A. Dobrescu, “Bounds on universal extra dimensions,” *Phys. Rev.*, vol. D64, p. 035002, 2001.
- [130] H.-C. Cheng, K. T. Matchev, and M. Schmaltz, “Radiative corrections to Kaluza-Klein masses,” *Phys. Rev.*, vol. D66, p. 036005, 2002.
- [131] Senjanović, G., “Course on grand unification,” *The Standard Model and Beyond*, pp. 137–179, 2008.
- [132] von Steinkirch, Marina, “Introduction to Group Theory for Physicists,” *Lecture Notes, SUNY, WS*, 2011.
- [133] A.-C. Davis and N. F. Lepora, “Embedded defects and symmetry breaking in flipped $SU(5)$,” *Phys. Rev.*, vol. D52, pp. 7265–7275, 1995.
- [134] J. L. Lopez and D. V. Nanopoulos, “Flipped $SU(5)$: A Grand unified superstring theory (GUST) prototype,” in *Vacuum and vacua: The physics of nothing. Proceedings, 33rd Course of the International School of Subnuclear Physics, Erice, Italy, July 2-9, 1995*, pp. 125–165, 1995.
- [135] M. O. Khojali, A. S. Cornell, A. Deandrea, and G. Cacciapaglia, “Evolution of the gauge couplings and Weinberg angle in 5-dimensions for a G_2 gauge group,” *J. Phys. Conf. Ser.*, vol. 889, no. 1, p. 012012, 2017.
- [136] Manton, N. S., “A new six-dimensional approach to the Weinberg-Salam model,” *Nuclear Physics B*, vol. 158, no. 1, pp. 141–153, 1979.
- [137] I. Antoniadis and K. Benakli, “Limits on extra dimensions in orbifold compactifications of superstrings,” *Phys. Lett.*, vol. B326, pp. 69–78, 1994.
- [138] N. Haba, M. Harada, Y. Hosotani, and Y. Kawamura, “Dynamical rearrangement of gauge symmetry on the orbifold $S1 / Z(2)$,” *Nucl. Phys.*, vol. B657, pp. 169–213, 2003. [Erratum: Nucl. Phys.B669,381(2003)].
- [139] I. Antoniadis, K. Benakli, and M. Quiros, “Production of Kaluza-Klein states at future colliders,” *Phys. Lett.*, vol. B331, pp. 313–320, 1994.
- [140] N. Kitazawa and Y. Sakai, “Constraints on gauge-Higgs unification models at the LHC,” *Mod. Phys. Lett.*, vol. A31, no. 07, p. 1650041, 2016.
- [141] T. Ohlsson and S. Riad, “Running of Neutrino Parameters and the Higgs Self-Coupling in a Six-Dimensional UED Model,” *Phys. Lett.*, vol. B718, pp. 1002–1007, 2013.

- [142] L.-X. Liu and A. S. Cornell, “Improved vacuum stability in a five dimensional model,” *Phys. Rev.*, vol. D86, p. 056002, 2012.
- [143] Burges, C. J. C and Schnitzer, Howard J., “Virtual effects of excited quarks as probes of a possible new hardonic mass scale,” *Nuclear Physics B*, vol. 228, no. 3, pp. 464–500, 1983.
- [144] Kühn, J. and Zerwas, P., “Excited quarks and leptons,” *Physics Letters B*, vol. 147, no. 1-3, pp. 189–196, 1984.
- [145] Arkani-Hamed, Nima and Dimopoulos, Savas and Dvali, Gia, “Phenomenology, astrophysics, and cosmology of theories with submillimeter dimensions and TeV scale quantum gravity,” *Phys. Rev.*, vol. D59, no. 8, p. 086004, 1999.
- [146] Antoniadis, Ignatios and Arkani-Hamed, Nima and Dimopoulos, Savas and Dvali, Gia, “New dimensions at a millimeter to a Fermi and superstrings at a TeV,” *Physics Letters B*, vol. 436, no. 3, pp. 257–263, 1998.
- [147] Randall, Lisa and Sundrum, Raman, “Large mass hierarchy from a small extra dimension,” *Physical Review Letters*, vol. 83, no. 17, p. 3370, 1999.
- [148] M. Schumann, “Dark Matter 2013,” *Braz. J. Phys.*, vol. 44, pp. 483–493, 2014. [,1314(2013)].
- [149] M. Cirelli, “Dark Matter Indirect Detection amid hints and constraints,” *PoS*, vol. NEUTEL2015, p. 020, 2015.
- [150] Abdallah, Jalal and Ashkenazi, Adi and Boveia, Antonio and Busoni, Giorgio and De Simone, Andrea and Doglioni, Caterina and Efrati, Aielet and Etzion, Erez and Gramling, Johanna and Jacques, Thomas and others, “Simplified models for dark matter and missing energy searches at the LHC,” *arXiv preprint arXiv:1409.2893*, 2014.
- [151] N. D. Christensen, P. de Aquino, N. Deutschmann, C. Duhr, B. Fuks, C. Garcia-Cely, O. Mattelaer, K. Mawatari, B. Oexl, and Y. Takaesu, “Simulating spin- $\frac{3}{2}$ particles at colliders,” *Eur. Phys. J.*, vol. C73, no. 10, p. 2580, 2013.
- [152] B. Hassanain, J. March-Russell, and J. G. Rosa, “On the possibility of light string resonances at the LHC and Tevatron from Randall-Sundrum throats,” *JHEP*, vol. 07, p. 077, 2009.
- [153] P. Langacker, “The Physics of Heavy Z' Gauge Bosons,” *Rev. Mod. Phys.*, vol. 81, pp. 1199–1228, 2009.

- [154] T. Han, P. Langacker, Z. Liu, and L.-T. Wang, “Diagnosis of a New Neutral Gauge Boson at the LHC and ILC for Snowmass 2013,” 2013.
- [155] F. del Aguila, J. de Blas, and M. Perez-Victoria, “Electroweak Limits on General New Vector Bosons,” *JHEP*, vol. 09, p. 033, 2010.
- [156] G. Arcadi, Y. Mambrini, M. H. G. Tytgat, and B. Zaldivar, “Invisible Z' and dark matter: LHC vs LUX constraints,” *JHEP*, vol. 03, p. 134, 2014.
- [157] E. W. Kolb and M. S. Turner, “The Early Universe,” *Front. Phys.*, vol. 69, pp. 1–547, 1990.
- [158] M. Cirelli, E. Del Nobile, and P. Panci, “Tools for model-independent bounds in direct dark matter searches,” *JCAP*, vol. 1310, p. 019, 2013.
- [159] M. Freytsis and Z. Ligeti, “On dark matter models with uniquely spin-dependent detection possibilities,” *Phys. Rev.*, vol. D83, p. 115009, 2011.
- [160] V. Barger, W.-Y. Keung, and G. Shaughnessy, “Spin Dependence of Dark Matter Scattering,” *Phys. Rev.*, vol. D78, p. 056007, 2008.
- [161] J. Abdallah *et al.*, “Simplified Models for Dark Matter Searches at the LHC,” *Phys. Dark Univ.*, vol. 9-10, pp. 8–23, 2015.
- [162] E. Aprile *et al.*, “Limits on spin-dependent WIMP-nucleon cross sections from 225 live days of XENON100 data,” *Phys. Rev. Lett.*, vol. 111, no. 2, p. 021301, 2013.
- [163] A. Drlica-Wagner *et al.*, “Search for Gamma-Ray Emission from DES Dwarf Spheroidal Galaxy Candidates with Fermi-LAT Data,” *Astrophys. J.*, vol. 809, no. 1, p. L4, 2015.
- [164] M. Ackermann *et al.*, “Searching for Dark Matter Annihilation from Milky Way Dwarf Spheroidal Galaxies with Six Years of Fermi Large Area Telescope Data,” *Phys. Rev. Lett.*, vol. 115, no. 23, p. 231301, 2015.
- [165] J. F. Cherry, M. T. Frandsen, and I. M. Shoemaker, “Direct Detection Phenomenology in Models Where the Products of Dark Matter Annihilation Interact with Nuclei,” *Phys. Rev. Lett.*, vol. 114, p. 231303, 2015.
- [166] V. Khachatryan *et al.*, “Search for dark matter, extra dimensions, and unparticles in monojet events in proton–proton collisions at $\sqrt{s} = 8$ TeV,” *Eur. Phys. J.*, vol. C75, no. 5, p. 235, 2015.

- [167] O. Buchmueller, M. J. Dolan, S. A. Malik, and C. McCabe, “Characterising dark matter searches at colliders and direct detection experiments: Vector mediators,” *JHEP*, vol. 01, p. 037, 2015.
- [168] P. Harris, V. V. Khoze, M. Spannowsky, and C. Williams, “Constraining Dark Sectors at Colliders: Beyond the Effective Theory Approach,” *Phys. Rev.*, vol. D91, p. 055009, 2015.
- [169] T. Jacques and K. Nordström, “Mapping monojet constraints onto Simplified Dark Matter Models,” *JHEP*, vol. 06, p. 142, 2015.
- [170] M. Chala, F. Kahlhoefer, M. McCullough, G. Nardini, and K. Schmidt-Hoberg, “Constraining Dark Sectors with Monojets and Dijets,” *JHEP*, vol. 07, p. 089, 2015.
- [171] A. Alves, S. Profumo, and F. S. Queiroz, “The dark Z' portal: direct, indirect and collider searches,” *JHEP*, vol. 04, p. 063, 2014.
- [172] A. Alves, A. Berlin, S. Profumo, and F. S. Queiroz, “Dark Matter Complementarity and the Z' Portal,” *Phys. Rev.*, vol. D92, no. 8, p. 083004, 2015.
- [173] J. Alwall, R. Frederix, S. Frixione, V. Hirschi, F. Maltoni, O. Mattelaer, H. S. Shao, T. Stelzer, P. Torrielli, and M. Zaro, “The automated computation of tree-level and next-to-leading order differential cross sections, and their matching to parton shower simulations,” *JHEP*, vol. 07, p. 079, 2014.
- [174] A. Alloul, N. D. Christensen, C. Degrande, C. Duhr, and B. Fuks, “FeynRules 2.0 - A complete toolbox for tree-level phenomenology,” *Comput. Phys. Commun.*, vol. 185, pp. 2250–2300, 2014.
- [175] S. Chang, R. Edezhath, J. Hutchinson, and M. Luty, “Effective WIMPs,” *Phys. Rev.*, vol. D89, no. 1, p. 015011, 2014.
- [176] A. DiFranzo, K. I. Nagao, A. Rajaraman, and T. M. P. Tait, “Simplified Models for Dark Matter Interacting with Quarks,” *JHEP*, vol. 11, p. 014, 2013. [Erratum: JHEP01,162(2014)].
- [177] H. An, L.-T. Wang, and H. Zhang, “Dark matter with t -channel mediator: a simple step beyond contact interaction,” *Phys. Rev.*, vol. D89, no. 11, p. 115014, 2014.
- [178] M. Papucci, A. Vichi, and K. M. Zurek, “Monojet versus the rest of the world I: t -channel models,” *JHEP*, vol. 11, p. 024, 2014.

- [179] G. Aielli *et al.*, “Proton-air cross section measurement with the ARGO-YBJ cosmic ray experiment,” *Phys. Rev.*, vol. D80, p. 092004, 2009.
- [180] G. Bélanger, F. Boudjema, A. Pukhov, and A. Semenov, “micrOMEGAs4.1: two dark matter candidates,” *Comput. Phys. Commun.*, vol. 192, pp. 322–329, 2015.
- [181] D. Korotkin and H. Samtleben, “Generalization of Okamoto’s equation to arbitrary 2 x 2 Schlesinger systems,” *Adv. Math. Phys.*, vol. 2009, p. 461860, 2009.
- [182] A. Goyal and M. Kumar, “Fermionic Dark Matter in a simple t -channel model,” *JCAP*, vol. 1611, no. 11, p. 001, 2016.
- [183] Y. Bai and J. Berger, “Fermion Portal Dark Matter,” *JHEP*, vol. 11, p. 171, 2013.
- [184] F. Giacchino, A. Ibarra, L. Lopez Honorez, M. H. G. Tytgat, and S. Wild, “Signatures from Scalar Dark Matter with a Vector-like Quark Mediator,” *JCAP*, vol. 1602, no. 02, p. 002, 2016.
- [185] Y. Hosotani and N. Yamatsu, “Gauge–Higgs grand unification,” *PTEP*, vol. 2015, p. 111B01, 2015.
- [186] A. Abdalgabar, A. S. Cornell, A. Deandrea, and A. Tarhini, “Evolution of Yukawa couplings and quark flavour mixings in 2UED models,” *Phys. Rev.*, vol. D88, p. 056006, 2013.
- [187] G. Cacciapaglia and B. Kubik, “Even tiers and resonances on the Real Projective Plane,” *JHEP*, vol. 02, p. 052, 2013.
- [188] A. Deandrea, J. Welzel, P. Hosteins, and M. Oertel, “Quantum corrections to the effective neutrino mass operator in 5D MSSM,” *Phys. Rev.*, vol. D75, p. 113005, 2007.